



SCHOOL of  
GRADUATE STUDIES  
EAST TENNESSEE STATE UNIVERSITY

East Tennessee State University  
**Digital Commons @ East  
Tennessee State University**

---

Electronic Theses and Dissertations

Student Works

---

12-2007

# 1, Structural and Functional Studies of Human Replication Protein A; 2 DNA Damage Responses and DNA Repair Defects in Laminopathy-Based Premature Aging.

Yiyong Liu

*East Tennessee State University*

Follow this and additional works at: <https://dc.etsu.edu/etd>

 Part of the [Molecular Genetics Commons](#)

---

## Recommended Citation

Liu, Yiyong, "1, Structural and Functional Studies of Human Replication Protein A; 2 DNA Damage Responses and DNA Repair Defects in Laminopathy-Based Premature Aging." (2007). *Electronic Theses and Dissertations*. Paper 2062. <https://dc.etsu.edu/etd/2062>

This Dissertation - Open Access is brought to you for free and open access by the Student Works at Digital Commons @ East Tennessee State University. It has been accepted for inclusion in Electronic Theses and Dissertations by an authorized administrator of Digital Commons @ East Tennessee State University. For more information, please contact [digilib@etsu.edu](mailto:digilib@etsu.edu).

1, Structural and Functional Studies of Human Replication Protein A; 2, DNA Damage  
Responses and DNA Repair Defects in Laminopathy-Based Premature Aging

---

A dissertation

presented to

the faculty of the Department of Biochemistry and Molecular Biology

East Tennessee State University

In partial fulfillment

of the requirements for the degree

Doctorate of Philosophy in Biomedical Sciences

---

by

Yiyong Liu

December, 2006

---

Yue Zou, Ph.D. Chair

David A. Johnson, Ph.D.

John J. Laffan, Ph.D.

Peter J. Rice, Pharm.D., Ph.D.

Douglas P. Thewke, Ph.D.

Keywords: DNA Repair, DNA Damage Responses, Replication Protein A, Laminopathy

## ABSTRACT

1, Structural and Functional Studies of Human Replication Protein A; 2, DNA Damage Responses and DNA Repair Defects in Laminopathy-Based Premature Aging

by

Yiyong Liu

The genome of mammalian cells is under constant attack from DNA-damaging agents. To maintain genomic integrity, cells activate an array of pathways primarily consisting of DNA repair and DNA damage checkpoints. Human replication protein A (RPA), a single-stranded DNA (ssDNA) binding protein, is essential for almost all DNA metabolic pathways. However, the role of RPA in nucleotide excision repair (NER), a DNA repair pathway for removing bulky DNA lesions, remains elusive. In this study, the binding of RPA to a battery of well-defined ssDNA substrates has been systematically examined using fluorescence spectroscopy. The results showed that RPA has a lower binding affinity for damaged ssDNA than for non-damaged ssDNA, and there was no direct contact between RPA residues and the lesion itself. These findings will help define the roles of RPA in DNA damage recognition in NER. In cells, RPA undergoes hyperphosphorylation in the N-terminus of RPA32 subunit after DNA damage. In this study, the hyperphosphorylation-induced conformational changes of RPA have been probed using mass spectrometry-based protein foot-printing, fluorescence spectroscopy, and limited proteolysis. The data show that upon hyperphosphorylation RPA undergoes a subtle structural change involving its DNA-binding domain B (DBD-B), reducing its affinity for short ssDNA. These results suggest that hyperphosphorylation may modulate RPA functions by altering DBD-

B-mediated RPA-DNA/protein interactions. Cellular accumulation of DNA damage has been widely implicated in premature aging. In Hutchinson-Gilford progeria syndrome (HGPS) and restrictive dermopathy (RD), premature aging is caused by defective maturation of lamin A and linked to accumulation of DNA double-strand breaks (DSBs). However, how lamin A dysfunction leads to genome instability and premature aging is not understood. Here evidence showed that in HGPS and RD fibroblasts DNA damage checkpoints are persistently activated and recruitment of repair factors to DSBs was impaired. Strikingly, xeroderma pigmentosum group A (XPA), a unique NER protein, formed foci and colocalized with the unrepairable DSBs in the patient cells. RNAi knockdown of XPA in HGPS cells significantly restored DSB repair. These results indicate that XPA dysfunction may play an important role in accumulating DSBs in HGPS, implicating a potential strategy for treatment of these premature aging diseases.

## DEDICATION

I dedicate this manuscript to my lovely wife, Jingru Sun, whose invaluable support made my journey towards my Ph.D. possible.

## ACKNOWLEDGEMENTS

I would like to thank Dr. Yue Zou for being a wonderful advisor and guiding me through these four years of my graduate study. I would also like to thank Mike Shell for his constant help with my research. I would like to acknowledge Dr. Nicholas E. Geacintov and Dr. Ashis K. Basu for synthesizing adducted ssDNA substrates; Dr. Mamuka Kvaratskhelia and Dr. Sonja Hess for conducting mass spectrometry; Dr. Antonio E. Rusinol and Dr. Michael Sinensky for their assistance with my research.

## CONTENTS

	Page
ABSTRACT .....	2
DEDICATION .....	4
ACKNOWLEDGEMENTS .....	5
LIST OF TABLES .....	11
LIST OF FIGURES .....	12
Chapter	
1. INTRODUCTION .....	14
DNA Damage and Cellular Responses .....	14
Nucleotide Excision Repair (NER).....	15
Double Strand Break (DSB) Repair.....	16
DNA Damage Checkpoints.....	19
Replication Protein A (RPA) and Hyperphosphorylation .....	19
RPA Structure and Interactions with ssDNA.....	21
RPA Hyperphosphorylation.....	22
DNA Repair Defects in Laminopathy-Based Premature Aging .....	24
Questions to be Answered in the Studies.....	25
2. INTERACTIONS OF HUMAN REPLICATION PROTEIN A WITH SINGLE-STRANDED DNA ADDUCTS .....	28
Abstract.....	28
Introduction.....	29
Materials and Methods.....	31
DNA Substrate Preparation .....	31
RPA Preparation .....	33

Chapter	Page
Gel Mobility-Shift Assays .....	34
Gel-Filtration Analysis and Scintillation Counting .....	34
Fluorescence Measurement of the Binding of RPA to ssDNA with a BPDE Adduct .....	35
Fluorescence Anisotropy Measurements .....	35
Data Processing .....	36
Results .....	37
Stoichiometry of RPA Binding to Different Sizes of ssDNA .....	37
Fluorescence Spectroscopic Characterization of RPA Binding to- Defined Substrates .....	41
RPA Binding to 5'F-30mer with or without (6-4)PP, BPDE, AAF, or AP Adduct .....	44
RPA Binding to Damaged and Undamaged 9mer and 11mer ssDNAs .....	48
Discussion .....	52
References .....	55
 3. MODULATION OF REPLICATION PROTEIN A FUNCTION BY ITS HYPERPHOSPHORYLATION-INDUCED COMFORMATIONAL CHANGE INVOLVING DNA BINDING DOMAIN B .....	
Abstract .....	59
Introduction .....	60
Materials and Methods .....	63
Protein Production and Purification .....	63
<i>In Vitro</i> Phosphorylation by DNA-PK .....	63
Chemical Modification and In-Gel Proteolysis .....	64
MS and MS/MS Analysis .....	65



Chapter	Page
Fluorescence Spectroscopy Determination .....	66
Partial Proteolysis and Identification of Proteolytic Fragments .....	66
Gel Mobility Shift Assay .....	67
Pull-Down Assays .....	68
Western Blotting .....	69
Results .....	69
<i>In Vitro</i> Hyperphosphorylation of RPA by DNA-PK .....	69
Surface Topology Analysis of Native and Hyperphosphorylation RPAs with Group-Specific Reagents and Mass Spectrometry .....	72
Fluorescence Measurements .....	76
Limited Proteolysis of RPA and hyp-RPA .....	79
Bindings of RPA and hyp-RPA to ssDNA and Partial DNA Duplex .....	82
Discussion .....	86
References.....	90
<b>4. DNA DAMAGE RESPONSES IN PROGEROID SYNDROMES ARISING FROM DEFECTIVE MATURATION OF PRELAMIN A .....</b>	<b>94</b>
Abstract .....	94
Introduction .....	95
Materials and Methods .....	97
Cell Culture and Drug Treatments .....	97
Immunofluorescence Microscopy .....	98
Transfection of Plasmid and siRNA .....	98
DNA Synthesis Assay .....	99
Western Blotting .....	99
Comet Assay .....	100

Chapter	Page
Results .....	101
Early Replication Arrest of RD Cells and HGPS Cells .....	101
Activation of ATM and ATR in RD Cells and HGPS cells .....	102
Restoration of Replication Activity by Inactivation of ATM and ATR .....	106
FTI Treatment, A Potential Therapy for HGPS and RD? .....	108
Discussion .....	111
References.....	114
 5. XERODERMA PIGMENTOSUM GROUP A (XPA) INHIBITS REPAIR OF DNA DOUBLE-STRAND BREAKS IN LAMINOPATHY-BASED PREMATURE AGING CELLS .....	
	118
Abstract .....	118
Introduction .....	119
Materials and Methods .....	120
Cell Cultures .....	120
Immunofluorescence Microscopy .....	120
Western Blotting .....	121
$\gamma$ -H2AX Association Assay and Co-Immunoprecipitation .....	121
Comet Assay .....	122
Results .....	122
Accumulation of DSBs in HGPS Cells and RD Cells .....	122
Mislocalization of DSB Repair Proteins and Colocalization of XPA with DSBs .....	124
Persistence of XPA-localized DSBs .....	130
Effects of XPA Knockdown on DSB Repair in HGPS Cells .....	131
Discussion .....	133

Chapter	Page
References.....	137
6. SUMMARY AND CONCLUSIONS .....	140
COMPREHENSIVE REFERENCES .....	144
APPENDIX: ABBREVIATIONS .....	159
VITA.....	162

## LIST OF TABLES

Table	Page
2-1. RPA binding to Damaged/Undamaged ssDNA .....	42
2-2. Fluorescence Anisotropy Titration of RPA Binding to 5'F-30mer or 5'F-BPDE-30mer .....	46
2-3. Fluorescence Anisotropy Titration of RPA Binding to 5'F-9mer or F(M)-9mer .....	49
2-4. Fluorescence Titration of RPA Binding to BPDE-11mer or 5'F-11mer .....	51
3-1. Identification of Modified Lysines or Arginines in RPA and hyp-RPA .....	73
3-2. Identification of Peptides of RPA or hyp-RPA Digested by Chymotrypsin .....	80
3-3. Fluorescence Anisotropy Titration of RPA or hyp-RPA Binding to 5'F-8mer .....	85

## LIST OF FIGURES

Figure	Page
1-1. Four DNA Damage Response Reactions in Mammalian Cells .....	14
1-2. Scheme of the Global Genomic Repair (GGR) Pathway .....	17
1-3. Schematic Representation of DSB Repair Pathways .....	18
1-4. Components of the DNA Damage Checkpoints in Human Cells .....	20
1-5. Schematic Representation of RPA Structures .....	21
2-1. Structures of ssDNA Substrates Used in the Present Study .....	32
2-2. Binding of RPA to Different Sizes of ssDNA .....	38
2-3. Gel Filtration Analysis of RPA-ssDNA Binding .....	40
2-4. Fluorescence Spectroscopic Characterization of RPA Binding to Defined ssDNA .....	43
2-5. Fluorescence Anisotropy Titration of RPA	
Binding to 5'F-30mer or 5'F-BPDE-30mer .....	47
2-6. Typical Fluorescence Binding Isotherms for Short ssDNA Titrated with RPA .....	50
3-1. <i>in vitro</i> Phosphorylation of RPA by DNA-PK .....	71
3-2. Mass Spectrometric Analysis of Relative Reactivity of Lysines in	
RPA and hyp-RPA with NHS-biotin .....	74
3-3. MALDI-TOF Analysis of Arginine Modification in RPA and hyp-RPA with HPG .....	75
3-4. Measurements of the Intrinsic Fluorescence of	
Tryptophans of RPA and Its Mutants .....	77
3-5. Partial Proteolysis of RPA and hyp-RPA with Chymotrypsin .....	81
3-6. Bindings of RPA and hyp-RPA to Oligo(dT) <sub>8</sub> and Partial DNA Duplexes .....	83
3-7. DBD-B Structure with Highlighted Residues .....	87
4-1. Early Replication Arrest of HGPS and RD Cells .....	101
4-2. Activation of ATM and ATR in HGPS and RD Cells .....	104

Figure	Page
4-3. Phosphorylation of Chk1, Chk2, and p53 in HGPS and RD Cells .....	105
4-4. Restoration of Replication Activity in HGPS Cells by Inactivation of ATM and ATR .....	107
4-5. FTI Treatment of HGPS and RD Cells .....	110
5-1. Prelamin A and DSB Accumulation in BJ, HGPS and RD Fibroblasts .....	123
5-2. Colocalization of $\gamma$ -H2AX Foci and the foci of DNA repair Proteins in BJ, HGPS and RD Fibroblasts .....	125
5-3. Specificity of Human XPA Antibodies Used in this Study.....	126
5-4. Chromatin-mediated XPA- $\gamma$ -H2AX Interaction .....	128
5-5. Laminopathy-induced DSBs Are Unrepairable .....	129
5-6. DSB Repair in HGPS Cells with XPA Knockdown by RNAi .....	133
5-7. The Localization of Rad51 Foci and $\gamma$ -H2AX Foci in HGPS Cells with or without XPA Knockdown .....	134

# CHAPTER 1

## INTRODUCTION

### DNA Damage and Cellular Responses

The genomic integrity of mammalian cells is constantly challenged by endogenous insults of metabolic byproducts such as reactive oxygen radicals as well as environmental factors such as chemical agents and ultraviolet (UV) radiation. Limits to the fidelity of DNA metabolism including replication, recombination, and repair also promote genomic instability. Damage to DNA elicits four types of cellular pathways, including DNA repair, DNA damage checkpoints, transcriptional response, and apoptosis (Figure 1-1), to either repair the DNA or eliminate cells with heavy damage (Sancar et al., 2004; Zhou and Elledge, 2000). Failure to correctly cope with DNA damage may cause accumulation of genomic rearrangements that promote tumorigenesis (Kolodner et al., 2002). It has been estimated that 80-90% of human cancers may partially result from DNA damage (Doll and Peto, 1981).

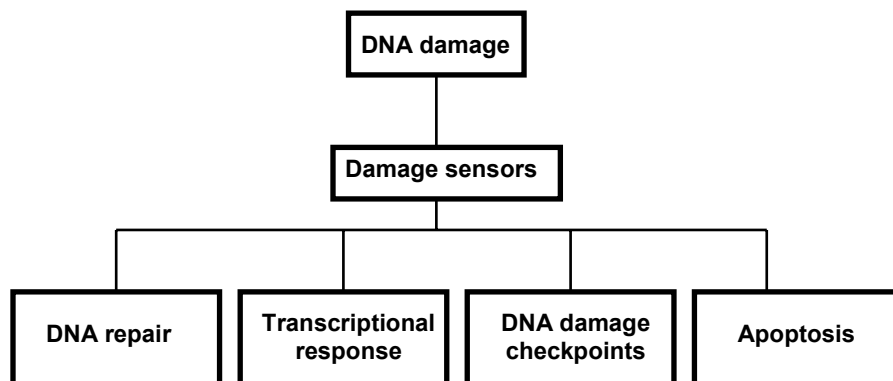


Figure 1-1. Four DNA damage response reactions in mammalian cells

Source: adapted from Sancar et al., 2004.

DNA can be damaged in a variety of ways, including base damage (reduced, oxidized, or fragmented bases), DNA backbone damage (abasic sites and single- or double-strand DNA breaks), and cross-links (DNA-protein cross-links and interstrand or intrastrand cross-links). There are six different types of DNA repair pathways including direct repair, base excision repair (BER), mismatch repair (MMR), nucleotide excision repair (NER), double-strand break (DSB) repair, and repair of interstrand cross-links. All these repair pathways have more than one subpathway to recognize and remove a specific type of DNA damage. Because my doctoral research focuses on NER and DSB repair, these two pathways will be introduced as follows.

### Nucleotide Excision Repair (NER)

NER is the major mechanism for removal of a variety of structurally and chemically unrelated bulky DNA lesions such as chemical adducts and the dimerized pyrimidine bases induced by UV radiation. Defects in NER cause diseases such as xeroderma pigmentosum (XP), Cockayne Syndrome (CS), and trichothiodystrophy (TTD) (Bootsma, 2002; Thoma and Vasquez, 2003). There are two major NER subpathways: global genomic repair (GGR) eliminates lesions from the entire genome, and transcription coupled repair (TCR) efficiently removes lesions from the transcribed strand of active genes. Both subpathways follow the same basic repair steps and require more than 25 proteins for DNA damage recognition, dual-incision, excision, repair synthesis, and ligation (Thoma and Vasquez, 2003). As depicted in Figure 1-2 (page 17), in GGR, DNA damage-induced helical distortion is recognized by the XPC-hHR23B (xeroderma pigmentosum group C-human homolog of RAD23B) complex, followed by recruitment of transcription factor IIIH (TFIIH). Xeroderma pigmentosum group A (XPA, a metalloprotein) and replication protein A (RPA, a eukaryotic single-stranded DNA binding



protein) arrive sequentially at the damage site and function in verifying the presence of DNA lesions. But how this verifying process is carried out and the exact spatial arrangement of the recognition factors at the damage site remain unknown. Endonuclease xeroderma pigmentosum group G (XPG) and the xeroderma pigmentosum group F-excision-repair cross-complementing group 1 (XPF-ERCC1) complex are responsible for the 3' and 5' DNA incisions, respectively. Binding of XPG induces the release of XPC-hHR23B, whereas XPF-ERCC1 triggers excision of the damaged DNA and the release of XPA and TFIIH. Subsequently, the newly formed gap in the DNA is filled by DNA polymerase  $\delta/\epsilon$ , replication factor C (RFC), proliferating cell nuclear antigen (PCNA), RPA and DNA ligase I (Park and Choi, 2006).

### Double Strand Break (DSB) Repair

Among the various forms of DNA damage that are inflicted by mutagens, DSB probably is the most dangerous lesion. DSBs can be caused by ionizing radiation, radio-mimetic chemicals, reactive oxygen species (ROS), and mechanical stress on chromosomes (Jackson, 2002). DSBs can also be the result of normal V(D)J recombination or abnormal replication fork arrest and collapse (Jackson, 2002; Sancar et al., 2004). Defects in DSB repair result in genomic instability and apoptosis at the cellular level, and lead to increased predisposition to cancer in animal models and in people. DSBs are repaired either by homologous recombination (HR) or nonhomologous end-joining (NHEJ) mechanisms (Figure 1-3, page 18).

HR is an accurate repair process that is carried out by the Rad52 epistasis group. The Mre11/Rad50/Xrs2 complex in budding yeast or the Mre11/Rad50/Nbs1 (MRN) complex in mammals resects the 5' ends of the DSB to generate 3' ssDNA overhangs. Rad51, RPA,

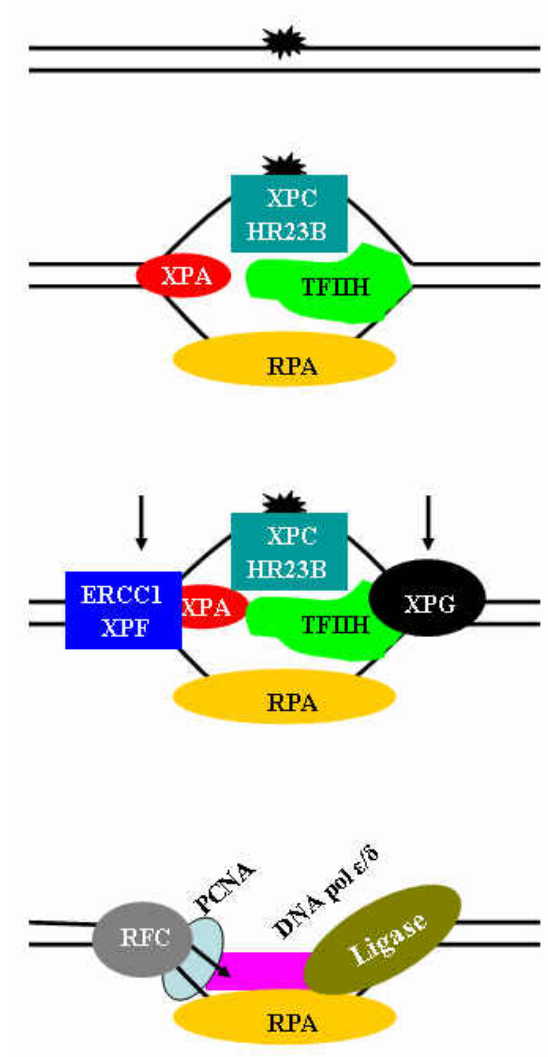
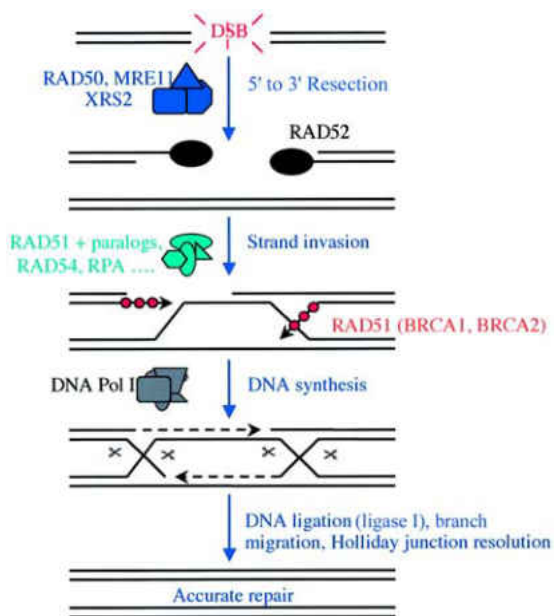


Figure 1-2. Scheme of the global genomic repair (GGR) pathway

The DNA damage such as UV-induced dimerized pyrimidines bases is recognized by the xeroderma pigmentosum protein C-human homolog of RAD23B (XPC-hHR23B) complex together with damage recognition factors xeroderma pigmentosum group A (XPA), replication protein A (RPA) and transcription factor IIIH (TFIIH). The damage site is then unwound by ~25 bp driven by ATR hydrolysis. The sequentially recruited endonucleases xeroderma pigmentosum group G (XPG) and xeroderma pigmentosum group F-excision-repair cross-complementing group 1 (XPF-ERCC1) complex are responsible for the 3' and 5' incisions, respectively. DNA polymerase  $\delta/\epsilon$ , replication factor C (RFC), proliferating cell nuclear antigen (PCNA), RPA and DNA ligase I fill the formed gap.

### Homologous recombination



### Nonhomologous end-joining

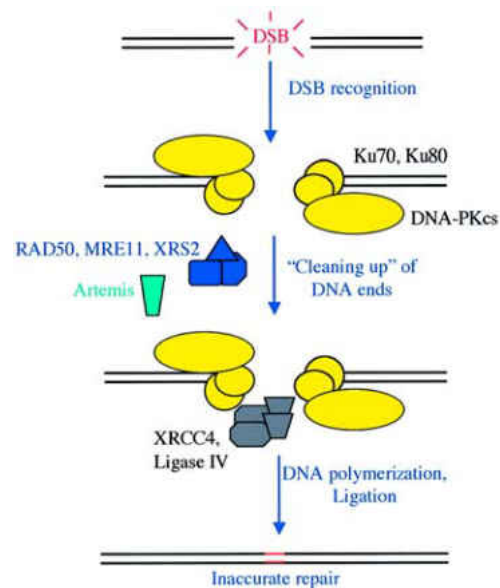


Figure 1-3. Schematic representation of DSB repair pathways

DSBs are repaired by either homologous recombination or nonhomologous end-joining. Source: adapted from Jackson, 2002.

Rad52 and Rad54 bind the resulting 3' ssDNA strands and form an  $\alpha$  helical nucleoprotein filament that facilitates the migration of the damaged DNA strand into the homologous double-strand DNA partner. DNA polymerase then extends the 3' ends of the damaged DNA and DNA ligase 1 ligates the ends, creating double Holliday junctions. After branch migration, the Holliday junctions are then cleaved and ligated (Binz et al., 2004; Jackson, 2002).

NHEJ rejoins the two broken ends directly. It generally leads to small deletions of DNA sequence. The first step of NHEJ is the binding of Ku 70/80 heterodimer to the double-stranded ends of the DSB. Ku then recruits the kinase DNA-dependent protein kinase catalytic subunit (DNA-PKcs). Some DSBs require processing by the Mrell/Rad50/Nbs1 (MRN) complex before ligation. Processing can also be carried out by other proteins including the Artemis complex (in

mammals) or Rad57 (yeast)/FEN-1 (mammals). The DNA-PK complex then recruits DNA ligase IV and x-ray repair cross-complementing protein 4 (XRCC4), and phosphorylates XRCC4. This is followed by DNA polymerization and ligation (Binz et al., 2004; Jackson, 2002).

### DNA Damage Checkpoints

In addition to the repair of DNA damage in response to genotoxic insults, cells also launch checkpoints to attenuate cell cycle progression and arrest replication, therefore preventing DNA lesions from being converted to inheritable mutations (Li and Zou, 2005; Sancar et al., 2004; Zhou and Elledge, 2000). The DNA damage checkpoint conceptually has four components: sensors, mediator, signal transducers, and effectors (Figure 1-4, page 20) (Sancar et al., 2004). Two protein kinases of the phosphoinositide 3-kinase-like kinase (PIKK) family, ATM and ATR, and the Rad9-Rad1-Hus1/Rad17-Rfc2-5 checkpoint complex play the central roles in initiating the checkpoints (Abraham, 2001; Li and Zou, 2005). ATM is activated primarily in response to DNA double-strand breaks (DSBs) (Shiloh, 2003), whereas ATR is activated by a broad array of DNA damage and replication interference (Abraham, 2001; Li and Zou, 2005). Upon activation, with the aid of mediator such as claspin, BRCA1, 53BP, or MDC1, ATM and ATR phosphorylate two major signal-transducing kinases Chk1 and Chk2, which in turn regulate downstream targets, such as Cdc25A, Cdc25C, and p53, to control cell cycle progression and DNA synthesis (Li and Zou, 2005; Sancar et al., 2004).

### Replication Protein A (RPA) and Hyperphosphorylation

RPA is a heterotrimer consisting of RPA70, RPA32, and RPA14, named after their molecular masses of 70, 32, and 14 kDa, respectively. RPA was originally defined as a

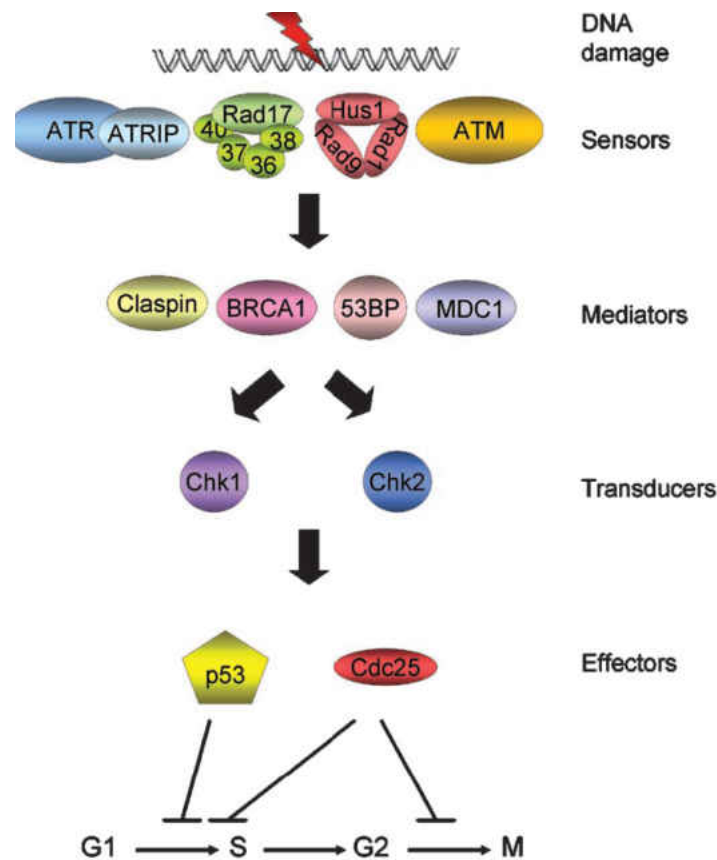


Figure 1-4. Components of the DNA damage checkpoints in human cells

The signal of DNA damage is transduced from sensors to transducers with the aid of mediators. The transducers activate or inactivate effectors to inhibit the G1/S transition, S-phase progression, or the G2/M transition. Source: from Sancar et al., 2004.

eukaryotic single-stranded DNA binding protein essential for the *in vitro* replication of simian virus 40 (SV40) DNA. Subsequent extensive studies revealed that RPA is required for almost all cellular DNA metabolism such as DNA replication, recombination, DNA damage checkpoints, and all major types of DNA repair including nucleotide excision, base excision, mismatch, and double-strand break repairs. RPA participates in such diverse pathways through its ability to interact with DNA and numerous proteins involved in these processes (Zou et al., 2006).

## RPA Structure and Interactions with ssDNA

Structurally, the heterotrimer RPA contains four DNA binding domains (DBDs) (Figure 1-5). The DBD is built around a central OB-fold (oligo-saccharide/oligonucleotide binding fold) (Bochkarev et al., 1999; Bochkarev et al., 1997; Bochkareva et al., 2001; Bochkareva et al., 2002; Jacobs et al., 1999), which consists of five  $\beta$ -strands in a Greek-key  $\beta$ -barrel and is found in many single-stranded DNA-binding proteins (Murzin, 1993). RPA70 can be divided into 4

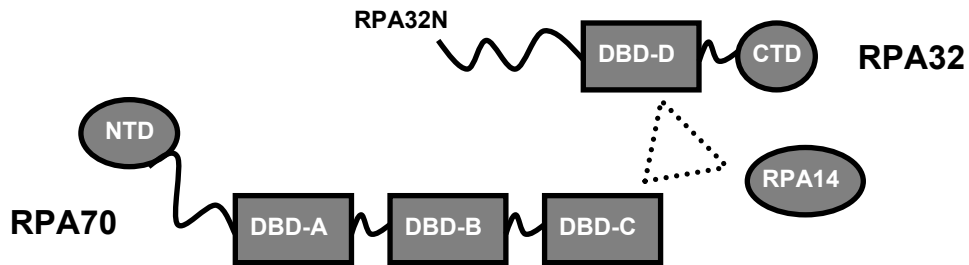


Figure 1-5. Schematic representation of RPA structures

The four DBDs (DNA binding domains) are presented as boxes. NTD stands for the N-terminal domain of RPA70, and CTD for the C-terminal domain of RPA32.

distinguishable regions, the N-terminal domain (RPA70N), DBD-A, -B, and -C, each having one OB-fold (Bochkarev et al., 1997; Brill and Bastin-Shanower, 1998; Iftode et al., 1999; Jacobs et al., 1999; Wold, 1997). The tandem DBD-A and DBD-B harbor the major ssDNA binding activity of RPA trimer (Arunkumar et al., 2003; Bastin-Shanower and Brill, 2001; Iftode et al., 1999; Wold, 1997). RPA32 consists of three domains, including an unstructured N-terminal phosphorylation domain (RPA32N), a central DNA-binding domain (DBD-D), and a C-terminal domain (RPA32C) largely involved in protein-protein interactions (Bochkarev et al., 1999; Bochkareva et al., 1998; Mer et al., 2000). RPA14 has a single OB-fold referred as DBD-E,

which is structurally important for the formation of RPA trimerization core (Bochkarev et al., 1999; Bochkareva et al., 2002), but no DNA binding activity was found for this domain.

The binding of RPA to ssDNA has been suggested to occur through a multi-step pathway (Bochkareva et al., 2002; Iftode et al., 1999). The binding is initiated by an interaction of the DBD-AB domains with a length of 8–10 nucleotides (nt) of the ssDNA (Bochkareva et al., 2002). Then, a significant conformational change of the protein allows ssDNA binding between 13 and 22 nt with the DBD-C domain additionally involved (Bastin-Shanower and Brill, 2001; Kolpashchikov et al., 1999). Finally, co-operative binding of RPA with all the four DBDs occurs, which involves a region of 30 nt (Bochkareva et al., 2002). It is now generally accepted that RPA needs an occluded size of approximately 30 nt for a minimum full and high-affinity binding (Blackwell and Borowiec, 1994; Iftode et al., 1999; Kim et al., 1992; Wold, 1997).

### RPA Hyperphosphorylation

It has been well reported that the unstructured N-terminal domain (residues 1-42) of RPA32 (RPA32N) becomes phosphorylated during the normal cell cycle (Din et al., 1990; Dutta and Stillman, 1992; Oakley et al., 2003) and hyperphosphorylated in response to DNA damage (Binz et al., 2004; Block et al., 2004; Cruet-Hennequart et al., 2006; Liu and Weaver, 1993; Sakasai et al., 2006; Zernik-Kobak et al., 1997). There are nine serines/threonines located in RPA32N. It remains unknown how many and which of these sites are concurrently phosphorylated on a single RPA molecule upon DNA damage. Phospho-peptide mapping has shown that at least five sites of RPA32N including Thr-21, Ser-23, Ser-29, Ser-33, and either Ser-11, -12, or -13, and probably two additional sites, Ser-4 and Ser-8, can be phosphorylated in UV-irradiated HeLa cells (Niu et al., 1997; Nuss et al., 2005; Zernik-Kobak et al., 1997). The

DNA damage-induced hyperphosphorylation of RPA32 is believed to be carried out by PI-3 kinases DNA-PK, ATM, and ATR (Barr et al., 2003; Binz et al., 2004; Block et al., 2004; Brush et al., 1994; Cruet-Hennequart et al., 2006; Iftode et al., 1999; Liu et al., 2006a; Pan et al., 1994; Sakasai et al., 2006; Shao et al., 1999). But the relative contribution of these kinases to RPA hyperphosphorylation and the potential different roles of the hyperphosphorylation by these kinases have not been defined.

Besides phosphorylatable sites in RPA32N, efficient phosphorylation of Thr-98 in DBD-D of RPA32 has been recently demonstrated by Nuss et al. (Nuss et al., 2005). In addition, like yeast RPA70 that can be phosphorylated (Brush et al., 1996; Clifford et al., 2004; Kim and Brill, 2003), phosphorylation of human RPA70 also has been detected *in vitro* and *in vivo* (Liu et al., 2006a; Nuss et al., 2005). There are no reports of phosphorylation of RPA14.

RPA is extensively involved in many DNA metabolic pathways by interacting with DNA and/or a large variety of proteins. Although how hyperphosphorylation alters the activities of RPA in these cellular reactions remains largely unknown, several recent studies began to reveal effects of hyperphosphorylation on RPA-DNA and RPA-protein interactions (Binz et al., 2004; Block et al., 2004; Iftode et al., 1999; Liu and Weaver, 1993; Zernik-Kobak et al., 1997; Zou et al., 2006). A recent review on RPA phosphorylation by Binz et al. (Binz et al., 2004) has suggested that hyperphosphorylation may make RPA less active in DNA replication and help the transition of RPA from replication to DNA damage response including DNA repair. However, how this occurs and the potential structural changes of RPA after hyperphosphorylation remain unknown.



## DNA Repair Defects in Laminopathy-Based Premature Aging

Recent studies showed that DNA damage accumulation and DNA damage responses resulting from repair defects can cause phenotypes reminiscent of premature ageing and may have causal roles in normal aging (Lombard et al., 2005). These DNA repair defects are usually caused by mutations in genes encoding DNA repair proteins (Karanjawala and Lieber, 2004; Lombard et al., 2005). Two premature aging diseases caused by defective maturation of lamin A have been recently found to involve DNA repair defects (Liu et al., 2005a; Varela et al., 2005). Lamin A is a component of nuclear lamina that functions to structurally support the nucleus and organize chromatin (Goldman et al., 2002). One of the diseases is Hutchinson-Gilford progeria syndrome (HGPS), which is rare (1 in 4 million children) and uniformly fatal. HGPS is characterized by retarded growth, partial lipodystrophy, osteoporosis, osteolytic lesions, thin skin, micrognathia, and premature atherosclerosis (Eriksson et al., 2003). All patients die as a consequence of myocardial infarction or cerebrovascular accident at an average age of 12 years (range from 8 to 21 years) (Capell et al., 2005). The defective maturation of Lamin A from its precursor, prelamin A, in HGPS is caused by a *de novo* point mutation (1824C → T) in the *LMNA* gene (De Sandre-Giovannoli et al., 2003; Eriksson et al., 2003). This mutation results in a deletion of 50 amino acids near the C terminus of prelamin A including an endoprotease (Zmpste 24) cleavage site required for the proteolytic maturation of lamin A (Eriksson et al., 2003). The consequence of this mutation is the accumulation of a truncated prelamin A, progerin, in the patient cells. Another premature aging disease is restrictive dermopathy (RD). RD is neonatally lethal, characterized by retarded growth, tight and rigid skin, alopecia, micrognathia, and other bone abnormalities (Navarro et al., 2005). The defective maturation of lamin A in RD is caused by the deficiency of protease Zmpste 24, which results in the

accumulation of prelamin A in cells. HGPS and RD have been suggested to be manifestations of the same cellular problem to different degrees (Misteli and Scaffidi, 2005). Recent studies showed that the genomic integrity has been compromised and DNA repair is defective in human HGPS fibroblasts and *Zmpste24*-deficient mouse embryonic fibroblasts (MEFs) (Liu et al., 2005a) (Varela et al., 2005). Moreover, an active p53 signalling pathway exists in *Zmpste24*-deficient MEF (Varela et al., 2005). The question remaining to be answered is, why is DNA repair compromised in HGPS and RD cells when the defects are in the nuclear structural protein lamin A and no evidence of mutations were found in repair genes?

#### Questions to be Answered in the Studies

In NER, RPA together with XPA and XPC-hHR23B are believed to be the DNA damage recognition factors. It is widely accepted that the XPA-RPA complex functions in verifying the presence of DNA lesions following the initial damage recognition by the XPC-hHR23B complex in a double-checking mechanism (Evans et al., 1997; Missura et al., 2001; Sugawara et al., 1998; Thoma and Vasquez, 2003). But how the DNA lesions are verified and the exact spatial arrangement of the recognition factors at the damage site remain unknown. Controversial results have been shown regarding the relative binding affinities of RPA with damaged or undamaged ssDNA (Hey et al., 2001; Lao et al., 2000; Patrick and Turchi, 1999; Patrick and Turchi, 2001; Schweizer et al., 1999). The apparent inconsistency has resulted in the notion that RPA binds preferentially to either undamaged or damaged ssDNA strand or both strands of DNA duplex that have been disrupted by a lesion. To clarify this inconsistency, the binding of RPA to a battery of well-defined ssDNA substrates containing different adducts was systematically examined using noninvasive fluorescence spectroscopy. This work has been published in *Biochemical Journal* (2005, 385:519-526) (Liu et al., 2005c) and is presented here as Chapter 2.

Although RPA hyperphosphorylation has been observed for more than a decade, the effects of hyperphosphorylation on RPA-DNA and RPA-protein interactions are only beginning to be elucidated. One of the most challenging issues regarding the cellular role of RPA hyperphosphorylation is how the functions of RPA, mediated by its interactions with DNA and proteins, are modulated by hyperphosphorylation. There are two possible mechanisms by which the modulation can be achieved: (i) the recognition of the hyperphosphorylated domain of RPA by hyperphospho-binding proteins; and (ii) a hyperphosphorylation-induced structural transformation of RPA affecting RPA-DNA and RPA-protein interactions. The potential structural change of RPA upon hyperphosphorylation was probed using mass spectrometric protein footprinting, fluorescence spectroscopy, and limited proteolysis. The effect of hyperphosphorylation on RPA-ssDNA binding was also examined. This work has been published in *The Journal of Biological Chemistry* (2005, 280:32775-32783) (Liu et al., 2005b) and is presented here as Chapter 3.

Mutations in genes encoding proteins involved in DNA repair may result in defective DNA repair, leading to DNA damage accumulation and DNA damage responses that can cause phenotypes reminiscent of premature ageing and may have causal roles in normal aging (Karanjawala and Lieber, 2004; Lombard et al., 2005). However, HGPS and RD cells that show no mutations in DNA repair genes exhibit DSB accumulation, impairment of DNA repair, and activation of the p53-dependent stress signaling pathway (Liu et al., 2005a; Manju et al., 2006; Varela et al., 2005). This suggests that genome instability caused by HGPS and RD might contribute to premature aging. To find out whether DNA damage responses similar to those caused by deficient DNA repair proteins exist in HGPS and RD, the activation of DNA damage checkpoints in the patient cells has been investigated. The results were summarized in a

manuscript “DNA Damage Responses in Progeroid Syndromes Arising from Defective Maturation of Prelamin A”, which has been accepted by Journal of Cell Science (in press) (Liu et al., 2006b). This work is present here as Chapter 4. Further studies were conducted to find out the causes of DNA repair defects in the patient cells. Using immunofluorescence microscopy and chromatin immunoprecipitation (ChIP) assay, we examined the localization of DNA repair proteins in relation to DSB sites. The results were summarized in a manuscript “Xeroderma Pigmentosum Group A (XPA) Inhibits Repair of DNA Double-Strand Breaks in Laminopathy-Based Premature Aging Cells” and submitted to Journal of Cell Science. The manuscript is currently under the process of review. This work is presented here as Chapter 5.

## CHAPTER 2

### INTERACTIONS OF HUMAN REPLICATION PROTEIN A WITH SINGLE-STRANDED DNA ADDUCTS

#### Abstract

Human replication protein A (hRPA), a single-stranded DNA-binding protein, is required for many cellular pathways including DNA repair, recombination, and replication. However, the role of RPA in nucleotide excision repair remains elusive. In the present study, we have systematically examined the binding of RPA to a battery of well-defined ssDNA (single-stranded DNA) substrates using fluorescence spectroscopy. These substrates contain adducts of (6-4) photoproducts, *N*-acetyl-2-aminofluorene-, 1-aminopyrene-, BPDE (benzo[*a*]pyrene diol epoxide)- and fluorescein that are different in many aspects such as molecular structure and size, DNA disruption mode (e.g. base stacking or non-stacking), as well as chemical properties. Our results showed that RPA has a lower binding affinity for damaged ssDNA than for non-damaged ssDNA and that the affinity of RPA for damaged ssDNA depends on the type of adduct. Interestingly, the bulkier lesions have a greater effect. With a fluorescent base-stacking bulky adduct, (+)-*cis*-anti-BPDE-dG, we demonstrated that on binding of RPA the fluorescence of BPDE-ssDNA was significantly enhanced by up to 8 to 9 folds. This indicated that the stacking between the BPDE adduct and its neighbouring ssDNA bases had been disrupted and there was a lack of substantial direct contacts between the protein residues and the lesion itself. For RPA interaction with short damaged ssDNA, we propose that on RPA binding the modified base of

ssDNA is looped out from the surface of the protein, permitting proper contacts of RPA with the remaining unmodified bases.

### Introduction

Human RPA (replication protein A) is a heterotrimeric protein consisting of three subunits of 70, 32, and 14 kDa [1]. RPA plays an indispensable role in replication, NER (nucleotide excision repair) and homologous recombination of DNA [1, 2]. The main activity of RPA is to bind to ssDNA (single-stranded DNA) during DNA metabolism, while RPA also binds to dsDNA with a much lower affinity. The association constant  $K_a$  for RPA–ssDNA interaction is in the range of  $10^8$ – $10^{11}$  M<sup>-1</sup> depending on the sequence and length of the ssDNA, the method of analysis and the experimental conditions [2-4]. The affinity of RPA for pyrimidine residues is approximately 50-fold higher than that for purine residues [5]. Structural studies revealed that RPA contains four DBDs (DNA-binding domains). Three of them (DBD-A, -B, and -C) are located in RPA70 in tandem with DBD-A and -B in the central region and DBD-C in the C-terminal region [6]. The fourth DBD resides in the central region of RPA32, referred to as DBD-D [7, 8]. The binding of RPA to ssDNA has been suggested to occur through a multi-step pathway [2, 7]. The binding is initiated by an interaction of the DBD-AB domains with a length of 8–10 nt of the ssDNA [7]. Then, a significant conformational change of the protein allows ssDNA binding between 13 and 22 nt with the DBD-C domain additionally involved [8, 9]. Finally, co-operative binding of RPA with all the four DBDs occurs, which involves a region of 30 nt [7]. It is now generally accepted that RPA needs an occluded size of approximately 30 nt for a minimum full and high-affinity binding [1, 2, 5, 10].

RPA has been suggested to be involved in DNA damage recognition of NER owing to its preference for the damaged DNA relative to undamaged DNA [11-20], although the specific role of RPA in the mechanism is not clear in recent studies [21-26]. Efforts have been made to understand the origin of the recognition and thus the functions of RPA in NER. It has been shown that RPA binds more efficiently to the undamaged ssDNA than to cisplatin-modified ssDNA [13, 16, 27]. In contrast, the affinity of RPA for UV-damaged ssDNA was up to 60-fold higher compared with that for undamaged ssDNA [12, 28]. These apparently inconsistent results have resulted in the unclear notions that RPA binds preferentially to either undamaged ssDNA or damaged ssDNA or both strands of DNA duplex that have been disrupted by the lesion. It has been noted that different methods and adducts were used in these investigations. More importantly, in most of these studies, the ssDNA substrates used were much longer than 30 nt, the occluded binding size of RPA. Use of such long ssDNA substrates appeared to be problematic due to the multiple binding sites available in a single ssDNA molecule and thus to the co-operative binding of RPA molecules to ssDNA. In addition, how RPA interacts with the adduct molecule itself in ssDNA remains unknown. Therefore, to address the controversy and to understand better the mechanism of RPA–ssDNA adduct interactions, a systematic study of RPA binding with well-defined damaged and undamaged ssDNA under strict conditions is necessary.

In the present study, we have systematically examined the interactions of human RPA with a series of modified and unmodified ssDNA substrates with a single protein-binding site (protein/ssDNA stoichiometry = 1) using the rigorous method of fluorescence anisotropy. These substrates contain adducts that are different in molecular size and structure, DNA-interacting structure (e.g. intercalating or non-intercalating), as well as chemical properties. Our results showed that RPA has no binding preference for damaged ssDNA over undamaged ssDNA.

Instead, RPA has lower binding affinities for damaged ssDNA than for undamaged ssDNA, and the extent of decrease in binding depends on the type of adduct. Also using BPDE (benzo[*a*]pyrene diol epoxide) as both a DNA adduct and a fluorescent DNA base-interaction and stacking sensor, we have analysed the nature of adduct due to binding of RPA. The results demonstrated that the interactions of the BPDE lesion with neighbouring bases were largely disrupted as a result of the protein binding. However, the results also suggested that there were no obvious direct interactions between the protein residues and the lesion itself.

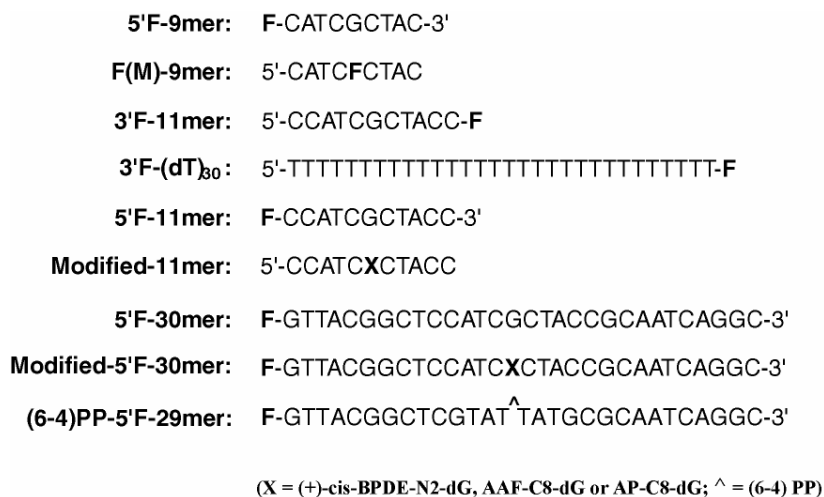
## Materials and Methods

### DNA Substrate Preparation

Oligodeoxynucleotides with or without fluorescein modification (except 30mers) were purchased from Qiagen (Alameda, CA, U.S.A.) in HPLC-purified quality. The 5'-fluorescein-labelled 30mer substrates with or without adduct were constructed by ligating the 5'-phosphorylated 11mer (with or without an adduct; Figure 2-1, page 32) with the 5'-fluorescein-labelled 9mer and 5'-phosphorylated 10mer, using T4 DNA ligase. The sequences of oligodeoxynucleotides used in the constructions are as follows: 9mer (GTTACGGCT); 11mer [CCATCXCTACC, X=G or (+)-*cis*-BPDE-*N*<sup>2</sup>-dG or C8-AAF-dG or C8-AP-dG; here, AAF stands for *N*-acetyl-2-acetylaminofluorene, AP for 1-aminopyrene, C8-AAF-dG for *N*-(deoxyguanosin-8-yl)-AAF, and C8-AP-dG for *N*-(deoxyguanosin-8-yl)-AP]; and 10mer (GCAATCAGGC). The adducted 11mer was synthesized by Dr. Nicholas E. Geacintov (New York University, New York, New York) and Dr. Ashis K. Basu (University of Connecticut, Storrs, Connecticut). The 5'-fluorescein-labelled 9mers (100 pmol) were incubated with



**A**



**B**

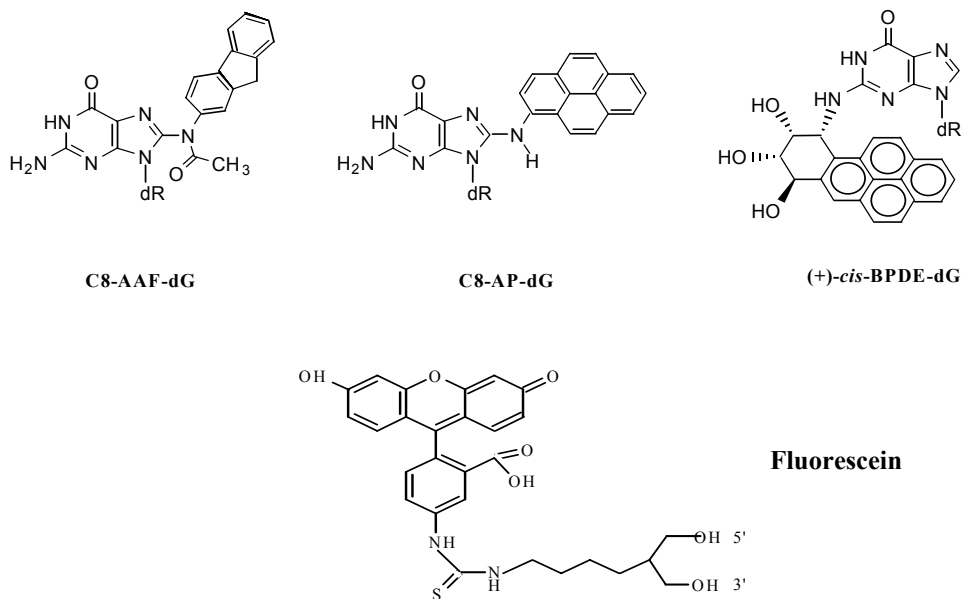


Figure 2-1. Structures of ssDNA substrates used in the present study  
(A) Schematic of ssDNA containing various modifications. F in the sequences stands for a fluorescein modification attached through a C5-linker to the 5' - or 3' -end of the respective ssDNA. X in the sequences represents the single adducted nucleotide. (B) Structures of specific DNA adducts.

equal moles of the phosphorylated 11mer (with or without an adduct) and 10mer in the presence of a 44mer template strand containing the complementary sequence (GATCTGGCCTGATTGCGGTAGCGATGGAGCCGTAACAGTACGTA) in 100 ml of ligation buffer containing 50 mM Tris/HCl (pH 7.8), 10 mM MgCl<sub>2</sub>, 10 mM dithiothreitol, 1 mM ATP and 50 mg/ml BSA. The mixture was brought to 85 °C for 5 min and then slowly cooled down to room temperature (25 °C) and finally to 16 °C, followed by the addition of 1 unit of T4 DNA ligase. The ligation was performed at 16 °C for 12 h. The sample was then reheated at 85 °C for 5 min with 8 M urea, followed by rapidly chilling on ice and then purified on a 12% (w/v) polyacrylamide sequencing gel under denaturing conditions. Using the 5'-<sup>32</sup>P-labelled 30mer and 44mer as controls, the band identified as 30mer which migrated much faster than the 44mer in the gel was excised, eluted, and precipitated with ethanol. For construction of the 29mer with or without a (6-4)PP [(6-4)-photoproduct] adduct, the same procedures were performed, except that the 11mer was substituted with the 10mer [CGTAT<sup>Δ</sup>TATGC, T<sup>Δ</sup>T=(6-4)PP] and a complementary 35mer (TGGCCTGATTGCGCATAATACGAGCCGTAACAGTA) was used for the ligation. The single-stranded nature of the constructed substrates was further confirmed by the ssDNA nuclease assays with S1 enzyme. All the substrates used in the fluorescence and anisotropy measurements are depicted in Figure 2-1 (page 32).

### RPA Preparation

Recombinant human RPA was expressed in *Escherichia coli* BL21(DE3)-RP cells and purified as described previously [29]. The concentration of RPA protein was determined using Bio-Rad Protein Assay kit.

### Gel Mobility-Shift Assays

Oligonucleotides poly(dT)<sub>8</sub>, poly(dT)<sub>30</sub>, poly(dT)<sub>40</sub>, and poly(dT)<sub>50</sub> were radiolabelled with [ $\gamma$ -<sup>32</sup>P]ATP and polynucleotide kinase. The substrate (5 nM) was incubated with the indicated amounts of RPA at 25 °C for 15 min in 20 ml of the binding buffer (40 mM HEPES–KOH, pH 7.9, 75 mM KCl, 8 mM MgCl<sub>2</sub>, 1 mM dithiothreitol, 5% (v/v) glycerol, and 100 mg/ml BSA). After incubation, 2 ml of 80% glycerol was added, and the mixture was immediately loaded on to a 3.5% native polyacrylamide gel in TBE running buffer (89 mM Tris/borate, pH 8.3, and 2 M EDTA) and electrophoresed at room temperature.

### Gel-Filtration Analysis and Scintillation Counting

Gel-filtration assay was performed on an HR 10/30 Superdex 200 column with an AKTApurifier system (Amersham Biosciences, Uppsala, Sweden) followed by scintillation counting. Poly(dT)<sub>8</sub> and poly(dT)<sub>40</sub> were radiolabelled with [ $\gamma$ -<sup>32</sup>P]ATP. Binding of RPA to these substrates was conducted the same way as in the gel mobility-shift assays, except that it was performed in a larger volume of 100 ml. After incubation at 25 °C for 15 min, the reaction mixture was loaded on to the column equilibrated with the same binding buffer. Fractions of 0.5 ml were collected at 0.5 ml/min, with the radioactivity of each fraction counted using a liquidscintillation counter. The column was calibrated with the following molecular-mass standards: RNase A, 13.7 kDa; chymotrypsinogen A, 25 kDa; ovalbumin, 43 kDa; bovine albumin, 67 kDa; aldolase, 158 kDa; catalase, 232 kDa; ferritin, 440 kDa; and thyroglobulin, 669 kDa.

### Fluorescence Measurement of the Binding of RPA to ssDNA with a BPDE Adduct

Measurements of the fluorescence emission spectra and the fluorescence titration were performed as described previously [30]. Fluorescence of the BPDE-ssDNA substrates was recorded at 25 °C on a SPEX Fluorolog-3 fluorimeter (Jobin Yvon, Edison, NJ, U.S.A.) with the excitation wavelength set at 350 nm, the slit width set at 5 nm for both excitation and emission beams and the integration time set at 0.5 second. Not more than 5% photobleaching was observed under these conditions. For titration, analysis was performed by measuring the emission at 380 nm with excitation at 350 nm. After sample equilibration, three data points with an integration time of 5 seconds and S.E.M. of 0.5% were collected for each titration point. RPA and the DNA substrates were placed in the same binding buffer before the titration to eliminate any change of the background on the addition of protein. All titrations were performed in a micro-quartz cuvette (4 mm × 4 mm) for a minimum sample volume of 200 µl with a 2 mm×2 mm stirring bar. Each addition of RPA was 0.5–1 µl, delivered by a 25-µl Hamilton syringe using a Hamilton repeating dispenser.

### Fluorescence Anisotropy Measurements

Measurements of fluorescence anisotropy provide information about the rotational behaviour of molecules. On binding of the fluorescently labelled DNA probe to proteins, the fluorescence anisotropy of the probe increased, serving as an indicator of the complex formation [16]. In the present investigation, ssDNA with fluorescein labelling at the 5'-end was used to monitor the RPA-ssDNA binding. The reason for choosing 5'-modification instead of 3'-modification is that, with the ssDNA fluorescein-labelled at the 5'-end, the intensities and shapes of the fluorescence spectra observed before and after the addition of saturating RPA

concentrations showed virtually no changes; however, with 3'-labelling the total fluorescence intensity decreased by approximately 30% upon binding.

The anisotropy titrations were performed on a SPEX Fluorolog-3 fluorimeter with automated polarizers at an excitation wavelength of 492 nm and monitored at an emission wavelength of 520 nm using a 500-nm cutoff filter with the slit width set at 14 nm for both excitation and emission beams for reliable signals. Other titrations were performed with the same procedure as described in the above fluorescence titrations of BPDE-DNA substrates.

### Data Processing

Three measurements of fluorescence titration or anisotropy titration for each sample were performed independently. The obtained data were expressed as mean value with standard deviation. The data were then processed to determine the equilibrium dissociation constant ( $K_{d,obs}$ ) or binding constant ( $K_{obs}$ ) using a one-site binding model and the non-linear least-squares method as described below [30].

For the equilibrium interaction of protein with DNA substrate:



For the spectroscopic titration, we have:

$$\Delta I = k[D]_t K [P] / (1 + K [P]) \quad [2]$$

where  $\Delta I$  represents fluorescence intensity change or anisotropy change,  $k$  is the proportional constant, and  $[D]_t$  stands for the total concentration of DNA, which is known.

From equation [1], it can be derived that:

$$K = [PD] / ([D]_t - [PD])([P]_t - [PD]) \quad [3]$$

where  $[P]_t$  is the total concentration of protein. Therefore, if the binding constant is known, the equilibrium free concentrations of RPA or DNA-bound RPA in the solution at all titration points can be determined by the following expression:

$$[PD] = (-b \pm (b^2 - 4ac)^{1/2}) / 2a \quad [4]$$

where  $a = K$ ,  $b = -K([D]_t + [P]_t) - 1$ , and  $c = K[D]_t[P]_t$ .

To obtain the binding constant  $K$  from the best fits of equation [2] to the data, an iteration process was established with [2] and [4] in the following fashion. (a) An initial estimated  $K$  was used in equation [4] to obtain the equilibrium free concentration of protein ( $[P] = [P]_t - [PD]$ ) corresponding to each experimental  $[P]_t$ . (b) The determined free protein concentration was then applied in equation [2] to calculate the new  $K$  and  $k$  by a non-linear least-squares fit. (c) Steps (a) and (b) were repeated with the newly determined protein free concentrations until the iteration process led to a convergence where the values of the equilibrium binding constant and protein free concentrations were no longer changed within the error limit ( $10^{-5}$ ).

## Results

### Stoichiometry of RPA Binding to Different Sizes of ssDNA

RPA needs an occluded binding site of approximately 30 nt for a full and high-affinity binding [1, 2]. However, two different modes of complexes of RPA may occur depending on the experimental conditions [10]. To select ssDNA substrates with a binding stoichiometry of one for the present study, we have performed gel mobility-shift assays of RPA with various sizes of ssDNA. As shown in Figure 2-2 (page 38), of the substrates poly(dT)<sub>8</sub>, poly(dT)<sub>30</sub>, poly(dT)<sub>40</sub>, and poly(dT)<sub>50</sub>, a single shifted band was observed with (dT)<sub>8</sub> (not shown) and (dT)<sub>30</sub> even in the presence of excess protein, suggesting a single RPA binding. In contrast, an additional slower

eluting band appeared with (dT)<sub>40</sub> and (dT)<sub>50</sub> as the concentration of RPA was increased to 25 nM, implying that multiple complexes may form with these longer oligonucleotides. This is not in agreement with the previous report by Kim et al. [5] who noted only one shifting band for

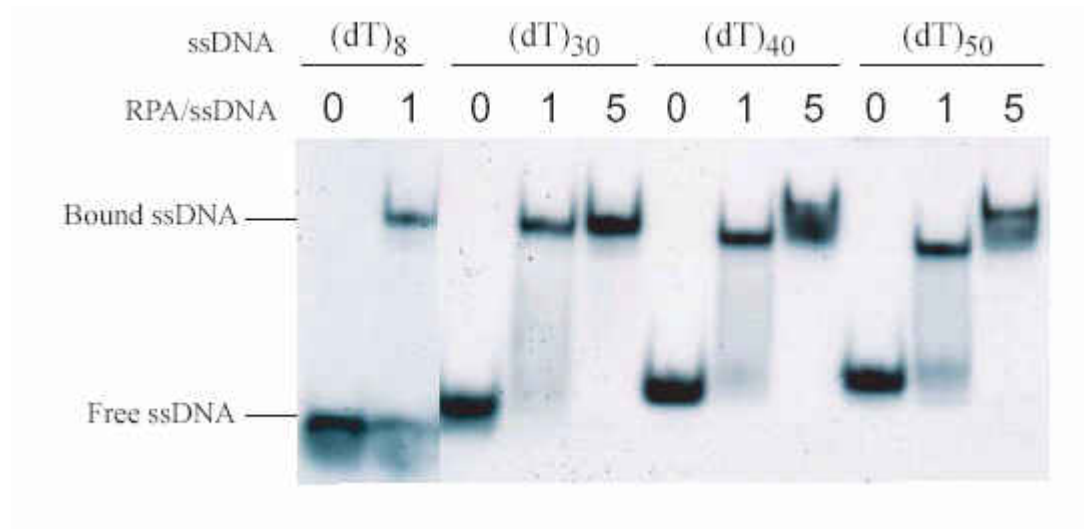


Figure 2-2. Binding of RPA to different sizes of ssDNA

RPA was incubated with 5 nM poly(dT)<sub>8</sub>, poly(dT)<sub>30</sub>, poly(dT)<sub>40</sub>, or poly(dT)<sub>50</sub> at different molar ratios (0, 1, and 5) at 25 °C for 15 minutes in 20 μL of the binding buffer. The binding products were analyzed on a 3.5% native polyacrylamide gel. The positions of RPA-ssDNA complexes and free oligonucleotides are indicated.

the RPA binding to (dT)<sub>50</sub>, although this may be the result of different conditions used in their assays. It is also worth noting that the electrophoretic mobility of the RPA-ssDNA complex increased as the length of the ssDNA increased from 8 to 40 nt, which was also noted in an earlier study [10]. Although the conformational change of the complex might affect the mobility [10], a more reasonable explanation could be that the ratio of the negative charges to the molecular mass (kDa) of the complex (charge/mass) influenced the mobility as a function of the

length of ssDNA. These ratios are consistent with the migration pattern observed with a single bound RPA.

To define the nature and stoichiometry of these complexes, a gel-filtration assay followed by scintillation counting was performed to determine the molecular masses of the complexes formed between radiolabelled (dT)<sub>8</sub> or (dT)<sub>40</sub> and RPA at different concentrations. Figure 2-3A (page 40) shows the elution profile of the RPA–DNA binding reaction mixtures, in which the two major peaks represent two types of DNA–protein complexes. When 10 times more RPA (in molar ratio) was incubated with (dT)<sub>8</sub>, a single peak appeared at 11.5 ml, which was also the retention volume for the RPA–(dT)<sub>40</sub> complex at a protein/DNA ratio of 1:1. The low peak intensity for (dT)<sub>8</sub> was due to the less efficient <sup>32</sup>P-labelling and the much lower binding affinity of RPA for such short substrates compared with d(T)<sub>40</sub>. Calculations based on mass standards showed that the retention volume of 11.5 ml corresponds to a molecular mass of 130 kDa (Figure 2-3B, page 40), which is consistent with the binding of a single RPA molecule in both cases. In contrast, incubation of the protein with (dT)<sub>40</sub> in a 10:1 ratio resulted in an RPA–(dT)<sub>40</sub> complex with a retention volume of 10.0 ml, which corresponds to a molecular mass of 238 kDa. This is consistent with a double-bound complex (RPA/DNA=2). Therefore, the (dT)<sub>40</sub> ssDNA allows double bindings by RPA, whereas (dT)<sub>8</sub> permits only single binding and the complex has a molecular mass similar to the complex from RPA–(dT)<sub>40</sub> single binding. Most probably, the single binding also occurred for (dT)<sub>30</sub> ssDNA. Thus we conclude that a length of 30 nt is sufficient for the binding of one RPA molecule under our experimental conditions.



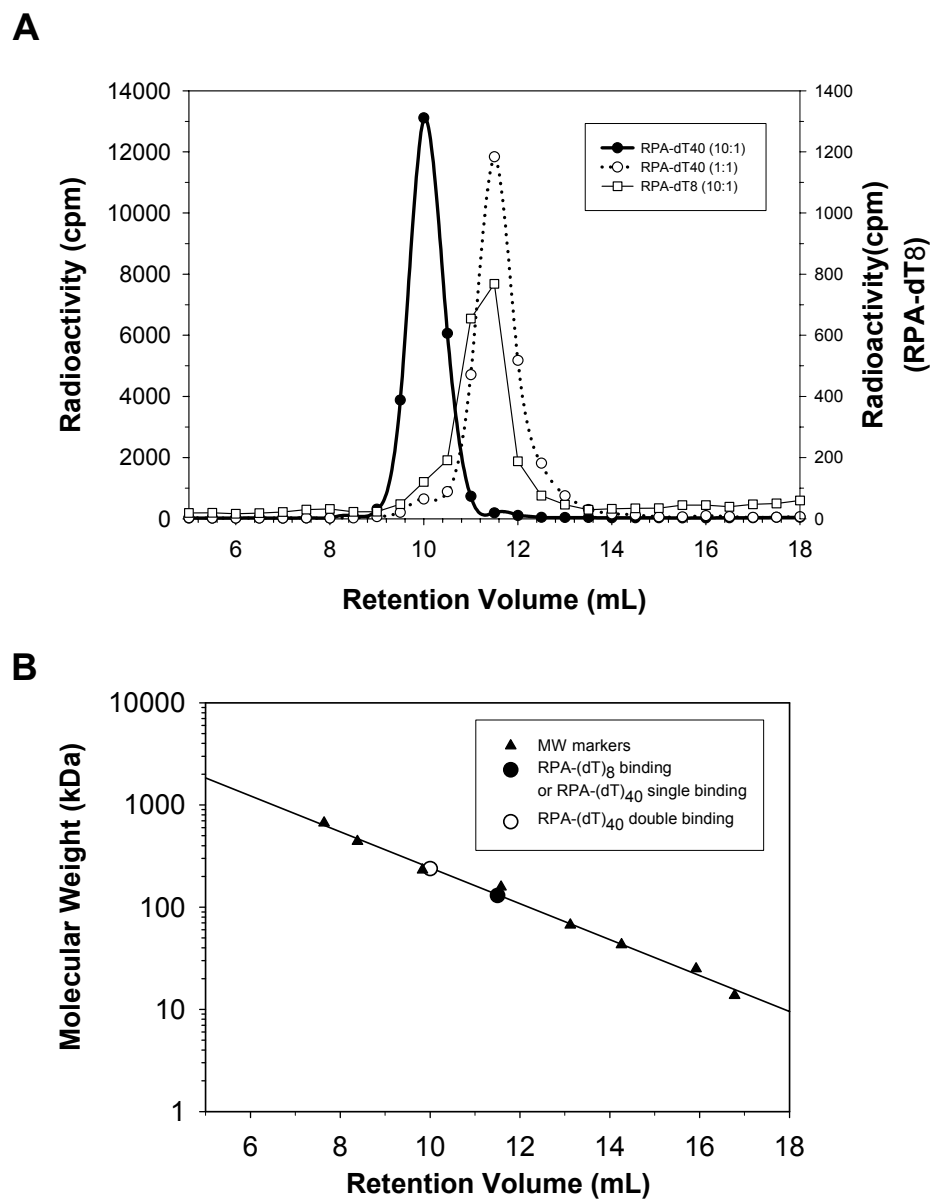


Figure 2-3. Gel filtration analysis of RPA-ssDNA binding

(A) Scintillation counting of RPA binding reactions with different sizes of ssDNA. The binding reactions of RPA with poly(dT)<sub>8</sub> and poly(dT)<sub>40</sub> at different molar ratios were constructed and gel-filtrated as described under Materials and Methods. (B) The apparent molecular masses of the RPA-ssDNA complexes were determined by gel filtration based on the relationship of the retention volumes of markers versus their molecular masses fitted with linear regression method.

## Fluorescence Spectroscopic Characterization of RPA Binding to Defined Substrates

Little is known about how RPA protein interacts with the adduct molecule of the damaged ssDNA. In the present study, we examined RPA binding to oligonucleotides containing a single BPDE lesion by monitoring the fluorescence of BPDE. Because aromatic amino acids are probably involved in the interactions of RPA with normal ssDNA through stacking with bases [4, 7, 31], it is of interest to determine how the pyrene-like residue of the BPDE-*N*<sup>2</sup>-dG adduct is affected. The fluorescence of this adduct is a very sensitive probe of its environment and we have previously used this in the study of a protein–DNA interaction system [30]. It is now known that the fluorescence of the pyrenyl residue of BPDE-*N*<sup>2</sup>-dG adducts in DNA is strongly quenched [32] by neighbouring T and C bases [33]. In DNA, the fluorescence of BPDE-*N*<sup>2</sup>-dG adducts is sensitive to the secondary structure, the aqueous solvent environment [32], and the adduct conformation [34]. Therefore, any disruption or weakening of the BPDE-base interactions may lead to an increase in the fluorescence of the adduct, providing evidence for structural alterations in the immediate environment of BPDE-*N*<sup>2</sup>-dG lesions. In ssDNA, significant BPDE–base stacking interactions are evident since the absorption spectrum of the pyrenyl residue is significantly red-shifted with an absorption maximum at approximately 352–354 nm [35]. When excited at 350 nm, the emission spectrum of the BPDE-adducted 11mer oligonucleotides (Figure 2-1, page 32) displays two fluorescence maxima, one at 384 nm and the other at 404 nm, consistent with previous observations [30, 36]. After binding to RPA, the  $\lambda_{\text{max}}$  at 384 nm blue-shifted to 380 nm, and the fluorescence intensity was enhanced by 8–9-fold (Figure 2-4A, page 43, and Table 2-1, page 42). This implies that, on binding of RPA, the interactions between the BPDE molecule and the neighbouring bases were lost due to a local conformational change in the ssDNA. This leads to diminished BPDE–nucleobase stacking interactions as indicated by a

significant blue shift in the fluorescence emission maxima and a large enhancement in the fluorescence yield. A (+)-*cis*-BPDE-30mer ssDNA substrate was also subjected to the same measurements. While similar results were observed, the fluorescence enhancement was not as large as with the BPDE-11mer (Table 2-1). It is probable that the BPDE molecule remained partially stacked in this case. Furthermore, these results suggested that no significant interactions between RPA residues and the BPDE molecule occurred. Otherwise, fluorescence quenching rather than enhancement would be observed upon RPA interaction.

In comparison, emission spectra for a non-stacking fluorescein, site-specifically adducted to the middle of a 9mer ssDNA, F(M)-9mer (Figure 2-1, page 32), were recorded with  $\lambda_{\text{ex}} = 492$  nm in the presence and absence of RPA (Figure 2-4B, page 43). No fluorescence variation was observed, indicating that fluorescence quenching interactions are absent from such adducts. Unlike the (+)-*cis*-BPDE-dG adduct, the fluorescein derivative is covalently attached to the nucleic acids of ssDNA through a long carbon linker.

Table 2-1. RPA binding to damaged / undamaged ssDNA

ssDNA	$K_{\text{d,obs}}$ (nM)	Fluorescence enhancement upon RPA binding (fold)
5'F-9mer	39.1 ± 4.5	
5'F-Abase(M)-9mer	43.0 ± 1.5	
F(M)-9mer	93.7 ± 6.2	
5'F-11mer	22.9 ± 2.6	
BPDE-11mer	146.0 ± 6.7	8 - 9
5'F-30mer	2.5 ± 0.4	
5'F-BPDE-30mer	11.8 ± 1.5	3
5'F-AAF-30mer	9.0 ± 1.9	
5'F-AP-30mer	16.5 ± 3.1	
5'F-(6-4) PP-29mer	6.1 ± 0.4	

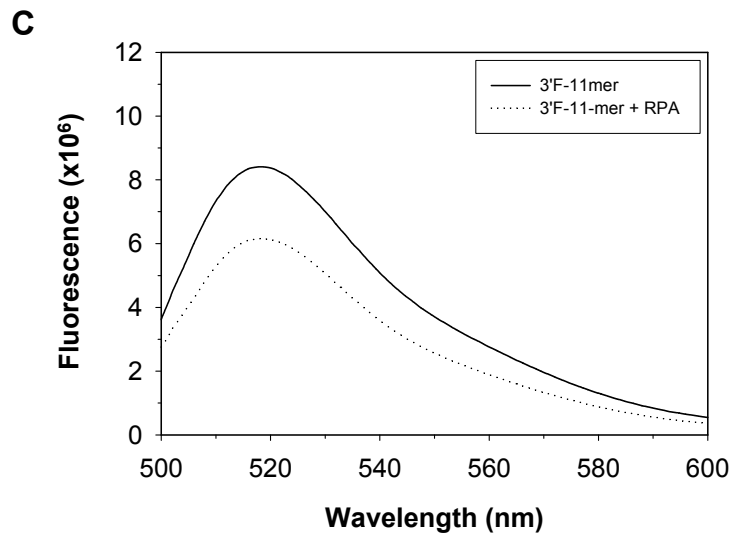
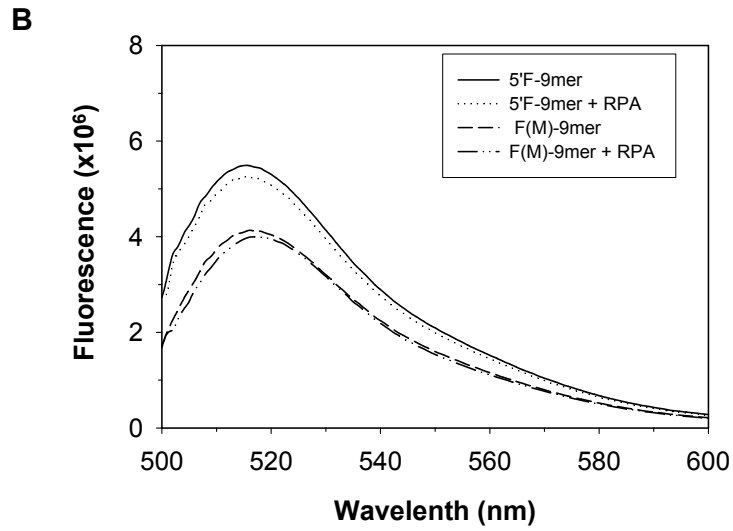
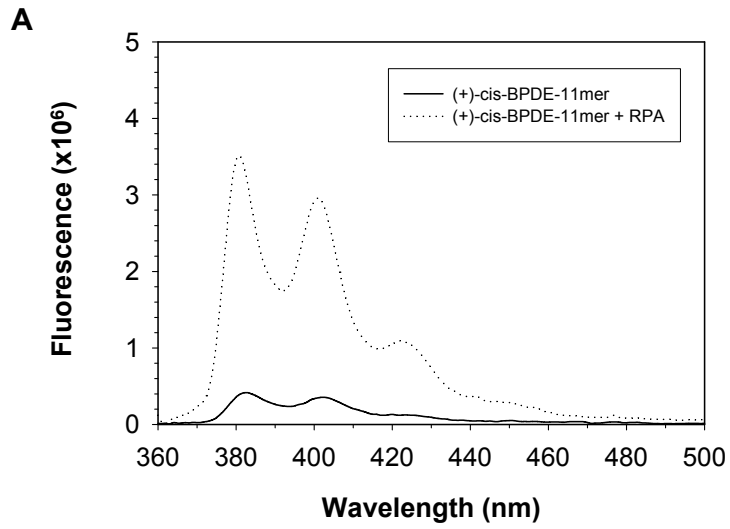


Figure 2-4. Fluorescence spectroscopic characterization of RPA binding to defined ssDNA (A) The emission spectra of (+)-*cis*-BPDE-11mer in the absence and presence of RPA were recorded with the excitation at 350 nm in 200  $\mu$ L of RPA binding buffer. (B) The fluorescence spectra of a 9mer with fluorescein modification in the middle of the sequence or at 5'-end in the absence and presence of RPA were recorded with the excitation at 492 nm in RPA binding buffer. (C) The fluorescence spectra of a 11mer with fluorescein labeling at 3'-end in the absence and presence of RPA were recorded as in (B). All the fluorescence measurement was presented in arbitrary units.

Additional structural information about the RPA–ssDNA interaction was obtained from fluorescence spectroscopic studies with a fluorescein labelled at either the 5' - or 3' -end ssDNA (Figures 2-4B and 2-4C, page 43). The fluorescence of the probe labelled at the 3' -end of ssDNA was quenched by approximately 30% on RPA–ssDNA complex formation, which was consistent with the results observed previously [16]. Interestingly, the binding of RPA to the ssDNA with the fluorescein labelled at the 5' -end led to no change in fluorescence, regardless of the length of the substrate. This implies that the 5' -terminus of ssDNA had no direct contact with RPA protein, while the 3' -end did.

#### RPA Binding to 5'F-30mer with or without (6-4)PP, BPDE, AAF, or AP Adduct

Experiments were conducted to assess the binding affinities of RPA with a series of damaged and undamaged ssDNAs of 9mer, 11mer, and 30mer nucleotides. Use of such short substrates eliminated the possibility of overlapping binding sites that are usually available with longer ssDNAs. In addition, for RPA interaction with damaged ssDNA, the protein may bind to the flanking undamaged DNA sequence of a lesion if the size of the substrate is too long and direct contact of RPA with the DNA lesion is thermodynamically unfavourable. Because a size

of approximately 30 nt is the minimum length of ssDNA required for RPA to have a full functional interaction with ssDNA, we first examined RPA binding to the 30mer ssDNAs containing different types of adduct using fluorescence spectroscopy. All the substrates were 5'-terminally labelled with fluorescein and used as substrates for fluorescence anisotropy measurements. The fluorescence intensity of fluorescein modified either at the 5'-end or in the middle of the sequence of ssDNA remained unaffected by RPA binding, indicating that there was no direct interaction of the protein with the fluorescein. This established the validity of the fluorescence anisotropy measurements. For the 3'-terminally labelled fluorescein, the fluorescence intensity changed due to RPA binding (Figure 2-4C, page 43). Therefore, the 3'-fluorescein is not suitable for use as a reporter for anisotropy measurements, although it was used previously for the determination of RPA-ssDNA interactions [16]. In addition, although the BPDE, AAF, and AP have intrinsic fluorescence when excited at appropriate wavelengths, emissions of these adducts occur at the wavelength range far shorter than 492 nm, the excitation wavelength for producing the anisotropy of fluorescein. Therefore, it is unlikely that the adduct fluorophore would interfere with the fluorescence of fluorescein through dipole-dipole coupling. Table 2-2 (page 46) shows the data collected from the fluorescence anisotropy titration of RPA binding to the 30mers adducted with or without BPDE. Figure 2-5 (page 47) shows the representative isotherms by fitting the data in a one-site binding model. As shown in Table 2-1 (page 42), RPA binding affinities for the substrates followed the order: ND>(6-4)PP>AAF>BPDE>AP, where ND stands for non-damaged ssDNA, suggesting that RPA binds less efficiently to these adducts than to the non-damaged ssDNA.

Table 2-2. Fluorescence anisotropy titration of RPA binding to 5'F-30mer or 5'F-BPDE-30mer

RPA(nM)	5'F-30mer		5'F-BPDE-30mer	
	Mean	Std	Mean	Std
0	0	0	0	0
0.5	0.0054	0.0012	0.0029	0.0008
1	0.0103	0.0014	0.0062	0.0006
1.5	0.0158	0.0021	0.0092	0.0006
2	0.0211	0.0030	0.0123	0.0009
2.5	0.0262	0.0029	0.0157	0.0008
3.5	0.0368	0.0032	0.0224	0.0024
4.5	0.0457	0.0029	0.0275	0.0015
5.5	0.0537	0.0029	0.0326	0.0018
6.5	0.0611	0.0027	0.0372	0.0020
7.5	0.0654	0.0029	0.0418	0.0023
9.5	0.0691	0.0021	0.0481	0.0033
11.5	0.0731	0.0019	0.0539	0.0047
13.5	0.0763	0.0018	0.0583	0.0030
15.5	0.0785	0.0027	0.0627	0.0029
17.5	0.0806	0.0016	0.0668	0.0030
21.5	0.0827	0.0016	0.0713	0.0020
25.5	0.0856	0.0017	0.0743	0.0017
29.5	0.0864	0.0019	0.0774	0.0032
33.5	0.0873	0.0019	0.0799	0.0028
37.5	0.0889	0.0023	0.0816	0.0026

Mean represents the mean value of three measurements for each titration point;

Std represents the standard deviation.

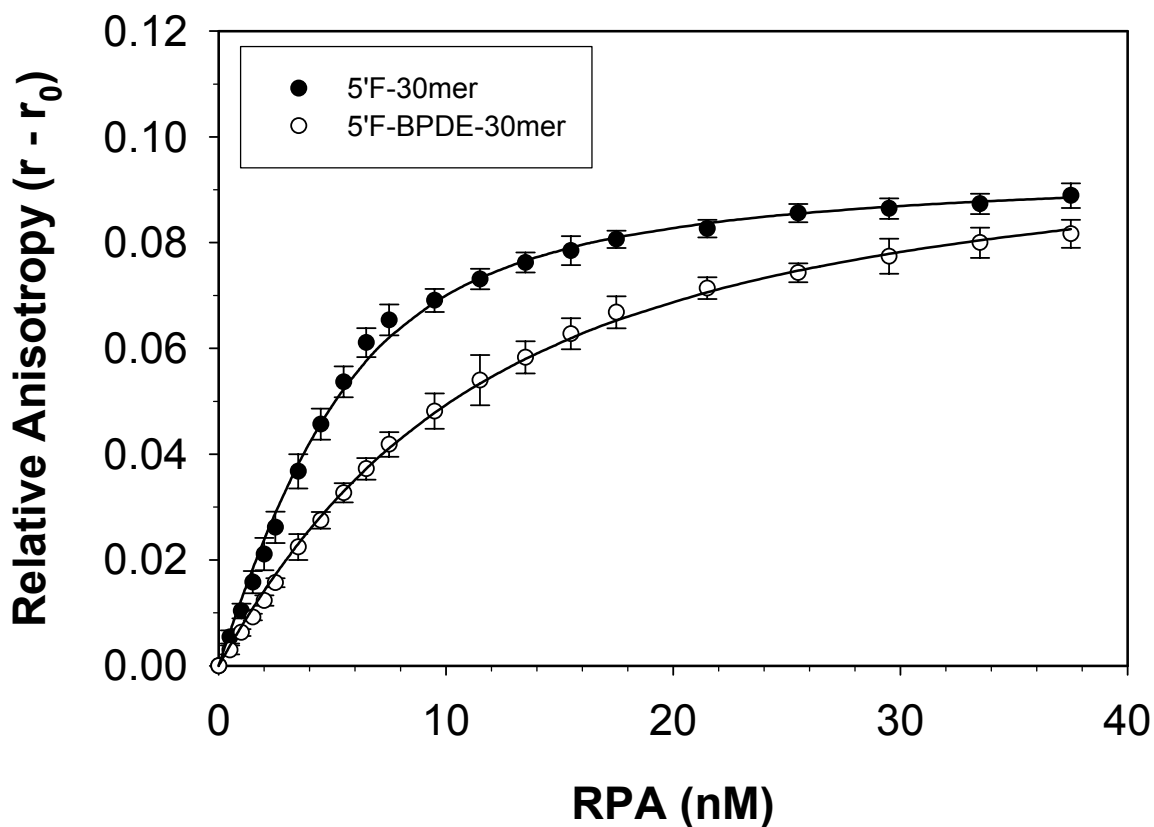


Figure 2-5. Fluorescence anisotropy titration of RPA binding to 5'F-30mer or 5'F-BPDE-30mer. Five nanomolar 5'F-30mer or 5'F-BPDE-30mer was titrated with RPA. The binding isotherms were best fitted to obtain the equilibrium dissociation constants ( $K_{d,obs}$ ). Each datum point was the mean value of three independent measurements. Error bars represent standard deviations.

To verify that the anisotropy titration and fluorescence titration gave the same results for RPA binding to BPDE-adducted ssDNA, titration was also conducted by measuring the BPDE fluorescence change of 5'F-BPDE-30mer. A non-linear least-squares fit of the data provided a dissociation constant of 14.1 nM. This is evidently in good agreement with the value of 11.8 nM determined from the anisotropy measurement, indicating the reliability of these two approaches used in our binding experiments.



### RPA Binding to Damaged and Undamaged 9mer and 11mer ssDNAs

We also examined the RPA binding to the damaged F(M)-9mer and undamaged 5'F-9mer ssDNAs by titrational fluorescence anisotropy measurements. For the substrate F(M)-9mer, the fluorescein also was considered as a lesion in the ssDNA. Figure 2-6A (page 50) showed the RPA-binding isotherms of titration data with substrates 5'F-9mer and F(M)-9mer (Table 2-3, page 49). The anisotropy data were normalized by subtracting the initial value of the respective free DNA and best fitted with the procedures described previously [30]. The results indicated that the affinity of RPA for the 5'F-9mer was significantly higher than that for the F(M)-9mer (Table 2-1, page 42), as demonstrated by the values of dissociation constants  $39.1 \pm 4.5$  and  $93.7 \pm 6.2$  nM for 5'F-9mer and F(M)-9mer respectively. Because the centrally located fluorescein was not attached to a base, the same anisotropic measurement was conducted for RPA binding to a 9mer (5'-end labelled with fluorescein) containing an abasic site in the middle of the same sequence (CATC[abase]CTAC). The binding affinity of RPA for this abasic substrate is very close to that for the undamaged 5'F-9mer (Table 2-1, page 42), indicating that the lack of base in the middle nucleotide had no effect on RPA binding. Thus, the decrease in the affinity for the F(M)-9mer was attributed to the presence of the fluorescein in the middle of the 9mer, although there was no direct interaction between the protein and the aromatic moiety of the fluorophore.

To determine how a base-stacking aromatic lesion adducted directly to a base influences RPA binding, BPDE, a different type of adduct with a larger aromatic ring system (Figure 2-1, page 32) was introduced into the 11mer. As described earlier, binding of RPA to BPDE-adducted ssDNA led to a large fluorescence enhancement. This fluorescence change can be used as a signal to monitor RPA-ssDNA interactions and to generate binding isotherms. As shown in

Table 2-4 (page 51) and Figure 2-6 B and C (page 50), titrations of RPA binding to the BPDE-ssDNA 11mer and the normal 11mer with the same sequence were performed and the binding affinities were determined for comparison. The dissociation constant for the damaged 11mer was  $146.0 \pm 6.7$  nM, while that for the undamaged 11mer ssDNA was  $22.9 \pm 2.6$  nM, indicating a much tighter binding with the undamaged DNA.

Table 2-3. Fluorescence anisotropy titration of RPA binding to 5'F-9mer or F(M)-9mer

RPA(nM)	5'F-9mer		F(M)-9mer	
	Mean	Std	Mean	Std
0	0	0	0	0
4	0.0114	0.0010	0.0056	0.0007
8	0.0217	0.0015	0.0110	0.0008
12	0.0303	0.0016	0.0157	0.0008
16	0.0378	0.0025	0.0195	0.0010
20	0.0445	0.0022	0.0235	0.0013
28	0.0577	0.0020	0.0323	0.0017
36	0.0680	0.0017	0.0396	0.0024
44	0.0757	0.0008	0.0464	0.0030
52	0.0826	0.0007	0.0508	0.0026
68	0.0914	0.0010	0.0586	0.0024
84	0.0979	0.0003	0.0648	0.0027
116	0.1050	0.0005	0.0774	0.0039
148	0.1112	0.0018	0.0869	0.0037
212	0.1173	0.0021	0.0998	0.0034
276	0.1209	0.0019	0.1097	0.0025

Mean represents the mean value of three measurements for each titration point;

Std represents the standard deviation.

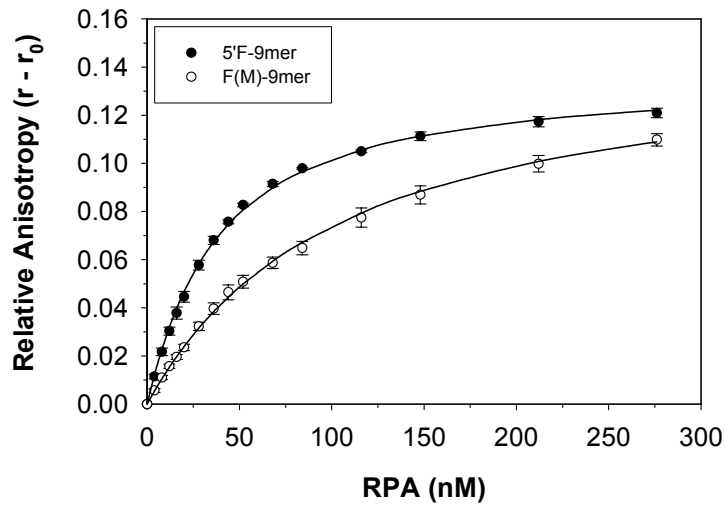
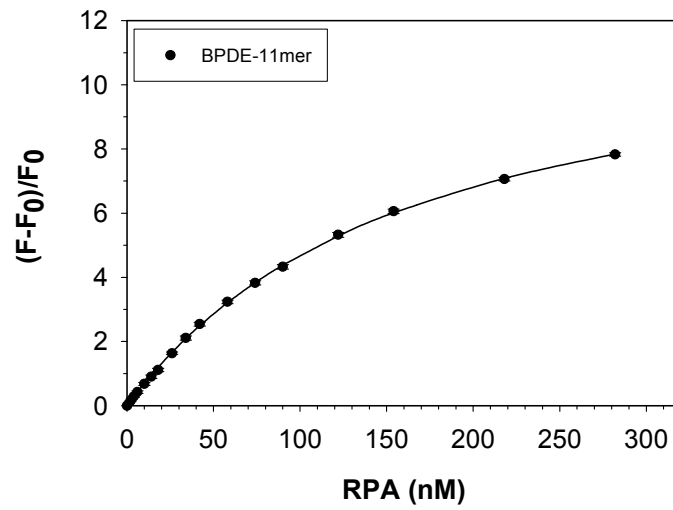
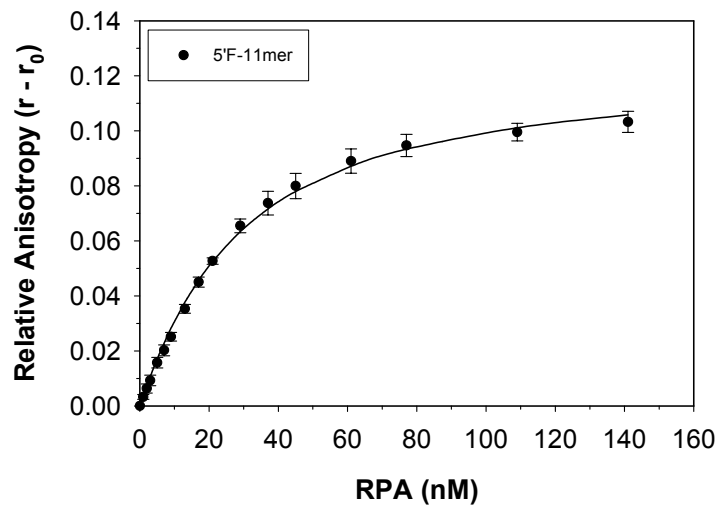
**A****B****C**

Figure 2-6. Typical fluorescence binding isotherms for short ssDNA titrated with RPA  
 (A) Fluorescence anisotropy measurements of RPA binding to 5'F-9mer and F(M)-9mer. (B)  
 Fluorescence titration of BPDE-11mer with RPA. Error bars are too small to see. (C)  
 Fluorescence anisotropy titration of 5'F-11mer with RPA. Data were collected from three  
 independent measurements. Error bars represent standard deviations.

Table 2-4. Fluorescence titration of RPA binding to BPDE-11mer or 5'F-11mer

RPA(nM)	BPDE-11mer		RPA (nM)	5'F-11mer	
	Mean	Std		Mean	Std
0	0	0	0	0	0
2	0.1381	0.0140	1	0.0032	0.0008
4	0.2841	0.0235	2	0.0063	0.0016
6	0.4232	0.0408	3	0.0092	0.0019
10	0.6777	0.0426	5	0.0156	0.0019
14	0.9041	0.0522	7	0.0202	0.0019
18	1.1148	0.0546	9	0.0251	0.0015
26	1.6337	0.0368	13	0.0352	0.0015
34	2.1078	0.0638	17	0.0449	0.0018
42	2.5423	0.0608	21	0.0526	0.0011
58	3.2353	0.0540	29	0.0654	0.0025
74	3.8279	0.0613	37	0.0737	0.0043
90	4.3257	0.0682	45	0.0799	0.0045
122	5.3244	0.0759	61	0.089	0.0043
154	6.0574	0.0687	77	0.0946	0.0040
218	7.0585	0.0569	109	0.0994	0.0032
282	7.8296	0.0554	141	0.1032	0.0038

Mean represents the mean value of three measurements for each titration point;

Std represents the standard deviation.

## Discussion

In the present study, we have systematically analysed the interactions of RPA with a group of damaged and undamaged ssDNA substrates by fluorescence spectroscopy under strict and comparable experimental conditions. Unlike most previous studies, the substrates used in the present study were no longer than 30 nt in length, which kept the binding stoichiometry at one RPA per ssDNA to avoid potential binding complications.

Our experiments designed to probe the nature of the adduct of ssDNA on RPA binding indicated that the protein-bound ssDNA involved a significant local structural alteration around the lesion. This structural change probably caused the disruption of BPDE-ssDNA base stacking and the exposure of the BPDE molecule on RPA binding, which was particularly evident for the short substrate of BPDE-11mer. The results also suggested that the exposed BPDE lesion may be in no or little direct contact with amino acids of RPA. For RPA binding to the BPDE-11mer, it is probable that the modified base resides in the DBDs-AB [2] and is probably flipped out of the protein-ssDNA interaction interface, permitting better contacts of RPA with the unmodified bases. For BPDE-30mer, two additional DBDs, DBD-C, and DBD-D of RPA are involved in the binding. Because binding of a protein to its substrate is a dynamic equilibrium process and RPA has a higher affinity (at least 50-fold) for ssDNA of 30 nt or longer than that for ssDNA of 8–10 nt [3], at equilibrium almost all RPA molecules bind to ssDNA starting from the 5'-end of the substrates. Thus, the modified base that is centrally located in the substrate sequence may reside in the entrance region of DBD-C in the DBDs-ABCD tandem [2], which may result in different and smaller structural changes at adduct. Because both the RPA-ssDNA binding modes of 8–10 nt and 30 nt are probably biologically important in cells (although the 8–10 nt binding mode is

not a full-length binding) [2], our results provide valuable information on RPA–ssDNA adduct interactions in the two cases.

The present study on RPA binding to various ssDNA substrates showed that RPA binds to undamaged ssDNA more favourably than adducted ssDNA, indicating that the presence of lesions in the ssDNA interrupts RPA binding. Two factors might be attributed to this observation: space restriction and the potential repulsion between the exposed aromatic lesion and non-hydrophobic or non-aromatic amino acids. Comparison between RPA binding to the AAF and AP (both being C8-guanine adducts) adducted ssDNAs indicated that AP has an apparent lower affinity than AAF (Table 2-1, page 42). This may be an indication that the larger the aromatic rings system of the adduct, the stronger the inhibition on RPA binding (Figure 2-1, page 32). This was also true when a comparison was made between the BPDE and fluorescein ssDNA. The affinity for BPDE-11mer was lower than that for F(M)-9mer, although it is generally believed that for undamaged ssDNA, longer ssDNA binds to RPA more tightly. It is conceivable that, unlike the fluorescein, which contains a long arm stretching the aromatic rings far away from the DNA, the large BPDE ring system is directly attached to the base.

One of the objectives of the present work was to understand better the biochemical basis for RPA binding to ssDNA and dsDNA and to determine the roles, if any, of RPA in damage recognition in the NER. Although RPA binds to both ssDNA and dsDNA, the binding affinity for duplex DNA is much lower than that for ssDNA. This can be attributed to three factors. First, the binding to ssDNA is facilitated by stacking and other interactions between DNA bases and the residues of RPA [4, 7, 31], while formation of dsDNA eliminates most of the intermolecular interactions due to the base-pairing and stacking. Second, the dsDNA is more rigid and thus more resistant to being bent than the ssDNA. At least local DNA bending could be a result of

efficient RPA binding. Third, dsDNA has a larger helix diameter relative to ssDNA, which may make the binding to dsDNA spatially less favourable. Our results for the unfavourable binding of RPA to damaged ssDNA compared with undamaged ssDNA suggested no direct adduct recognition power from RPA. Several other groups have suggested that the function of RPA in DNA damage recognition in NER is to recognize the local single-stranded character induced by lesions in the duplex [13, 16, 19, 27, 37]. However, efficient binding of RPA to the ssDNA requires a minimum length of approximately 8 nt [10, 31] and, in most of the cases, the local DNA denaturation induced by bulky DNA lesions is much smaller than 8 nt. Based on the results of the present study, we, therefore, propose that base stacking disruption and DNA strand flexibility induced by the lesions may play a role in the binding of RPA to damaged DNA. The base stacking disruption and strand flexibility would allow the exposure of the DNA bases to specific amino acid residues of the RPA. The strand flexibility for bending could in turn structurally facilitate intermolecular interactions. Our hypothesis was also supported by the fact that even without any lesions RPA discriminates the ssDNA of different sequences and this discrimination is probably based on the strength of base stacking in the sequences. Previous studies [3, 5] reported that affinity of RPA for pyrimidine sequences was approximately 50-fold higher than that for purine sequences. It is conceivable that this preference for pyrimidine residues is the result of a weaker base stacking between the relatively smaller aromatic rings of the pyrimidines compared with those of the purine residues.

## References

- 1 Wold, M. S. (1997) Replication protein A: a heterotrimeric, single-stranded DNA-binding protein required for eukaryotic DNA metabolism. *Annu Rev Biochem* **66**, 61-92
- 2 Iftode, C., Daniely, Y. and Borowiec, J. A. (1999) Replication protein A (RPA): the eukaryotic SSB. *Crit Rev Biochem Mol Biol* **34**, 141-180
- 3 Kim, C., Paulus, B. F. and Wold, M. S. (1994) Interactions of human replication protein A with oligonucleotides. *Biochemistry* **33**, 14197-14206
- 4 Kim, C. and Wold, M. S. (1995) Recombinant human replication protein A binds to polynucleotides with low cooperativity. *Biochemistry* **34**, 2058-2064
- 5 Kim, C., Snyder, R. O. and Wold, M. S. (1992) Binding properties of replication protein A from human and yeast cells. *Mol Cell Biol* **12**, 3050-3059
- 6 Brill, S. J. and Bastin-Shanower, S. (1998) Identification and characterization of the fourth single-stranded-DNA binding domain of replication protein A. *Mol Cell Biol* **18**, 7225-7234
- 7 Bochkareva, E., Korolev, S., Lees-Miller, S. P. and Bochkarev, A. (2002) Structure of the RPA trimerization core and its role in the multistep DNA-binding mechanism of RPA. *Embo J* **21**, 1855-1863
- 8 Bastin-Shanower, S. A. and Brill, S. J. (2001) Functional analysis of the four DNA binding domains of replication protein A. The role of RPA2 in ssDNA binding. *J Biol Chem* **276**, 36446-36453
- 9 Kolpashchikov, D. M., Weissart, K., Nasheuer, H. P., Khodyreva, S. N., Fanning, E., Favre, A. and Lavrik, O. I. (1999) Interaction of the p70 subunit of RPA with a DNA template directs p32 to the 3'-end of nascent DNA. *FEBS Lett* **450**, 131-134
- 10 Blackwell, L. J. and Borowiec, J. A. (1994) Human replication protein A binds single-stranded DNA in two distinct complexes. *Mol Cell Biol* **14**, 3993-4001
- 11 Burns, J. L., Guzder, S. N., Sung, P., Prakash, S. and Prakash, L. (1996) An affinity of human replication protein A for ultraviolet-damaged DNA. *J Biol Chem* **271**, 11607-11610



- 12 Lao, Y., Gomes, X. V., Ren, Y., Taylor, J. S. and Wold, M. S. (2000) Replication protein A interactions with DNA. III. Molecular basis of recognition of damaged DNA. *Biochemistry* **39**, 850-859
- 13 Patrick, S. M. and Turchi, J. J. (1999) Replication protein A (RPA) binding to duplex cisplatin-damaged DNA is mediated through the generation of single-stranded DNA. *J Biol Chem* **274**, 14972-14978
- 14 Sancar, A. (1996) DNA excision repair. *Annu Rev Biochem* **65**, 43-81
- 15 He, Z., Henriksen, L. A., Wold, M. S. and Ingles, C. J. (1995) RPA involvement in the damage-recognition and incision steps of nucleotide excision repair. *Nature* **374**, 566-569
- 16 Hey, T., Lipps, G. and Krauss, G. (2001) Binding of XPA and RPA to damaged DNA investigated by fluorescence anisotropy. *Biochemistry* **40**, 2901-2910
- 17 Clugston, C. K., McLaughlin, K., Kenny, M. K. and Brown, R. (1992) Binding of human single-stranded DNA binding protein to DNA damaged by the anticancer drug cis-diamminedichloroplatinum (II). *Cancer Res* **52**, 6375-6379
- 18 Lao, Y., Lee, C. G. and Wold, M. S. (1999) Replication protein A interactions with DNA. 2. Characterization of double-stranded DNA-binding/helix-destabilization activities and the role of the zinc-finger domain in DNA interactions. *Biochemistry* **38**, 3974-3984
- 19 de Laat, W. L., Appeldoorn, E., Sugawara, K., Weterings, E., Jaspers, N. G. and Hoeijmakers, J. H. (1998) DNA-binding polarity of human replication protein A positions nucleases in nucleotide excision repair. *Genes Dev* **12**, 2598-2609
- 20 Missura, M., Buterin, T., Hindges, R., Hubscher, U., Kasparikova, J., Brabec, V. and Naegeli, H. (2001) Double-check probing of DNA bending and unwinding by XPA-RPA: an architectural function in DNA repair. *Embo J* **20**, 3554-3564
- 21 Reardon, J. T. and Sancar, A. (2002) Molecular anatomy of the human excision nuclease assembled at sites of DNA damage. *Mol Cell Biol* **22**, 5938-5945
- 22 Reardon, J. T. and Sancar, A. (2003) Recognition and repair of the cyclobutane thymine dimer, a major cause of skin cancers, by the human excision nuclease. *Genes Dev* **17**, 2539-2551
- 23 Riedl, T., Hanaoka, F. and Egly, J. M. (2003) The comings and goings of nucleotide excision repair factors on damaged DNA. *Embo J* **22**, 5293-5303

- 24 Volker, M., Mone, M. J., Karmakar, P., van Hoffen, A., Schul, W., Vermeulen, W., Hoeijmakers, J. H., van Driel, R., van Zeeland, A. A. and Mullenders, L. H. (2001) Sequential assembly of the nucleotide excision repair factors in vivo. *Mol Cell* **8**, 213-224
- 25 Sugasawa, K., Ng, J. M., Masutani, C., Iwai, S., van der Spek, P. J., Eker, A. P., Hanaoka, F., Bootsma, D. and Hoeijmakers, J. H. (1998) Xeroderma pigmentosum group C protein complex is the initiator of global genome nucleotide excision repair. *Mol Cell* **2**, 223-232
- 26 Wakasugi, M. and Sancar, A. (1999) Order of assembly of human DNA repair excision nuclease. *J Biol Chem* **274**, 18759-18768
- 27 Patrick, S. M. and Turchi, J. J. (2001) Stopped-flow kinetic analysis of replication protein A-binding DNA: damage recognition and affinity for single-stranded DNA reveal differential contributions of  $k_{on}$  and  $k_{off}$  rate constants. *J Biol Chem* **276**, 22630-22637
- 28 Schweizer, U., Hey, T., Lipps, G. and Krauss, G. (1999) Photocrosslinking locates a binding site for the large subunit of human replication protein A to the damaged strand of cisplatin-modified DNA. *Nucleic Acids Res* **27**, 3183-3189
- 29 Yang, Z. G., Liu, Y., Mao, L. Y., Zhang, J. T. and Zou, Y. (2002) Dimerization of human XPA and formation of XPA2-RPA protein complex. *Biochemistry* **41**, 13012-13020
- 30 Zou, Y., Bassett, H., Walker, R., Bishop, A., Amin, S., Geacintov, N. E. and Van Houten, B. (1998) Hydrophobic forces dominate the thermodynamic characteristics of UvrA-DNA damage interactions. *J Mol Biol* **281**, 107-119
- 31 Bochkarev, A., Pfuetzner, R. A., Edwards, A. M. and Frappier, L. (1997) Structure of the single-stranded-DNA-binding domain of replication protein A bound to DNA. *Nature* **385**, 176-181
- 32 Geacintov, N. E., Zinger, D., Ibanez, V., Santella, R., Grunberger, D. and Harvey, R. G. (1987) Properties of covalent benzo[a]pyrene diol epoxide-DNA adducts investigated by fluorescence techniques. *Carcinogenesis* **8**, 925-935
- 33 Geacintov, N. E., Solntsev, k., Johnson, L. W., Chen, J. X., Kolbanovskiy, A. D., Liu, T. M. and Shafirovich, V. Y. (1998) Photoinduced electron transfer and strand cleavage in pyrenyl-DNA complexes and adducts. *J. Phys.Org. Chem.* **11**, 561-565

- 34 Huang, W., Amin, S. and Geacintov, N. E. (2002) Fluorescence characteristics of site-specific and stereochemically distinct benzo[a]pyrene diol epoxide-DNA adducts as probes of adduct conformation. *Chem Res Toxicol* **15**, 118-126
- 35 Cosman, M., Ibanez, V., Geacintov, N. E. and Harvey, R. G. (1990) Preparation and isolation of adducts in high yield derived from the binding of two benzo[a]pyrene-7,8-dihydroxy-9,10-oxide stereoisomers to the oligonucleotide d(ATATGTATA). *Carcinogenesis* **11**, 1667-1672
- 36 Geacintov, N. E., Gagliano, A. G., Ibanez, V. and Harvey, R. G. (1982) Spectroscopic characterizations and comparisons of the structures of the covalent adducts derived from the reactions of 7, 8-dihydroxy-7,8,9,10-tetrahydrobenzo [a] pyrene-9,10-oxide, and the 9, 10-epoxides of 7,8,9,10-tetrahydrobenzo [a] pyrene and 9,10,11,12-tetrahydrobenzo [e] pyrene with DNA. *Carcinogenesis* **3**, 247-253
- 37 Mu, D., Hsu, D. S. and Sancar, A. (1996) Reaction mechanism of human DNA repair excision nuclease. *J Biol Chem* **271**, 8285-8294

## CHAPTER 3

### MODULATION OF REPLICATION PROTEIN A FUNCTION BY ITS HYPERPHOSPHORYLATION-INDUCED CONFORMATION CHANGE INVOLVING DNA BINDING DOMAIN B

#### Abstract

Human replication protein A (RPA), composed of RPA70, RPA32, and RPA14 subunits, undergoes hyperphosphorylation in cells in response to DNA damage. Hyperphosphorylation that occurs predominately in the N-terminal region of RPA32 is believed to play a role in modulating the cellular activities of RPA essential for almost all DNA metabolic pathways. In order to understand how the hyperphosphorylation modulates the functions of RPA, we compared the structural characteristics of full length native and hyperphosphorylated RPAs using mass spectrometric protein foot-printing, fluorescence spectroscopy, and limited proteolysis. Our mass spectrometric data showed that of 24 lysines and 18 arginines readily susceptible to small chemical reagent modification in native RPA, the three residues K343, R335, and R382 located in DNA binding domain B (DBD-B) of RPA70 were significantly shielded in the hyperphosphorylated protein. Tryptophan fluorescence studies indicated significant quenching of W361, located in the DBD-B domain, induced by hyperphosphorylation of RPA. Consistently, DBD-B became more resistant to the limited proteolysis by chymotrypsin after RPA hyperphosphorylation. Taken together, our results suggest that upon hyperphosphorylation of RPA32 N-terminus (RPA32N), RPA undergoes a subtle conformational change with specific involvement of the ssDNA binding cleft of DBD-B. Comparison of interactions of native and

hyperphosphorylated RPAs with short single stranded oligonucleotides or partial DNA duplexes with a short 5' or 3' ssDNA tails showed reduced affinity for the latter protein. We propose that the hyperphosphorylation may play a role in modulating the cellular pathways by altering the DBD-B-mediated RPA-DNA and RPA-protein interactions, hypothetically via the interaction of hyperphosphorylated RPA32N with DBD-B.

### Introduction

Replication protein A (RPA) is a eukaryotic single-stranded DNA (ssDNA) binding protein essential for DNA replication, repair, recombination (1-3), and cellular DNA-damage checkpoints (4,5). RPA is composed of three subunits, RPA70, RPA32, and RPA14, named after their molecular weights of 70, 32, and 14 kDa, respectively. Although the structure of full length RPA trimer remains unsolved, X-ray crystallography, NMR, and biochemical studies reveal that RPA70 contains four domains, the N-terminal domain of RPA70, DNA-binding domain (DBD) A, B, and C (6-8). The tandem DBD-A and DBD-B harbor the major ssDNA binding activity of RPA heterotrimer (9). DBD-C has a conserved zinc finger (10) and exhibits low affinity for ssDNA but interacts with the other two subunits to form a RPA trimerization core (11). RPA32 consists of three domains, including an unstructured N-terminal phosphorylation domain (RPA32N), a central DNA-binding domain (DBD-D), and a C-terminal domain (RPA32C) largely involved in protein-protein interactions (12-14). RPA14 is referred to as DBD-E. All the DBDs in RPA have similar structures, built around a central OB-fold: oligo-saccharide/oligonucleotide binding fold (6,7,11,12,15). However, the N-terminal domain of RPA70 (also referred to as DBD-F or RPA70N) has been only implicated in protein-protein interactions in DNA metabolism (1-3, 6). In contrast, DBD-E (RPA14) shows no binding affinity

for ssDNA but is structurally important for the formation of RPA trimerization core (11, 12). Slight differences in structure and residue compositions of the binding clefts of the DBDs may explain their differences in ssDNA binding (16,17).

It has been reported that the N-terminal domain of RPA32 (RPA32N) becomes phosphorylated in a cell cycle-dependent manner (18-20) and hyperphosphorylated in response to DNA damage (21-24). The cell cycle-dependent phosphorylation is carried out by cyclin-dependent kinases (Cdks) and occurs at two consensus sites, Ser-23 and Ser-29 of RPA32 (19,22,25). More sites in RPA32N are phosphorylated in cells in response to DNA damage (22,23,26) or apoptosis (27). Phospho-peptide mapping has shown that at least five sites of RPA32N including Thr-21, Ser-23, Ser-29, Ser-33, and either Ser-11, -12, or -13, and probably two additional sites, Ser-4 and Ser-8, can be phosphorylated in UV-irradiated HeLa cells (22,25,28). The DNA damage-induced hyperphosphorylation of RPA32 is believed to be carried out by the members of phosphatidylinositol 3-kinase-like serine/threonine protein kinase (PIKK) family that includes DNA-dependent protein kinase (DNA-PK), ataxia-telangiectasia mutated kinase (ATM), and ATM- and Rad3-related kinase (ATR) (2,4,23,24,29-31). DNA-PK phosphorylates RPA32 *in vitro* at many of the same sites that are phosphorylated *in vivo* in HeLa cells after UV-irradiation (22,24,25).

One of the most striking aspects of RPA is that the protein is involved in almost all DNA metabolic pathways in cells. It is believed that such broad cellular activities of RPA are mediated by its interactions with ssDNA and numerous proteins engaged in cellular processes (9,14). RPA phosphorylation may play a role in regulation of these interactions and thus the cellular functions of RPA (24). It has been shown that RPA hyperphosphorylation down-regulates DNA replication (24,32). In particular, hyperphosphorylation of RPA32 may modulate RPA interactions with

DNA and proteins involved in the DNA repair and signaling pathways in response to DNA damage (2,24). For instance, hyperphosphorylated RPA (hyp-RPA) has shown decreased interactions with simian virus 40 (SV40) T antigen, DNA polymerase  $\alpha$ , DNA-PK, ATM, and p53, while the hyperphosphorylation has no effects on RPA interactions with XPA, Rad51, and Rad52 (20,24,33-37). In addition, hyp-RPA binds double-stranded DNA (dsDNA) with a reduced affinity (20,38), whereas the effects of hyperphosphorylation on RPA interaction with ssDNA remain controversial (20,38,39). Despite the significant role of hyperphosphorylation of RPA in modulating its cellular functions, the biochemical basis of the effects is still poorly understood. A possible scenario is that RPA may change its structure or conformation upon hyperphosphorylation and thus alter the protein activities and functions. A synthetic peptide fragment with eight Ser/Thr substituted to Asp to mimic the hyperphosphorylated RPA32N was shown to interact with DBD-F (RPA70N) fragment (RPA70<sub>1-168</sub>) (38). However, the structural characteristics of the hyperphosphorylated RPA trimer of full length remain to be elucidated.

In the present study, we determined the hyperphosphorylation-induced structural alterations of human RPA protein using mass spectrometric protein foot-printing, limited proteolysis, and tryptophan fluorescence spectroscopy. Out of 42 basic residues readily susceptible to modification with small chemical reagents in the native protein, the three amino acids: K343, R335, and R382 in DBD-B of RPA70 were shielded in the context of the hyperphosphorylated RPA. Our results indicate that these residues were exclusively involved in a limited structural alteration of the protein upon hyperphosphorylation of the RPA32 N-terminus. In particular, this local structural change showed effects on the RPA interactions with 8mer ssDNA or partial DNA duplexes containing ssDNA tails. Considering the essential role of RPA in most of cellular DNA metabolic processes including those mediated with short ssDNA-

associated partial DNA duplexes, our results provide the biochemical basis for the roles of hyperphosphorylation in regulation of RPA functions.

## Materials and Methods

### Protein Production and Purification

Recombinant human RPA was expressed in *E. coli* BL21(DE3)-RP cells harboring the plasmid pTYB-RPA and purified as previously described (40). Two RPA mutants, W107/528 and W212/361, which had all tryptophans of RPA being replaced by phenylalanine except for residues 107 and 528 or residues 212 and 361, were expressed from BL21(DE3)-RP cells containing the plasmids constructed by site-directed mutagenesis. The mutant proteins were purified by the same procedures as for native RPA.

### In Vitro Phosphorylation by DNA-PK

For hyperphosphorylation, the purified RPA or mutants were incubated with DNA-PK isolated from HeLa nuclear extracts as a complex consisting of a 400kDa catalytic subunit and the DNA-binding component of 85kDa and 70kDa Ku subunits (Promega) at 30°C for 30 minutes in the phosphorylation buffer (40 mM HEPES, pH 7.5, 10 mM MgCl<sub>2</sub>, 1 mM DTT, 200 μM ATP, and 10 μg/mL calf thymus DNA). A mock treatment of proteins was carried out in parallel under the exact same conditions except that no ATP was added in the phosphorylation buffer. The reaction mixtures were then loaded onto an HR10/30 Superdex 200 column equipped with an AKTApurifier system (Amersham Pharmacia Biotech, Sweden). To purify the hyperphosphorylated RPA, the column was pre-equilibrated with the FPLC running buffer containing high concentration of salt (40 mM HEPES, pH 7.5, 2 M NaCl, 10 mM MgCl<sub>2</sub>, 10 μM



ZnCl<sub>2</sub>, and 1 mM DTT) and run with the same buffer at 4 °C. The fractions containing hyperphosphorylated proteins or mock-treated proteins were pooled and dialyzed against RPA storage buffer (40 mM HEPES, pH 7.5, 50 mM NaCl, 10 mM MgCl<sub>2</sub>, 10 μM ZnCl<sub>2</sub>, 1 mM DTT, and 50% glycerol). Protein concentration was determined using Bio-Rad Protein Assay Kit.

### Chemical Modification and in Gel Proteolysis

Biotinylation of lysine residues of RPA was carried out as described previously (41). Briefly, 2 μM hyp-RPA or RPA was incubated with *N*-hydroxysuccinimidobiotin (NHS-biotin, Pierce) in 50 mM HEPES (pH 7.5), 50 mM NaCl at 25 °C for 30 minutes. The reactions were then quenched by addition of 10 mM lysine. The three subunits of RPA were separated by SDS-PAGE and visualized by Coomassie blue stain. The corresponding bands were excised and the gel slices were destained, dehydrated, and digested with 1 μg of trypsin (Roche) in 50 mM NH<sub>4</sub>HCO<sub>3</sub> at 25 °C overnight. Proteolytic peptides were recovered and subjected to MS and MS/MS analysis.

Modification of arginine residues was performed by incubating 2 μM hyp-RPA or RPA with *p*-hydroxyphenylglyoxal (HPG, Pierce) in 50 mM HEPES / 50 mM boric acid (pH 8.0) at 37 °C in dark for 60 minutes. The modification was quenched by addition of 100 mM arginine. Then samples were subjected to SDS-PAGE and protein bands were excised and processed as described above.

## MS and MS/MS Analysis

MS spectra were obtained using matrix-assisted laser desorption time of flight (MALDI-TOF) and quadrupole-time of flight (Q-TOF) techniques. MALDI-TOF was done by Dr. Mamuka Kvaratskhelia (The Ohio State University, Columbus, Ohio). Q-TOF was done by Dr. Sonja Hess (National Institutes of Health, Bethesda, Maryland). MALDI-TOF experiments were performed using a Kratos Axima-CRF instrument (Kratos Analytical Instruments) with  $\alpha$ -cyano-4-hydroxy-cinnamic acid matrix. MS and MS/MS analyses were performed on a Micromass (Manchester, U.K.) Q-TOF-II instrument equipped with an electrospray source and Micromass cap-LC. Peptides were separated with a Waters Symmetry300 5  $\mu$ m precolumn (Waters, Milford, MA) and a Micro-Tech Scientific (Vista, CA) ZC-10-C18SBWX-150 column using two sequential gradients of 5-40% acetonitrile for 35 minutes and 40-90% acetonitrile for 20 min. MS/MS sequence data and the MASCOT automated peptide search engine ([www.matrixscience.com](http://www.matrixscience.com)) were used to identify RPA peptide peaks from the NCBI nr primary sequence database, and matched peaks were then located in the primary MS spectra. Protection events were qualitatively assigned as the appearance of a peak corresponding to a modified peptide in the modified protein spectrum and the absence of the modification peak in the modified hyperphosphorylated protein spectrum. A protection was considered to be significant only when the intensity of a modifiable peak was reduced by at least 85% in the hyp-RPA spectrum. In order to accurately identify protection events, at least two unmodified proteolytic peptide peaks present in all four spectra (unmodified protein, modified protein, unmodified hyp-protein, and modified hyp-protein) were used as controls. These control peaks served to standardize the peak intensities in each spectrum for accurate qualitative assignment of

protection. Data were reproducibly compiled and analyzed from six independent experimental groups.

### Fluorescence Spectroscopy Determination

The tryptophan fluorescence spectra of RPA, its mutants, and their hyperphosphorylated forms were recorded on a SPEX Fluorolog-3 fluorometer (Jobin Yvon Inc.) with the excitation wavelength at 295 nm and the slit widths set at 3 nm for excitation and 5 nm for emission beams. After equilibration of 100 nM protein in RPA buffer (40 mM HEPES-KOH, pH 7.9, 75 mM KCl, 8 mM MgCl<sub>2</sub>, 1 mM DTT, and 5% glycerol) at 25 °C for 10 min, the fluorescence spectra were obtained by recording emission from 310 nm to 500 nm. For the constant wavelength analysis, the emission at 355 nm was measured with excitation at 295 nm.

The rotational behavior of fluorescently labeled molecules can be monitored by fluorescence anisotropy. Increase of anisotropy may indicate complex formation (42). Fluorescence anisotropy measurements were performed to compare the binding of RPA and hyp-RPA to an oligo(dT)<sub>8</sub>. The (dT)<sub>8</sub> with a fluorescein labeled at 5' end (5'F-dT8) was purchased from Qiagen in HPLC-purified quality. The anisotropy titrations were performed as described in chapter 2 (43) and the data were processed using a one-site binding model and the non-linear least-squares method for the determination of the binding constants (44).

### Partial Proteolysis and Identification of Proteolytic Fragments

Four microgram of recombinant human RPA or hyp-RPA was incubated with chymotrypsin (1:80) at room temperature for the indicated periods in a reaction buffer (10 µL) containing 40 mM HEPES, pH 7.8, 1 mM EDTA, 70 mM MgCl<sub>2</sub>, and 10 mM DTT. At each

time point (5, 20, or 60 minutes), 2.5  $\mu$ L of the reaction mixture was removed and terminated by addition of Laemmli sample buffer and boiling for 10 minutes. The proteolytic products were resolved by 14% SDS-PAGE and stained with SYPRO Ruby protein gel stain (Bio-Rad). After destained with a solution containing 10% methanol and 7% acetic acid, the gel was imaged by a PhosphorImager (FLA-5000, FUJIFILM) using 473 nm laser line. For automated N-terminal sequencing, the proteolytic fragments separated on the 14% SDS-PAGE were transferred to a polyvinylidene difluoride (PVDF) membrane, followed by staining with Coomassie Brilliant Blue G-250. The protein bands of interest were excised and sent to the protein chemistry laboratory at the University of Texas Medical Branch for sequencing.

#### Gel Mobility Shift Assays

ssDNA was radio-labeled with [ $\gamma$ - $^{32}$ P]ATP and T4 polynucleotide kinase. The labeled substrate (1 nM) was then incubated with indicated amounts of hyp-RPA or RPA at room temperature for 15 min in 20  $\mu$ L of the binding buffer (40 mM HEPES-KOH, pH 7.9, 75 mM KCl, 8 mM MgCl<sub>2</sub>, 1 mM DTT, 5% glycerol, and 100  $\mu$ g/mL BSA). After incubation, 2  $\mu$ L of 80% (v/v) glycerol was added, and the mixture was immediately loaded onto a 4% native polyacrylamide gel in 1 x TBE running buffer (89 mM Tris-borate and 2 mM EDTA, pH8.3) and electrophoresed at room temperature. The gel was then dried. The free and bound DNA was visualized using a PhosphorImager (FLA-5000, FUJIFILM).

## Pull-Down Assays

The binding of RPA to partial DNA duplexes containing 5'-protruding 11 nucleotides (DNA-11) or 3'-protruding 10 nucleotides (DNA-10) were investigated by a streptavidin-agarose pull-down assay. The sequences of the oligonucleotides used to construct the partial DNA duplexes are as follows: 55mer, Biotin-GGACCTGAACACGTACGGAATTCGATATCCTCGAGCCAGATCTGCGCC AGCTGGC; 44mer, GCCAGCTGGCGCAGATCTGGCTCGAGGATATCGAATTCCG TACG; 45mer, GCAGATCTGGCTCGAGGATATCGAATTCCGTACGTGTTTCAGGT CC. The 44mer and 45mer were 5'-<sup>32</sup>P-labeled and annealed to their complementary biotinylated 55mer at a molar ratio of 1:1, respectively. The annealing mixture was then loaded onto an 8% native polyacrylamide gel in 1 x TBE running buffer and electrophoresed at 80 volts for 3 hours at room temperature. Using the 5'-<sup>32</sup>P-labeled 44mer, 45mer, and 55mer as controls, the bands identified as the partial DNA duplexes, which migrated slower than the single-stranded oligonucleotides in the gel, were excised, eluted, and precipitated with ethanol. After the purification, 5 pmol of the partial DNA duplex were incubated with the indicated amounts of mixed hyp-RPA and RPA in 500 µL of the binding buffer at room temperature for 15 minutes. Then 20 µL of streptavidin-conjugated agarose beads (Invitrogen) pre-washed with the binding buffer was added. The mixture was placed on a rotating shaker with gentle mixing at room temperature for 30 minutes. The beads were collected by centrifugation and washed 3 times with the binding buffer. The proteins in the complex were assessed by Western blotting using an antibody specific for RPA32 as described below.

## Western Blotting

Protein samples were separated by 10% SDS-PAGE and transferred to a PVDF membrane in Tris-glycine buffer (0.375 M Tris, 0.192 M glycine, 20% methanol). The membrane was blocked with 5% nonfat milk at room temperature for 1 hour and then treated with a monoclonal anti-RPA32 antibody (Kamiya Biomedical) at 0.5 µg/mL in PBS supplemented with 5% nonfat milk at 4 °C overnight with shaking. The RPA32 protein bands were visualized using anti-mouse IgG conjugated with horseradish peroxidase as the secondary antibody (Santa Cruz) by following the protocol of the ECL Western Blotting System (Amersham Biosciences).

## Results

### *In Vitro* Hyperphosphorylation of RPA by DNA-PK

It has been well established that DNA-PK is involved in the DNA damage-induced RPA hyperphosphorylation in cells (23,29-31,39,45-47). DNA-PK is composed of the Ku70/80 heterodimer and the catalytic subunit DNA-PKcs (48). The sites of RPA phosphorylated by DNA-PK *in vitro* are similar to those phosphorylated *in vivo* after UV-irradiation of human cells (22,25). Although RPA may also be hyperphosphorylated by other PIKK family members such as ATR and ATM in response to DNA damage *in vivo*, hyperphosphorylation of RPA by DNA-PK represents a typical one for study of the DNA damage-induced RPA hyperphosphorylation. To investigate the changes of RPA structure and activity upon hyperphosphorylation, we prepared the hyperphosphorylated RPA by incubating purified recombinant RPA with DNA-PK in the presence of calf thymus DNA (Promega). After hyperphosphorylation reaction, the RPA (116 kDa) was separated from DNA-PK (three subunits: 400, 80, and 85 kDa respectively) and

DNA by gel filtration with the running buffer containing 2 M NaCl, followed by dialysis against RPA storage buffer. A high salt concentration was used to dissociate RPA from the kinase and DNA, while the RPA remained in the form of trimer (Figure 3-1A, page 71). The SDS-PAGE and Western Blotting analyses of the RPA hyperphosphorylation showed that more than 85% of RPA32 was hyperphosphorylated by DNA-PK as indicated by the band shifted from the native RPA32 (Figure 3-1A, lane 3 and Figure 3-1B, lane 1, page 71). And this phosphorylation was fully reversed after the treatment of the hyp-RPA with calf intestinal phosphatase (CIP) as the retardation was diminished (Figure 3-1A, lane 4, page 71). No phosphorylation by DNA-PK was observed in RPA70 and RPA14 subunits, as confirmed by the labeling with [ $\gamma$ - $^{32}$ P]ATP (data not shown), which is also in agreement with that of a previous report (49). It has been generally known that *in vivo* phosphorylation results in five isoforms of RPA that represent different levels of phosphorylation as indicated by the mobility shifts of RPA32 on SDS-PAGE (20-22,50) (Figure 3-1B, lane 3, page 71). Of them, forms 2-3 occur in a cell cycle dependent manner, while forms 4-5 are the hyperphosphorylated RPA32 and appear upon cellular DNA damage. Comparison of RPAs phosphorylated *in vitro* and *in vivo* by Western blotting revealed that most of the DNA-PK-hyperphosphorylated RPA had the same mobility shifts as did forms 4 and 5 of RPA from UV-irradiated HeLa cells.

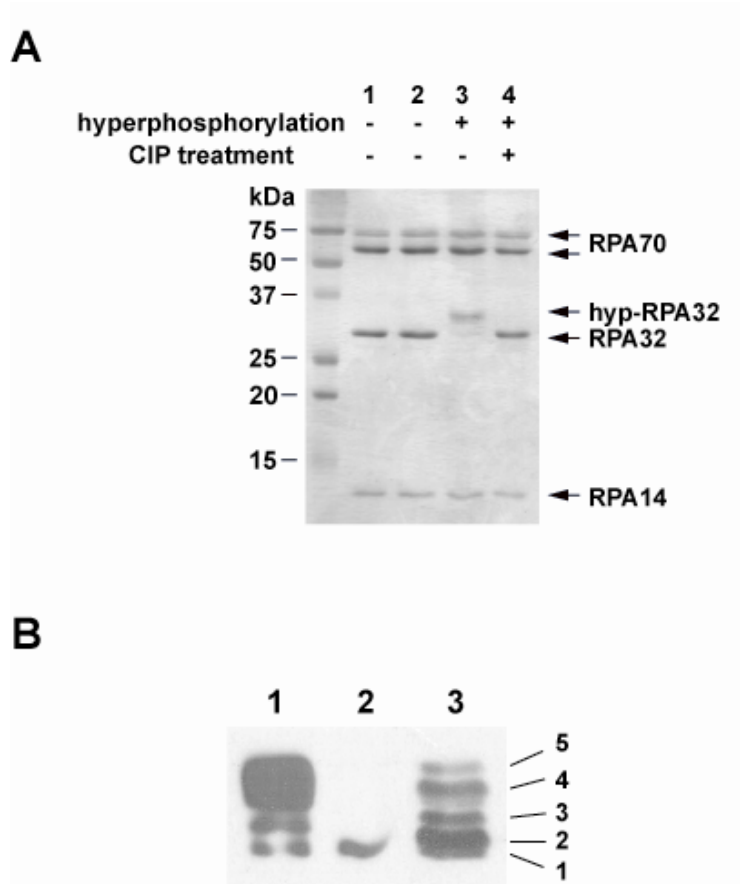


Figure 3-1. *in vitro* phosphorylation of RPA by DNA-PK

(A) The phosphorylation reaction was conducted as described in Experimental Procedures. Proteins including untreated RPA (lane 1), mock-treated RPA (lane 2), hyp-RPA (lane 3), and CIP-treated hyp-RPA (lane 4) were visualized by 14% SDS-PAGE and Coomassie blue staining.

(B) Immunoblot of RPA32 from RPA hyperphosphorylated by DNA-PK (lane 1), RPA (lane 2), and RPA in UV-irradiated HeLa cells (lane 3). To prepare the RPA in UV-irradiated HeLa cells, whole cell lysates were prepared from HeLa cells at 8 h following irradiation with 20 J/m<sup>2</sup> UV. Proteins were separated on a 10% SDS-PAGE followed by Western blotting using an antibody specific for RPA32.



## Surface Topology Analysis of Native and Hyperphosphorylated RPAs with Group Specific Reagents and Mass Spectrometry

Chemical modifications coupled with mass spectrometry have been used to probe the surface topology of proteins (51-53). Recently, a strategy of protein footprinting has been developed by Kvaratskhelia et al. for accurate mapping of protein-nucleic acid interactions using mass spectrometry (54). Here we extend this method to probe conformational changes of RPA after hyperphosphorylation by monitoring the changes of surface accessibility of lysine and arginine residues susceptible to NHS-biotin and hydroxyphenylglyoxal (HPG) modifications, respectively. Comparison of surface topologies of native and hyperphosphorylated RPAs would enable us to identify conformational changes in the full length protein induced by hyperphosphorylation.

Of note, maintenance of the structural integrity of proteins under the modification conditions is crucial for the success of these experiments. Therefore, we optimized concentrations of NHS-biotin and HPG. Our recent work indicated that upon treatment of RPA-ssDNA complex with 400  $\mu$ M NHS-biotin the integrity of nucleoprotein complex was fully preserved (41). Therefore, in the present study we employed the same reaction conditions. A similar approach was used to optimize the HPG modification. We found that integrity of RPA-ssDNA complex was fully preserved with treatment of 1.25 mM HPG and employed this concentration in the present study.

NHS-biotin reacts specifically with primary amines on the surface of proteins, resulting in covalent addition of a biotin molecule (226 Daltons) to lysine and release of an N-hydroxysuccinimide (54). The modified residues could be readily identified with subsequent MS and MS/MS analysis of the proteolytic fragments. We have recently reported NHS-biotin

Table 3-1. Identification of modified lysines or arginines in RPA and hyp-RPA

RPA Subunits	Biotin-Modified Lysines <sup>a</sup>	HPG-Modified Arginines <sup>a</sup>
RPA70	88, 163, 167, 183, 206, 220, 244, 263, 259, 324, 331, <b><u>343</u></b> , 379, 489, 502, 577, 588, 595	91, 92, 202, 210, 216, <b><u>335</u></b> , <b><u>382</u></b> , 472, 573, 575, 586, 600, 604, 605, 611
RPA32	38, 93, 138, 139	40, 133
RPA14	33, 49	30

a. The residues that were protected from modification in hyper-RPA are indicated in bold and underlined.

modification pattern of the full length RPA and RPA-ssDNA complex (41). In the present study, we compared the biotinylation sites of the native and hyp-RPA proteins by MALDI-TOF. Twenty-four biotinylated tryptic peptides were identified for native RPA including 18 fragments from RPA70, 4 from RPA32, and 2 from RPA14 (Table 3-1). The biotinylation patterns and intensities of the biotinylated peptides were almost identical between the native and hyp-RPA proteins, except that of the biotinylated peptide of amino acids 340-344 of DBD-B (Figure 3-2, page 74). This peptide peak was readily detectable in the MS spectra of native RPA, but was significantly diminished in hyp-RPA (Figure 3-2A, page 74). Figure 3-2B (page 74) is a representative segment of MALDI-TOF spectra showing that K88 and K379, other 2 of the 24 modified lysines, were biotinylated equally well in both native and hyp-RPA proteins. MS/MS analysis of the aa 340-344 peptide peak, which exhibited protection in the context of hyp-RPA, indicated the biotinylation of K343 (Figure 3-2C, page 74). Given that 23 modified lysines distributed on the surfaces of almost all the domains of RPA trimer, the exhibited similar

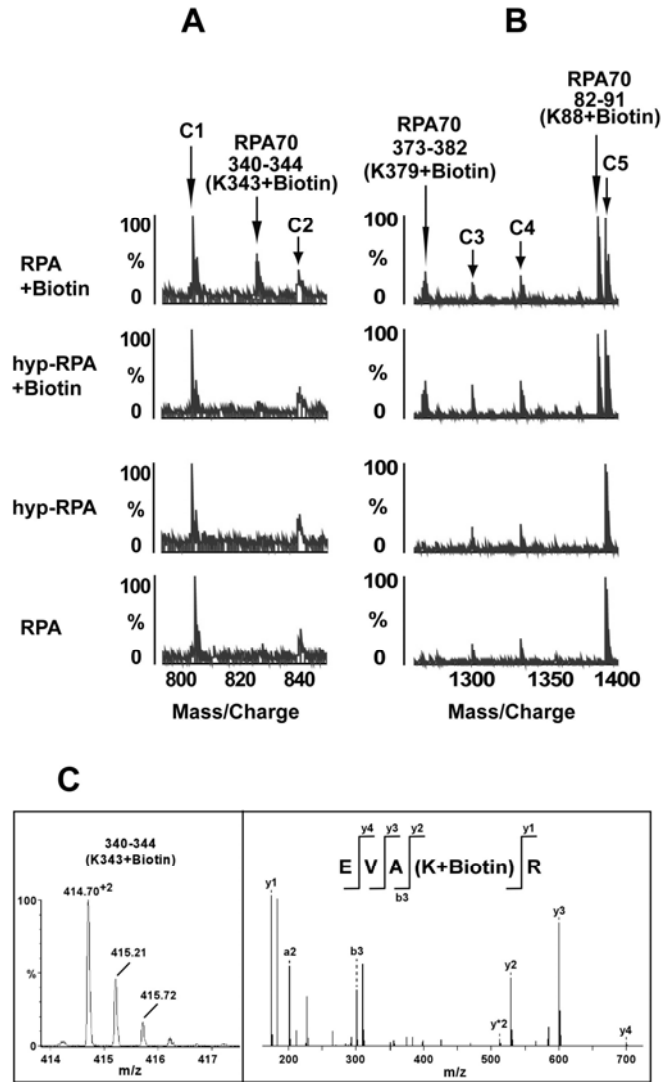


Figure 3-2. Mass spectrometric analysis of relative reactivity of lysines in RPA and hyp-RPA with NHS-biotin

(A) Representative segment of MALDI-TOF data to show that K343 was readily biotinylated in native RPA and not in hyp-RPA. (B) MALDI-TOF data illustrate the biotinylated peptide peaks (aa373-382 and aa82-91) were unchanged in RPA and hyp-RPA. C1-C5 were control peaks that serve as references for peak intensity. (C) MS/MS analysis of the doubly charged ion 414.70 representing the modified peptide aa340-344 with Q-ToF instrument reveals biotinylated K344. Left panel shows doubly charged parent ions; right panel shows fragmentation results.

modification patterns in native and hyp-RPA suggest that no significant global conformational changes occurred in RPA after hyperphosphorylation. However, the inaccessibility of residue K343 of RPA70 to NHS-biotin modification in hyp-RPA suggested occurrence of a limited structural re-arrangement involving the DBD-B domain containing K343 and the hyperphosphorylated N-terminus of RPA32. Because K343 is located in the DNA-binding cleft of DBD-B, adjacent to the L12 loop (aa 330-342), it is possible that the hyperphosphorylation resulted in at least partial shielding of the binding cleft of DBD-B from biotinylation via intramolecular interactions.

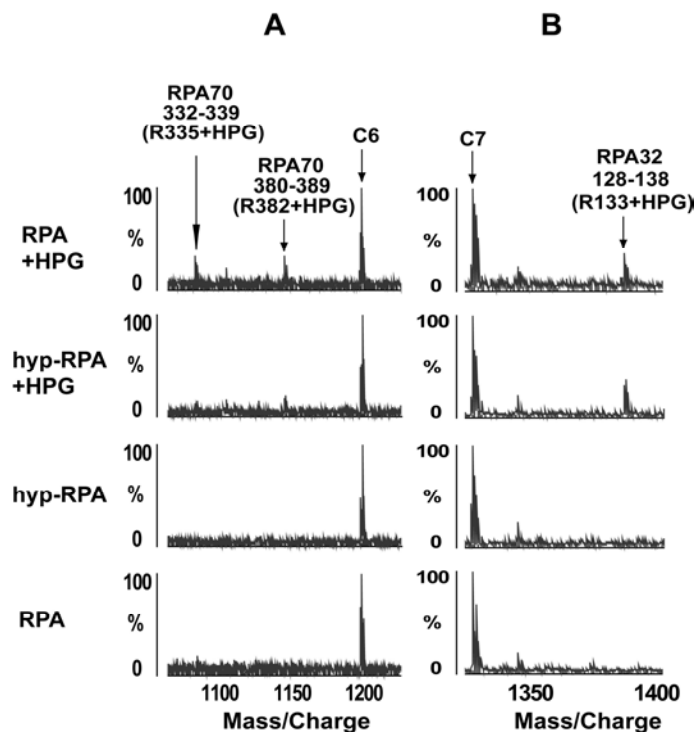


Figure 3-3. MALDI-TOF analysis of arginine modification in RPA and hyp-RPA with HPG (A) Representative segment of mass spectra to show that R335 and R382 in RPA70 were readily modified with HPG in native protein but were significantly protected from the modification in hyper-RPA. (B) Control data to demonstrate that the peak corresponding to the peptide (128-138) with R133 modified by HPG in RPA32 of RPA and hyp-RPA remained unchanged. Unmodified peptide peaks C6 and C7 serve as references for peak intensity.

We next examined the arginine modifications of RPA and hyp-RPA with HPG. HPG reacts specifically with the guanidyl group of arginine under mild conditions (pH 7-9, 25 °C) resulting in addition of a mass of 131 Daltons to the modified molecule (55). We observed modification of 18 arginines in the context of native RPA, of which 16 residues were identically susceptible to modification in hyper-RPA (Table 3-1, page 73). However, the following two peptide peaks: aa 332-339 (R335 + HPG) and aa 380-389 (R382 + HPG) of RPA70 were significantly diminished in hyper-RPA (Figure 3-3A, page 75). Figure 3-3B (page 75) depicts representative segments of MALDI-TOF spectra to show equal intensities of mass signal for the modifications at R133 of RPA32 in both RPA and hyp-RPA. Residue R335 is located in L12 loop of DBD-B, while R382 at the edge of the DNA-binding cleft of DBD-B adjacent to L45 (7,15). These results are fully consistent with those of biotinylation studies above.

### Fluorescence Measurements

RPA has eight tryptophan residues. The locations of the tryptophans are shown in Figure 3-4A (page 77): W197 and W212 in DBD-A, W361 and W414 in DBD-B, W442 and W528 in DBD-C, W107 in DBD-D, and W2 in the unstructured RPA32N. W212 and W361 have been shown to be located in the binding clefts of DBD-A and DBD-B, respectively, and to be involved in the interactions with ssDNA (7). W528 and W107 are located in the putative binding clefts of DBD-C and DBD-D, respectively, and were predicted to interact with ssDNA (11,12). Indeed, we previously found that the intrinsic fluorescence of all these in-cleft tryptophans were quenched upon ssDNA binding to RPA (unpublished data). If an intramolecular interaction involving any of the binding clefts occurs in hyp-RPA, the hyperphosphorylation could result in quenching of the tryptophan fluorescence in the clefts.

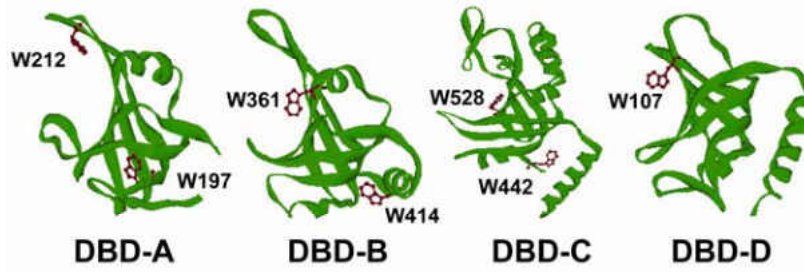
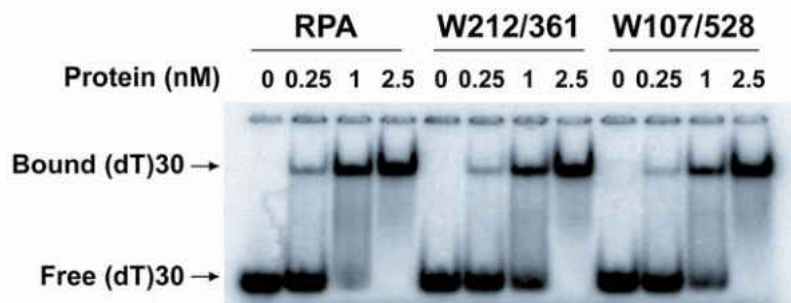
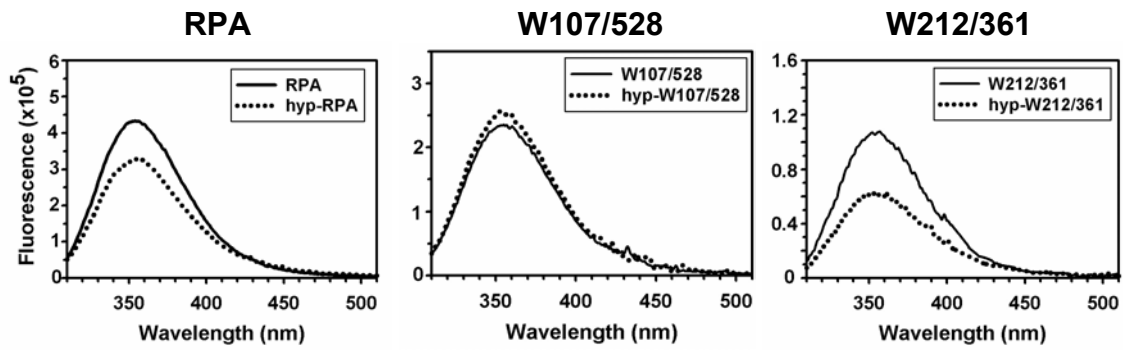
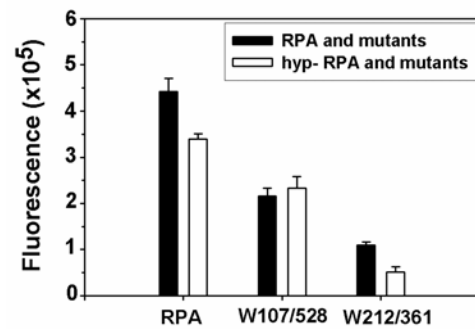
**A****B****C****D**

Figure 3-4. Measurements of the intrinsic fluorescence of tryptophans of RPA and its mutants (A) Structural exhibition of the tryptophans in RPA. The DBDs (16, 18, 21) are positioned by projecting the ssDNA binding clefts or the putative clefts in the same direction. The tryptophans of each DBD are marked. (B) Bindings of RPA and its mutants to oligo(dT)<sub>30</sub>. RPA or the mutants was incubated with 1 nM (dT)<sub>30</sub> at increasing concentrations at 25 °C for 15 minutes in 20 µL of the binding buffer. The binding products were analyzed on a 4% native polyacrylamide gel. The positions of the bound and free oligonucleotides are indicated. (C) Emission spectra of RPA, its mutants, and their hyperphosphorylated forms. The tryptophan fluorescence of the proteins (100 nM) was recorded from 310 nm to 500 nm at 25 °C with excitation at 295 nm in 200 µL of RPA buffer. The slit widths were set at 3 and 5 nm for excitation and emission beams, respectively. All the fluorescence measurement was presented in arbitrary units. (D) Constant wavelength analyses of RPA, its mutants, and their hyperphosphorylated forms. The intensity of tryptophan fluorescence of the proteins (100 nM) was recorded at 25 °C with excitation at 295 nm and emission at 355 nm in 200 µL of RPA buffer. Three data points with an integration time of 5 seconds and S.E.M. of 0.5% were collected for each measurement. Three measurements for each sample were performed independently. All the fluorescence measurement was presented in arbitrary units.

To dissect the roles of individual tryptophans in these interactions we prepared the following two mutant proteins. The W212/361 protein was obtained by preserving these two tryptophans and replacing the other 6 tryptophans with phenylalanines. Similarly, in the W107/528 mutant the residues W107 and W528 were preserved and the other tryptophans were substituted with phenylalanines. The binding of RPA mutants to ssDNA was tested to ensure that the mutants were active. Figure 3-4B (page 77) shows that both mutants bound a (dT)<sub>30</sub> with an affinity comparable to that of native RPA, indicating that the substitutions of tryptophans with phenylalanines had minimum effects on the binding activity of RPA. Then these mutants together with wild type RPA were subjected to a series of fluorescence measurements. As shown in Figures 3-4C and D (page 77), the tryptophan fluorescence of the wild type RPA decreased

upon hyperphosphorylation, suggesting that a structural re-arrangement in hyp-RPA occurred. However, no fluorescence changes were observed for the W107/528 mutant before and after hyperphosphorylation. By contrast, about one-half fluorescence was quenched for hyp-W212/361 (Figures 3-4C and D, page 77), suggesting that one of the two tryptophans was involved in the structural re-arrangement induced by hyperphosphorylation. Given that W361 is located in the proximity of K343 and R335 residues that were inaccessible to small chemical modification in hyp-RPA, we propose that the fluorescence of W361 was quenched due to the intramolecular interaction involving hyperphosphorylated RPA32N and binding cleft of DBD-B. The fluorescence quenching for hyp-W212/361 mutant was much more pronounced than that for wild type RPA. This suggests that more tryptophans in wild type RPA did not exhibit quenching upon hyperphosphorylation resulting in a higher fluorescence background for the wild type protein.

#### Limited Proteolysis of RPA and hyp-RPA

Partial proteolysis could be employed for probing conformational changes of a protein upon ligand binding or macromolecular interactions via domain mapping (56-58). Because proteolytic cleavage sites are usually located in the linking regions or loops between domains on the surface of a protein (59), structural variation of the protein with domain rearrangement may change the accessibility of some of the cleavage sites, resulting in altered proteolytic profiles. Previously, proteolytic experiments were carried out to show that RPA changed its conformation upon binding to ssDNA (56,57) or partial duplex DNA containing a 5'-protruding tail (57). Here we employed this method to compare the domain structures of native and hyperphosphorylated RPAs. The two proteins were partially digested with the fixed amount of chymotrypsin for the



indicated time periods (Figure 3-5, page 81). As shown in Figure 3-5A (page 81), chymotrypsin digestion revealed several peptide fragments that were more resistant in hyp-RPA compared to native RPA. Amino acid sequencing enabled us to determine that all these fragments were resulted from cleavages at the sites located in/near DBD-A and DBD-C of RPA70 (Figure 3-5B, page 81 and Table 3-2). In other words, these fragments contain no cleavages in DBD-B. Taken together, these partial hydrolysis data indicated that hyperphosphorylation of RPA32N could lead to conformational changes in RPA70 and the relatively resistance of DBD-B to partial proteolysis, which is consistent with the higher resolution results obtained from mass spectrometric foot-printing and tryptophan fluorescence studies.

Table 3-2. Identification of peptides of RPA or hyp-RPA digested by chymotrypsin

Peptide			
fragment	Size (kDa)	Origin	N-terminal sequence
1	51	RPA70	<sup>166</sup> GKAAG (major) <sup>a</sup> <sup>160</sup> GASKT (minor) <sup>a</sup>
2	46	RPA70	<sup>213</sup> SNSRG
3	36	RPA70	<sup>166</sup> GKAAG
4	34	RPA70	<sup>166</sup> GKAAG
5	20	RPA70	<sup>166</sup> GKAAG (major) <sup>a</sup> <sup>160</sup> GASKT (minor) <sup>a</sup>

- a. N-terminal sequencing gave two different sequences corresponding to two peptide fragments that migrated at the same position on SDS-PAGE. The amount of one peptide (major) was larger than the other (minor).

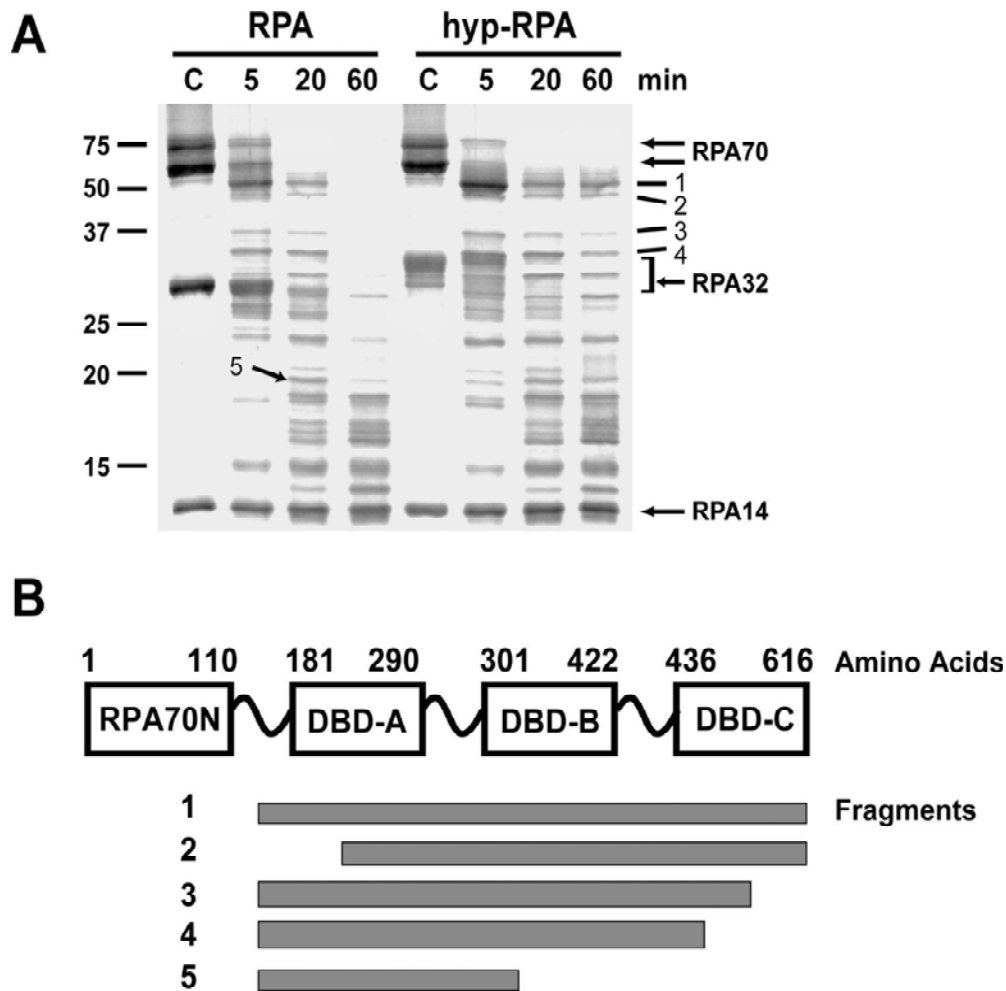


Figure 3-5. Partial proteolysis of RPA and hyp-RPA with chymotrypsin

(A) 4  $\mu$ g of RPA or hyp-RPA was digested with chymotrypsin (1:80) at room temperature for the times indicated. The reactions were then terminated, resolved by 14% SDS-PAGE, and visualized using SYPRO Ruby stain. Untreated RPA and hyp-RPA were loaded as controls (the lanes marked as 'C'). The molecular mass markers are shown on the left. Designations of individual fragments (dashes) and RPA subunits (arrows) are marked on the right. (B) Schematic map of proteolytic peptides generated upon RPA or hyp-RPA treatment with chymotrypsin. Domains are presented as boxes. The cleavage sites of chymotryptic peptide fragments are roughly shown.

### Bindings of RPA and hyp-RPA to ssDNA and Partial DNA Duplex

How the structural changes of RPA affect its activities may determine the role of RPA hyperphosphorylation in DNA metabolism. Our previous study showed that the K343 residue in DBD-B was directly involved in the RPA interaction with ssDNA (41). Because the 8-10 nt binding mode of RPA-ssDNA interaction has been suggested to be important for the initiation of replication, replication lagging strand synthesis, and nucleotide excision repair (2,60), here we examined the bindings of hyp-RPA and RPA to an oligo(dT)<sub>8</sub> by gel mobility shift assays (Figure 3-6A, page 83) and fluorescence anisotropy measurements (Table 3-3, page 85 and Figure 3-6B, page 83). Both assays revealed that hyp-RPA had a lower affinity for the (dT)<sub>8</sub> compared with the native RPA. The anisotropy data were best fitted using a one-site binding model as described previously (43) and the resulting dissociation constants were  $28.9 \pm 3.3$  nM and  $60.8 \pm 3.1$  nM for native and hyp-RPAs, respectively. To test whether this affinity change was specific to DNA sequence, an 8mer ssDNA with random sequences (CATCCTAC) also was used in our binding assays. Our results indicated similar reduction of the binding affinity for this DNA species (data not shown).

To examine how hyp-RPA changes its interaction with physiologically relevant DNA substrates, a set of partial DNA duplexes that mimic *in vivo* intermediates that occur during DNA replication and DNA repair was subject to the binding assays. For this purpose, partial DNA duplexes containing 5'-protruding 11 nucleotides (DNA-11) or 3'-protruding 10 nucleotides (DNA-10) were constructed. Figure 3-6C (page 83) shows the binding of a mixture of hyp-RPA and RPA to biotin-labeled DNA-11 and DNA-10 as analyzed by the pull-down assay with streptavidin-agarose and by Western blotting with an antibody against RPA32.

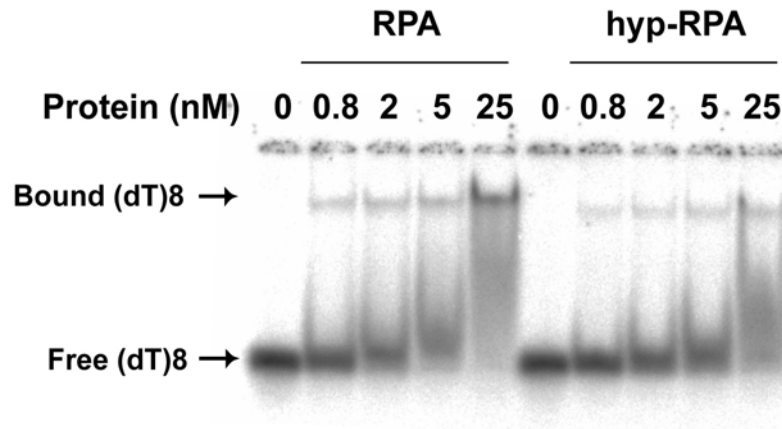
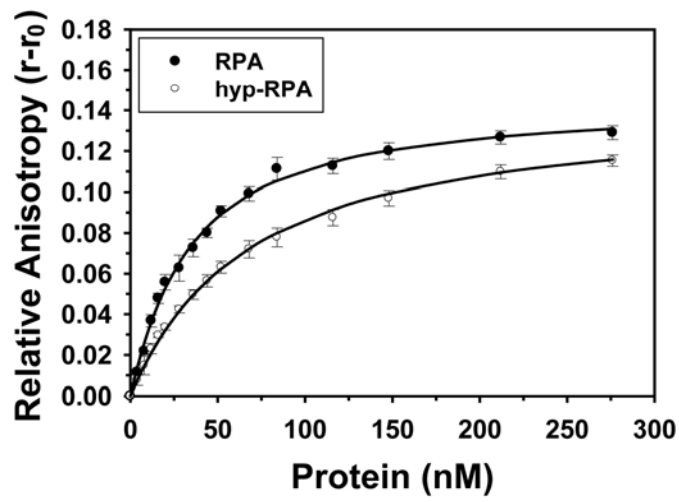
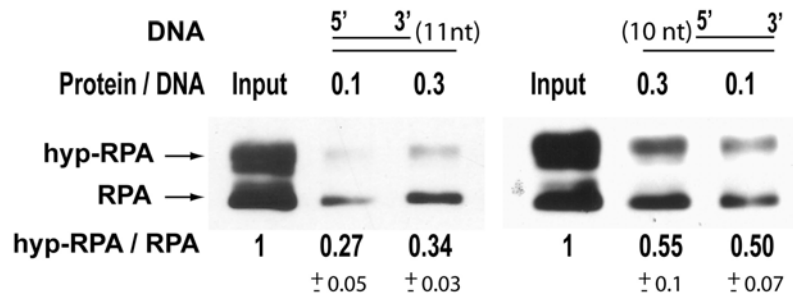
**A****B****C**

Figure 3-6. Bindings of RPA and hyp-RPA to oligo(dT)<sub>8</sub> and partial DNA duplexes

(A) RPA was incubated with 1 nM (dT)<sub>8</sub> at different molar ratios at 25 °C for 15 minutes in 20 μL of the binding buffer. The binding products were analyzed on a 4% native polyacrylamide gel. The positions of bound (dT)<sub>8</sub> and free (dT)<sub>8</sub> are indicated. (B) 10 nM 5'F-dT8 was titrated with RPA or hyp-RPA. The anisotropy was measured at 520 nm with excitation at 492 nm. The binding isotherms were best fitted to obtain the equilibrium dissociation constants ( $K_{d, \text{obs}}$ ) (44).

(C) Bindings of RPA and hyp-RPA to partial DNA duplexes containing 5'-protruding 11 nucleotides (DNA-11, left) or 3'-protruding 10 nucleotides (DNA-10, right). DNA-11 and DNA-10 were constructed by annealing a biotinylated 55mer with its complementary 44mer and 45mer, respectively. The biotinylated partial DNA duplex was incubated with a mixture of RPA and hyp-RPA. The protein bound to DNA was pulled down with streptavidin beads and detected by immunoblotting using an antibody against RPA32. The ratio of hyp-RPA to RPA in each binding was quantified.

The pull-down assay allowed the bindings of RPA and hyp-RPA to ssDNA to be monitored simultaneously and individually as the two forms of RPA protein were well separated on the SDS-PAGE. Thus, the binding of native RPA to ssDNA could serve as an internal control for determination of relative ssDNA binding efficiency of hyp-RPA. As shown in Figure 3-6C (page 83), the hyperphosphorylation led to a significant decrease in binding of RPA to the DNA-11 and DNA-10 substrates by about 70% and 50%, respectively, demonstrating that hyp-RPA had significantly lower affinity for these partial DNA duplexes than native RPA.

Table 3-3. Fluorescence anisotropy titration of RPA or hyp-RPA binding to 5'F-8mer

Protein (nM)	RPA		hyp-RPA	
	Mean	Std	Mean	Std
0	0	0	0	0
4	0.0115	0.0010	0.0076	0.0024
8	0.0217	0.0015	0.0147	0.0045
12	0.0367	0.0030	0.0230	0.0025
16	0.0478	0.0025	0.0295	0.0010
20	0.0557	0.0038	0.0335	0.0013
28	0.0627	0.0063	0.0423	0.0017
36	0.0726	0.0042	0.0496	0.0024
44	0.0800	0.0023	0.0564	0.0030
52	0.0906	0.0027	0.0631	0.0029
68	0.0991	0.0034	0.0720	0.0042
84	0.1112	0.0055	0.0778	0.0046
116	0.1126	0.0037	0.0874	0.0039
148	0.1199	0.0040	0.0969	0.0037
212	0.1266	0.0032	0.1098	0.0034
276	0.1289	0.0033	0.1152	0.0028

Mean represents the mean value of three measurements for each titration point;

Std represents the standard deviation.

## Discussion

As a single stranded DNA binding protein in eukaryotic cells, RPA interacts with a large variety of proteins required for DNA replication, repair, recombination, and DNA damage checkpoints, suggesting that RPA plays a regulatory role in the cellular DNA metabolic processes (2,24). In response to DNA damage, RPA undergoes hyperphosphorylation in cells carried out by the protein kinases of PIKK family (24). The hyperphosphorylation may play a role in modulating the cellular activities of RPA by altering its ability to interact with DNA and proteins and is critical to the success of cellular responses to protect against genotoxic stresses. In the present study, we characterized the structural alterations of RPA upon hyperphosphorylation by DNA-PK. Our findings provide new and important structural information regarding the changes introduced in the full length PRA trimer upon hyperphosphorylation of the protein.

Mass spectrometric foot-printing indicated that several basic residues were surface inaccessible in DBD-B of RPA 70 upon hyperphosphorylation of RPA32N. Tryptophan fluorescence studies suggested that W361 located in DBD-B was greatly quenched in response to hyperphosphorylation. Limited proteolysis revealed the structural changes in RPA70 and the relative resistance of DBD-B to the proteolytic digestion upon phosphorylation of RPA32N. Taken together, our findings suggest that a structural re-arrangement involving the RPA32N and a number of residues in the ssDNA binding cleft of DBD-B occurs after hyperphosphorylation of RPA (Figure 3-7, page 87). Given that the N-terminus of RPA32 becomes highly acidic (pI was estimated to be around 2) upon hyperphosphorylation, we propose that this structurally flexible protein segment of 40 residues could then be electrostatically attracted to the more positively charged basic region in the DNA binding cleft of DBD-B. This is supported by an estimation that

the fragment aa 330-345 in the DNA binding cleft of DBD-B, where K343 and R335 are located, is more basic ( $pI = \sim 12$ ) than the equivalent regions of other DBDs.

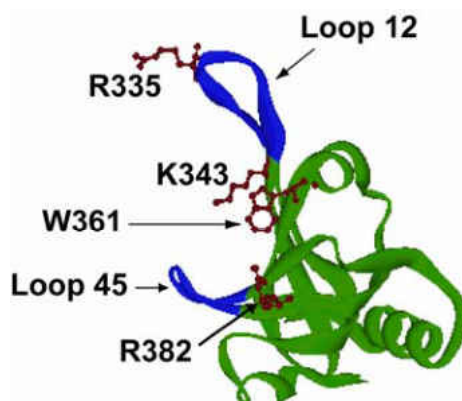


Figure 3-7. DBD-B structure with highlighted residues Arg-335, Lys-343, Trp-361 and Arg-382 in brown that could directly interact with hyperphosphorylated RPA32N. Two loops, Loop12 and Loop45, are indicated in blue. This figure was drawn based on the RPA70B crystal structure reported by Bochkareva *et al.* (*EMBO J.* 20, 612-618, PDB ID# 1FGU).

A previous NMR study showed that a synthesized acidic peptide mimicking hyperphosphorylated RPA32N was able to establish electrostatic interactions with the basic cleft of the purified DBD-F (RPA70N) domain fragment (RPA70<sub>1-168</sub>). However, in the study protein fragments rather than the full length RPA trimer were used (38). In the context of the full length protein DBD-B is located closer than DBD-F to interact with hyp-RPA32N. Indeed, based on the direction of the backbone at amino acid 45 of RPA32 in a crystal structure of RPA trimerization core (DBD-C/DBD-D/RPA14) unphosphorylated RPA32N was predicted to be located in the vicinity of the putative ssDNA-binding cleft of DBD-C (11). RPA32N in this position is closer to DBD-B than to DBD-F, and thus hyperphosphorylation of RPA32N is more likely to have effects on the closely positioned DBD-B rather than on the more distant DBD-F. Of note, our



results implicate a possible interaction of DBD-B with RPA32N without major structural changes in the RPA trimer.

A possible immediate effect of the hyperphosphorylation-induced shielding of the ssDNA-binding cleft of DBD-B from molecular access on RPA function is the inhibition of RPA binding to ssDNA, particularly short ssDNA. Indeed, we observed that hyperphosphorylation of RPA could affect the protein's ability to bind short oligonucleotides. It has been generally accepted that RPA binds to ssDNA in three modes in terms of the ssDNA lengths, 8-10 nt, 13-22 nt, and 30 nt, respectively (2,11). Of these modes, the binding to 8-10 nt (2,7,11,61) or short ssDNA tails of partial DNA duplexes (57,62,63) were exclusively carried out by DBD-A and DBD-B, while the other two modes required additional domains: DBD-C and DBD-C/DBD-D. Our results suggest that the potential intramolecular interaction induced by RPA32N hyperphosphorylation may compete with ssDNA binding to DBD-B. Such competition may provide a regulatory mechanism for modulating the RPA activities. However, the effect of the hyperphosphorylation of RPA appeared to be limited to the short ssDNA binding. It has been generally reported that the dissociation constant for the interaction of RPA with 10 nt or shorter oligonucleotides was in the order of  $10^{-7}$  M, while the dissociation constant for the RPA interaction with ssDNA longer than 15 nt was in the order of  $10^{-10}$  to  $10^{-9}$  M (64). Because DBD-B is believed to participate in all modes of ssDNA binding, it is likely that the two- to three-order higher affinity of RPA to longer ssDNA may allow DBD-B to predominately bind ssDNA, so that the effect of the hyperphosphorylation becomes minimal. Indeed, our results (data not shown) and also those from others showed that the hyperphosphorylation had negligible effect on the RPA binding to the ssDNA of 30 nt or longer lengths (20,38).

In contrast, our results indicate significant competition between hyperphosphorylation-elicited DBD-B shielding (probably due to the hyp-RPA32N and DBD-B interaction) and DBD-B binding to (dT)<sub>8</sub> or partial DNA duplexes with a short ssDNA tail. Such data suggest that the association constant for the possible intramolecular interaction causing DBD-B shielding could be in the order of  $10^7 \text{ M}^{-1}$ . Interestingly, interactions of RPA with these short ssDNA or partial DNA duplexes with short ssDNA tails were believed to play a role in the initiation of DNA replication and replicative lagging strand synthesis (2,38,60,65). Therefore, it is likely that the hyperphosphorylation of RPA could disrupt this process. Consistently, Vassin et al. (32) recently reported that a hyperphosphorylation-mimic RPA failed to associate with replication centers *in vivo*. Similarly, the DBD-B-engaged intramolecular interactions of RPA due to the hyperphosphorylation in N-terminus of RPA32 could also affect the RPA-protein interactions (with dissociation constants in the order of  $10^{-7} \text{ M}$ ) involved in various DNA metabolic pathways.

## References

1. Wold, M. S. (1997) *Annu Rev Biochem* **66**, 61-92
2. Iftode, C., Daniely, Y., and Borowiec, J. A. (1999) *Crit Rev Biochem Mol Biol* **34**(3), 141-180
3. Shivji, M. K., Podust, V. N., Hubscher, U., and Wood, R. D. (1995) *Biochemistry* **34**(15), 5011-5017
4. Barr, S. M., Leung, C. G., Chang, E. E., and Cimprich, K. A. (2003) *Curr Biol* **13**(12), 1047-1051
5. Dart, D. A., Adams, K. E., Akerman, I., and Lakin, N. D. (2004) *J Biol Chem* **279**(16), 16433-16440
6. Jacobs, D. M., Lipton, A. S., Isern, N. G., Daughdrill, G. W., Lowry, D. F., Gomes, X., and Wold, M. S. (1999) *J Biomol NMR* **14**(4), 321-331
7. Bochkarev, A., Pfuetzner, R. A., Edwards, A. M., and Frappier, L. (1997) *Nature* **385**(6612), 176-181
8. Brill, S. J., and Bastin-Shanower, S. (1998) *Mol Cell Biol* **18**(12), 7225-7234
9. Arunkumar, A. I., Stauffer, M. E., Bochkareva, E., Bochkarev, A., and Chazin, W. J. (2003) *J Biol Chem* **278**(42), 41077-41082
10. Bochkareva, E., Korolev, S., and Bochkarev, A. (2000) *J Biol Chem* **275**(35), 27332-27338
11. Bochkareva, E., Korolev, S., Lees-Miller, S. P., and Bochkarev, A. (2002) *Embo J* **21**(7), 1855-1863
12. Bochkarev, A., Bochkareva, E., Frappier, L., and Edwards, A. M. (1999) *Embo J* **18**(16), 4498-4504
13. Bochkareva, E., Frappier, L., Edwards, A. M., and Bochkarev, A. (1998) *J Biol Chem* **273**(7), 3932-3936
14. Mer, G., Bochkarev, A., Gupta, R., Bochkareva, E., Frappier, L., Ingles, C. J., Edwards, A. M., and Chazin, W. J. (2000) *Cell* **103**(3), 449-456
15. Bochkareva, E., Belegu, V., Korolev, S., and Bochkarev, A. (2001) *Embo J* **20**(3), 612-618
16. Bochkarev, A., and Bochkareva, E. (2004) *Curr Opin Struct Biol* **14**(1), 36-42

17. Kerr, I. D., Wadsworth, R. I., Cubeddu, L., Blankenfeldt, W., Naismith, J. H., and White, M. F. (2003) *Embo J* **22**(11), 2561-2570
18. Din, S., Brill, S. J., Fairman, M. P., and Stillman, B. (1990) *Genes Dev* **4**(6), 968-977
19. Dutta, A., and Stillman, B. (1992) *Embo J* **11**(6), 2189-2199
20. Oakley, G. G., Patrick, S. M., Yao, J., Carty, M. P., Turchi, J. J., and Dixon, K. (2003) *Biochemistry* **42**(11), 3255-3264
21. Liu, V. F., and Weaver, D. T. (1993) *Mol Cell Biol* **13**(12), 7222-7231
22. Zernik-Kobak, M., Vasunia, K., Connelly, M., Anderson, C. W., and Dixon, K. (1997) *J Biol Chem* **272**(38), 23896-23904
23. Block, W. D., Yu, Y., and Lees-Miller, S. P. (2004) *Nucleic Acids Res* **32**(3), 997-1005
24. Binz, S. K., Sheehan, A. M., and Wold, M. S. (2004) *DNA Repair (Amst)* **3**(8-9), 1015-1024
25. Niu, H., Erdjument-Bromage, H., Pan, Z. Q., Lee, S. H., Tempst, P., and Hurwitz, J. (1997) *J Biol Chem* **272**(19), 12634-12641
26. Lee, S. H., and Kim, D. K. (1995) *J Biol Chem* **270**(21), 12801-12807
27. Treuner, K., Okuyama, A., Knippers, R., and Fackelmayer, F. O. (1999) *Nucleic Acids Res* **27**(6), 1499-1504
28. Nuss, J. E., Patrick, S. M., Oakley, G. G., Alter, G. M., Robison, J. G., Dixon, K., and Turchi, J. J. (2005) *Biochemistry* **44**(23), 8428-8437
29. Pan, Z. Q., Amin, A. A., Gibbs, E., Niu, H., and Hurwitz, J. (1994) *Proc Natl Acad Sci U S A* **91**(18), 8343-8347
30. Shao, R. G., Cao, C. X., Zhang, H., Kohn, K. W., Wold, M. S., and Pommier, Y. (1999) *Embo J* **18**(5), 1397-1406
31. Brush, G. S., Anderson, C. W., and Kelly, T. J. (1994) *Proc Natl Acad Sci U S A* **91**(26), 12520-12524
32. Vassin, V. M., Wold, M. S., and Borowiec, J. A. (2004) *Mol Cell Biol* **24**(5), 1930-1943
33. Park, J. S., Park, S. J., Peng, X., Wang, M., Yu, M. A., and Lee, S. H. (1999) *J Biol Chem* **274**(45), 32520-32527
34. Jackson, D., Dhar, K., Wahl, J. K., Wold, M. S., and Borgstahl, G. E. (2002) *J Mol Biol* **321**(1), 133-148

35. Abramova, N. A., Russell, J., Botchan, M., and Li, R. (1997) *Proc Natl Acad Sci U S A* **94**(14), 7186-7191
36. Wu, X., Shell, S.M., and Zou, Y. (2005) *Oncogene* **24**, 4728-4735
37. Patrick, S. M., Oakley, G. G., Dixon, K., and Turchi, J. J. (2005) *Biochemistry* **44**(23), 8438-8448
38. Binz, S. K., Lao, Y., Lowry, D. F., and Wold, M. S. (2003) *J Biol Chem* **278**(37), 35584-35591
39. Fried, L. M., Koumenis, C., Peterson, S. R., Green, S. L., van Zijl, P., Allalunis-Turner, J., Chen, D. J., Fishel, R., Giaccia, A. J., Brown, J. M., and Kirchgessner, C. U. (1996) *Proc Natl Acad Sci U S A* **93**(24), 13825-13830
40. Yang, Z. G., Liu, Y., Mao, L. Y., Zhang, J. T., and Zou, Y. (2002) *Biochemistry* **41**(43), 13012-13020
41. Shell, S. M., Hess, S., Kvaratskhelia, M., and Zou, Y. (2005) *Biochemistry* **44**(3), 971-978
42. Hey, T., Lipps, G., and Krauss, G. (2001) *Biochemistry* **40**(9), 2901-2910
43. Liu, Y., Yang, Z., Utzat, C. D., Liu, Y., Geacintov, N. E., Basu, A. K., and Zou, Y. (2005) *Biochem J* **385**(Pt 2), 519-526
44. Zou, Y., Bassett, H., Walker, R., Bishop, A., Amin, S., Geacintov, N. E., and Van Houten, B. (1998) *J Mol Biol* **281**(1), 107-119
45. Boubnov, N. V., and Weaver, D. T. (1995) *Mol Cell Biol* **15**(10), 5700-5706
46. Gately, D. P., Hittle, J. C., Chan, G. K., and Yen, T. J. (1998) *Mol Biol Cell* **9**(9), 2361-2374
47. Oakley, G. G., Loberg, L. I., Yao, J., Risinger, M. A., Yunker, R. L., Zernik-Kobak, M., Khanna, K. K., Lavin, M. F., Carty, M. P., and Dixon, K. (2001) *Mol Biol Cell* **12**(5), 1199-1213
48. Smith, G. C., and Jackson, S. P. (1999) *Genes Dev* **13**(8), 916-934
49. Henriksen, L. A., Carter, T., Dutta, A., and Wold, M. S. (1996) *Nucleic Acids Res* **24**(15), 3107-3112
50. Carty, M. P., Zernik-Kobak, M., McGrath, S., and Dixon, K. (1994) *Embo J* **13**(9), 2114-2123
51. Bennett, K. L., Matthiesen, T., and Roepstorff, P. (2000) *Methods Mol Biol* **146**, 113-131

52. Suckau, D., Mak, M., and Przybylski, M. (1992) *Proc Natl Acad Sci U S A* **89**(12), 5630-5634
53. Leite, J. F., and Cascio, M. (2002) *Biochemistry* **41**(19), 6140-6148
54. Kvaratskhelia, M., Miller, J. T., Budihas, S. R., Pannell, L. K., and Le Grice, S. F. (2002) *Proc Natl Acad Sci U S A* **99**(25), 15988-15993
55. Yamasaki, R. B., Vega, A., and Feeney, R. E. (1980) *Anal Biochem* **109**(1), 32-40
56. Gomes, X. V., Henriksen, L. A., and Wold, M. S. (1996) *Biochemistry* **35**(17), 5586-5595
57. Pestryakov, P. E., Weisshart, K., Schlott, B., Khodyreva, S. N., Kremmer, E., Grosse, F., Lavrik, O. I., and Nasheuer, H. P. (2003) *J Biol Chem* **278**(19), 17515-17524
58. Heyduk, E., and Heyduk, T. (1994) *Biochemistry* **33**(32), 9643-9650
59. Zappacosta, F., Pessi, A., Bianchi, E., Venturini, S., Sollazzo, M., Tramontano, A., Marino, G., and Pucci, P. (1996) *Protein Sci* **5**(5), 802-813
60. Mass, G., Nethanel, T., Lavrik, O. I., Wold, M. S., and Kaufmann, G. (2001) *Nucleic Acids Res* **29**(18), 3892-3899
61. Blackwell, L. J., and Borowiec, J. A. (1994) *Mol Cell Biol* **14**(6), 3993-4001
62. Lavrik, O. I., Kolpashchikov, D. M., Weisshart, K., Nasheuer, H. P., Khodyreva, S. N., and Favre, A. (1999) *Nucleic Acids Res* **27**(21), 4235-4240
63. Pestryakov, P. E., Khlimankov, D. Y., Bochkareva, E., Bochkarev, A., and Lavrik, O. I. (2004) *Nucleic Acids Res* **32**(6), 1894-1903
64. Kim, C., Paulus, B. F., and Wold, M. S. (1994) *Biochemistry* **33**(47), 14197-14206
65. Lao, Y., Gomes, X. V., Ren, Y., Taylor, J. S., and Wold, M. S. (2000) *Biochemistry* **39**(5), 850-859

## CHAPTER 4

### DNA DAMAGE RESPONSES IN PROGEROID SYNDROMES ARISING FROM DEFECTIVE MATURATION OF PRELAMIN A

#### Abstract

The genetic diseases Hutchinson-Gilford progeria syndrome (HGPS) and restrictive dermopathy (RD) arise from accumulation of farnesylated prelamin A due to defects in the lamin A maturation pathway. Both of these diseases exhibit symptoms that can be viewed as accelerated aging. The mechanism by which accumulation of farnesylated prelamin A leads to these accelerated aging phenotypes is not understood. Here, we present evidence that in HGPS and RD fibroblasts, DNA damage checkpoints are persistently activated due to the compromise of genomic integrity. Inactivation of checkpoint kinases ATM and ATR in these patient cells can partially overcome their early replication arrest. Treatment of patient cells with a protein farnesyltransferase inhibitor (FTI) did not result in reduction of DNA double strand breaks and damage checkpoint signaling, although the treatment significantly reversed the aberrant shape of their nuclei. This suggests that DNA damage accumulation and aberrant nuclear morphology are independent phenotypes arising from prelamin A accumulation in these progeroid syndromes. Because DNA damage accumulation is an important contributor to the symptoms of HGPS, our results call into question on the possibility of treatment of HGPS with FTIs alone.

## Introduction

Hutchinson-Gilford progeria syndrome (HGPS) is a severe childhood disease characterized by accelerated aging that is caused by a *de novo* point mutation (1824C → T) in the *LMNA* gene that encodes lamin A and the splice variant lamin C and germ cell-specific lamin C2 (De Sandre-Giovannoli et al., 2003; Eriksson et al., 2003). These lamins are intermediate filament proteins composing the nuclear lamina, a scaffold underlying the inner nuclear membrane that structurally supports the nucleus and organizes chromatin (Goldman et al., 2002). The point mutation (1824C → T) of *LMNA* results in defective maturation of lamin A from its precursor prelamin A by causing a deletion of 50 amino acids near the C terminus of prelamin A that contains an endoprotease (*Zmpste 24*) cleavage site required for the proteolytic maturation of lamin A (Eriksson et al., 2003). *Zmpste 24* mutation leads to another progeroid disorder, restrictive dermopathy (RD) that is neonatally lethal (Navarro et al., 2005). Loss of *Zmpste 24* activity arrests the processing of prelamin A at a stage similar to HGPS, although a unique truncated prelamin A (progerin) is accumulated in HGPS cells. Based on the prior elucidation of the prelamin A processing pathway (Sinensky et al., 1994b), these mutations are predicted to result in accumulation of farnesylated and carboxymethylated prelamin A. These two diseases have been suggested to be manifestations of the same cellular problem to different degrees (Misteli and Scaffidi, 2005). Although the molecular mechanisms by which these mutations result in premature aging are far from full understanding, Liu *et al.* (Liu et al., 2005a) recently reported that human HGPS fibroblasts and *Zmpste24*-deficient mouse embryonic fibroblasts (MEFs) showed increased DNA damage and repair defects. In addition, Varela *et al.* (Varela et al., 2005) showed that *Zmpste24* deficiency in mouse elicits the upregulation of p53 target genes.



These studies suggest that the genomic integrity was compromised in HGPS and RD cells due to the accumulation of progerin and prelamin A, respectively.

Accumulation of DNA damage may activate DNA damage and replication checkpoints that attenuate cell cycle progression and arrest replication, thereby preventing DNA lesions from being converted to inheritable mutations (Li and Zou, 2005). Two protein kinases of the phosphoinositide 3-kinase-like kinase (PIKK) family, ATM and ATR, play the central roles in initiating the damage and replication checkpoints (Abraham, 2001; Li and Zou, 2005). ATM is activated primarily in response to DNA double-strand breaks (DSBs) (Shiloh, 2003), whereas ATR is activated by a broad range of DNA damage and replication interference (Abraham, 2001; Li and Zou, 2005). Upon activation, ATM and ATR phosphorylate two major signal-transducing kinases Chk1 and Chk2, which in turn regulate downstream targets, such as Cdc25A, Cdc25C, and p53, to control cell cycle progression and DNA synthesis (Li and Zou, 2005; Sancar et al., 2004). It has been reported that in telomere-initiated senescence, a checkpoint response similar to that in the cells with DNA-damage stress was activated involving ATM, ATR, and downstream kinases Chk1 and Chk2 (d'Adda di Fagagna et al., 2003; von Zglinicki et al., 2005). Kinase inactivation experiments showed that this signaling pathway has to be maintained in order to keep cells in a senescent state (d'Adda di Fagagna et al., 2003; von Zglinicki et al., 2005). DNA damage accumulation and responses resulting from repair defects may lead to phenotypes associated with premature aging and may have causal roles in normal aging (Lombard et al., 2005). Furthermore, evidence has been presented that progerin expression occurs during the normal aging process (Scaffidi and Misteli, 2006). Given the similarities between these progeroid syndromes and normal aging, we speculated that the same signaling pathway of DNA damage response is activated in HGPS and RD cells as in telomere-initiated senescence.

Several recent studies have shown that inhibition of prelamin A farnesylation by protein farnesyltransferase inhibitors reversed the aberrant nuclear morphology of progeroid cells (Capell et al., 2005; Mallampalli et al., 2005; Toth et al., 2005). However, the important question as to whether treatment with farnesyltransferase inhibitors concurrently restores the genomic integrity in these cells remains to be addressed.

In this study, we report that DNA damage checkpoints were constantly activated in HGPS and RD cells due to DNA repair defects. Strikingly, inactivation of ATR and ATM by specific kinase inhibitor or RNAi partially restored DNA replication in HGPS cells. Also importantly, treatment of the patient cells with a protein farnesyltransferase inhibitor (FTI) was found to have no effect on DNA damage in these cells.

## Materials and Methods

### Cell Culture and Drug Treatments

Fibroblasts from a HGPS patient with the point mutation 1824 C → T were obtained from the Coriell Cell Repository (no. AG11513A). Human RD fibroblasts were a gift from Dr. J.H. Miner (Washington University School of Medicine, St Louis, MO). BJ cells and HeLa cells were purchased from American Type Culture Collection (ATCC, nos. CRL-2522 and CCL-2, respectively). All cultures were maintained in DMEM (for RD cells and HeLa cells) or EMEM (for HGPS cells and BJ cells) supplemented with 10% FBS and antibiotics (50 units/ml penicillin and 50 µg/ml streptomycin) at 37°C under an atmosphere containing 5% CO<sub>2</sub>. For FTI treatment, cells were cultured to 70% confluence, and treated with 5 µM FTI L-744832 (Biomol, Plymouth Meeting, PA) daily for 72 hours before harvest. For the inactivation of ATR and ATM, cells

were treated with caffeine at a final concentration of 5 mM for at least 2 hours before further analysis.

### Immunofluorescence Microscopy

Cells were grown on coverslips to 70% confluence, washed twice with PBS, and then fixed with cold methanol (-20°C) or with 1% formaldehyde followed by permeabilization with 0.5% Triton X-100. The fixed cells were blocked with 15% FBS and then incubated with a primary antibody against ATR (rabbit or mouse, GeneTex), ATM (mouse, GeneTex), GFP (rabbit, ABCAM), or  $\gamma$ -H2AX (mouse, Stressgen). After three washes with PBS/1% Tween 20, the cells were incubated with a secondary antibody Alexa fluor 488-conjugated donkey anti-rabbit IgG or Alexa fluor 568-conjugated goat anti-mouse IgG (Molecular Probes). Nuclei were counterstained with DAPI. Cells were visualized by using a Zeiss Axioscope microscope.

### Transfection of Plasmids and siRNA

HeLa cells grown on coverslips were transiently transfected with plasmid pEGFP-LA $\Delta$ 50, pEGFP-LA $\Delta$ 50-SSIM (both were gifts from Dr. Francis Collins, NIH), control plasmid pEGFP, or empty parent vector using GeneJammer transfection reagent (Stratagene) following manufacture's instruction. Twenty-four hours post-transfection, the cells were processed differently for the following experiments. For examining the activation of ATM and ATR, the cells were irradiated with 20 J/m<sup>2</sup> UV or mock treated. Two hours post-treatment, the cells were processed for immunofluorescence microscopy as described above. To measure the amount of  $\gamma$ -H2AX, the cells were harvested and lysed for Western blotting as described below. For detecting

the formation of  $\gamma$ -H2AX foci, the cells were fixed with 1% formaldehyde and processed for immunofluorescence.

For the knockdown of ATR and ATM by RNAi, the cells were transfected with ATR siRNA and ATM siRNA (Wu et al., 2006), or GFP siRNA as a control using TransIT-TKO transfection reagent (Mirus) following manufacture's instruction. Further analyses were performed 72 hours after transfection.

### DNA Synthesis Assay

DNA synthesis was assayed by the method of thymidine incorporation modified from Shao et al. (Shao et al., 1997). Briefly,  $2 \times 10^5$  cells were seeded in a 35-mm dish 24 hours before pulse-labeling with 0.5  $\mu$ Ci/ml [methyl- $^3$ H]thymidine (Amersham Biosciences) for 30 minutes. The cells were then rinsed with PBS three times and harvested by lysis with 5% trichloroacetic acid (TCA) at 4 °C for 1 hour. Cell lysates were subjected to filtering using Whatman glass microfibre filters and a vacuum manifold. The filters were washed twice with 5 ml of 5% TCA, once with 70% ethanol, and then dried. The radioactivity of each sample was counted by liquid scintillation.

### Western Blotting

Cells cultured in 100-mm dishes were grown to 70% confluence and then trypsinized. Cell number was counted by using a hemacytometer. The cells were centrifuged at 1500 rpm for 5 minutes and washed twice with PBS. Cell pellet was lysed in 2 x SDS gel loading buffer and volumes corresponding to  $5 \times 10^6$  cells were subjected to SDS-PAGE. Immunoblotting was carried out as previously described (Liu et al., 2005b) with primary antibodies directed against

p53 (Santa Cruz), p53 (ser-15) (Cell Signaling), Chk2 (thr-68) (Cell Signaling), Chk1 (ser-345) (Santa Cruz),  $\gamma$ -H2AX (Bethyl), GAPDH (Santa Cruz), LaminA/C (Santa Cruz), and  $\beta$ -actin (Santa Cruz). The rabbit anti-mouse prelamin A antiserum used was generated specifically against the carboxyl-terminal prelamin A and cannot bind mature lamin A or lamin C (Sinensky et al., 1994a).

### Comet Assay

The neutral comet assay was performed to assess DNA strand breaks in cells. The first layer of agarose on microscope slides were prepared by dipping the slides into 1% normal melting point agarose (NMA) followed by drying. Eighty-five microliters of 0.5% low melting point agarose (LMA) containing  $4 \times 10^5$  cells was made by mixing 10  $\mu$ l of cell suspension with 75  $\mu$ l of LMA. The mixture was then poured onto the pre-coated slides. Slides were immersed in freshly prepared ice-cold buffer (2.5 M NaCl, 100 mM Na<sub>2</sub>EDTA, 10 mM Tris-HCl, 1% Triton X-100, pH 10) to lyse the cells for at least 1 hour at 4 °C in the dark. The slides were then placed in the alkaline buffer (0.3 M NaOH, 1 mM EDTA, pH > 13) for 30 minutes for DNA unwinding. The slides were equilibrated in TBE buffer for 5 minutes twice followed by electrophoresis at 1 volt/cm in TBE buffer for 10 minutes. The slides were then dipped in 70% ethanol for 5 minutes and dried at room temperature for 1 hour. Fifty microliters of 600  $\mu$ M DAPI was used for staining. All steps described above were conducted under dimmed light to prevent additional DNA damage. The quantification of the comets was conducted for randomly chosen 50 cells, and DNA damage was expressed as the percentage of DNA in tail.

## Results

### Early Replication Arrest of RD Cells and HGPS Cells

Results from our studies (Figure 4-3, page 105) and others (Liu et al., 2005a; Varela et al., 2005) showed that a considerable amount of phosphorylated histone H2AX ( $\gamma$ -H2AX), a molecular marker for DNA double-strand breaks (DSBs) (Sedelnikova et al., 2002), formed in HGPS and RD cells. This indicates that DNA damage accumulates in patient cells. To determine the status of DNA replication in these cells, a DNA replication assay with replicative incorporation of [methyl- $^3$ H] thymidine was performed. As shown in Figure 4-1,

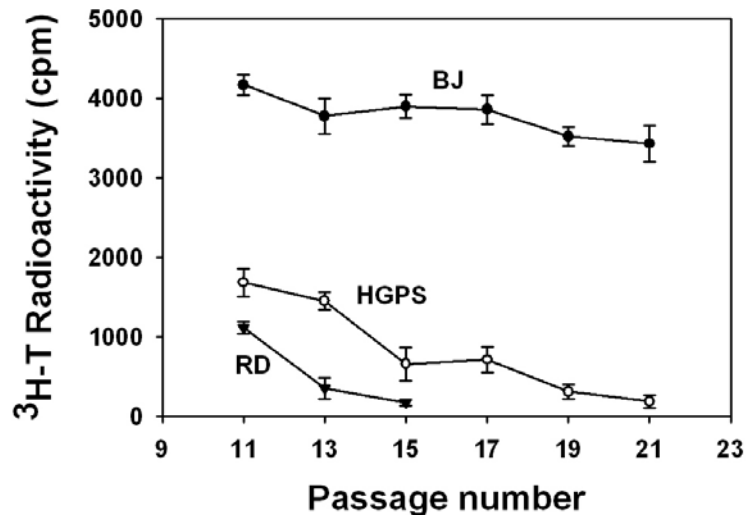


Figure 4-1. Early replication arrest of HGPS and RD cells

The replication assay was carried out with [methyl- $^3$ H] thymidine labeling as described in Materials and Methods. Symbols represent radioactivity values as follows: ● for BJ cells; ○ for HGPS cells; and ▼ for RD cells. The values were calculated from three independent experiments. Error bars represent standard deviations.

DNA synthesis in the HGPS and RD cells of passage 11 occurred at rates more than 2-fold slower than that in BJ cells, a non-transformed human diploid fibroblast cell line. Moreover, replicative capacity was lost at passage 15 for RD cells and at passage 21 for HGPS cells (Figure

4-1, page 101) in contrast to the more typical replicative behavior of BJ cells that exhibit many more passages before undergoing replicative senescence (Steinert et al., 2000). This premature replicative senescence of the patient cells is consistent with the previous reports that the percentage of S-phase cells in *Zmpste24*-deficient mouse embryonic fibroblasts (MEFs) was lower than that in normal MEFs (Liu et al., 2005a; Varela et al., 2005).

#### Activation of ATM and ATR in RD Cells and HGPS Cells

The premature replicative senescence of HGPS and RD cells suggested that G1/S and/or intra-S checkpoints were likely activated. To test this notion, we assessed the activation of ATM and ATR, two central initiators of DNA damage checkpoints (McGowan and Russell, 2004), in HGPS and RD cells using the method of immunofluorescence microscopy. In BJ cells, the majority of ATM was homogenously distributed in the nucleus (Figure 4-2A, page 104). The treatment of BJ cells with camptothecin (CPT), a radiomimetic agent widely used to induce DSBs and activate ATM in cells (Shiloh, 2003), caused ATM focus formation in the nuclei (Figure 4-2A, page 104). Interestingly, a very similar pattern of ATM nuclear focus formation was observed in HGPS and RD cells even without treatment with CPT, suggesting that ATM was activated in these cells (Figure 4-2A, page 104). By contrast, a different pattern of activation was observed for ATR in these patient cells. In unstressed BJ cells, ATR was mainly localized in cytoplasm, with little or no nuclear staining (Figure 4-2B, page 104). After UV irradiation, a known DNA damaging stress that induces ATR activation (Abraham, 2001), ATR translocated from cytoplasm into the nucleus. Interestingly, while the majority of ATR was in the nuclei of untreated RD cells, only part of ATR was distributed in the nuclei of HGPS cells and formed large foci or aggregates (Figure 4-2B, page 104). The nuclear distribution of ATR in RD and

HGPS cells suggests its activation in these cells, which is confirmed by the phosphorylation of its primary substrate Chk1 (see below). To verify that nuclear translocation of checkpoint kinases in the patient cells arises from expression of prelamin A, HeLa cells were transfected with a plasmid encoding progerin (LA $\Delta$ 50) for immunofluorescence analysis. As shown in Figure 4-2C (page 104), the majority of ATR was in cytoplasm in HeLa cells transfected with an empty parent vector. In contrast, ATR was mainly located in nuclei, forming large foci in the HeLa cells transfected with the LA $\Delta$ 50-expression plasmid. This indicated that the nuclear translocation of checkpoint kinases was indeed induced by the presence of progerin. Thus, DNA damage in HGPS and RD cells, arising from prelamin A accumulation, results in nuclear redistribution of ATR and ATM, consistent with activation of cell cycle checkpoints.

To confirm the presence of checkpoint response pathways in HGPS and RD cells, we next examined the activation of downstream signal-transducers Chk1 and Chk2 and the effector p53 by assessing their phosphorylation status at specific sites (Helt, 2005). As shown in Figure 4-3 (page 105), besides phosphorylation of H2AX, phosphorylation of Chk1 (Ser-345), Chk2 (Thr-68), and p53 (Ser-15) were all readily detected in HGPS and RD cells, confirming the activation and signaling of checkpoint pathways in these cells.



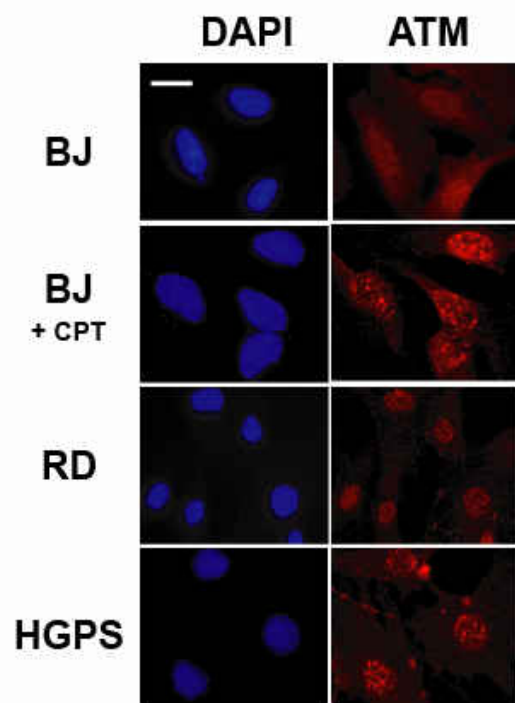
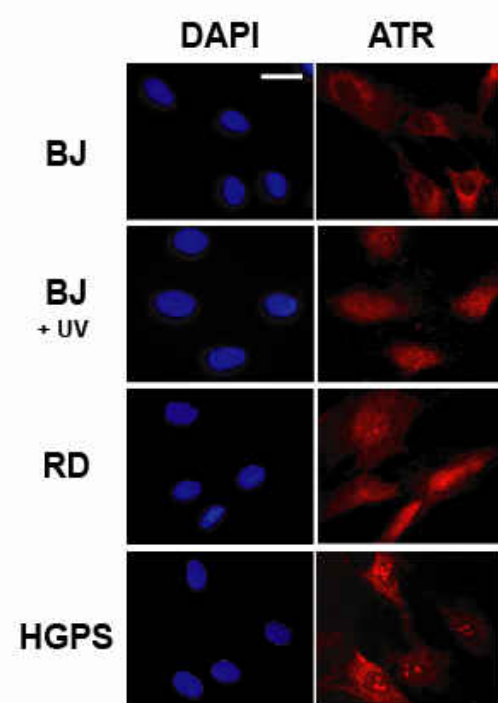
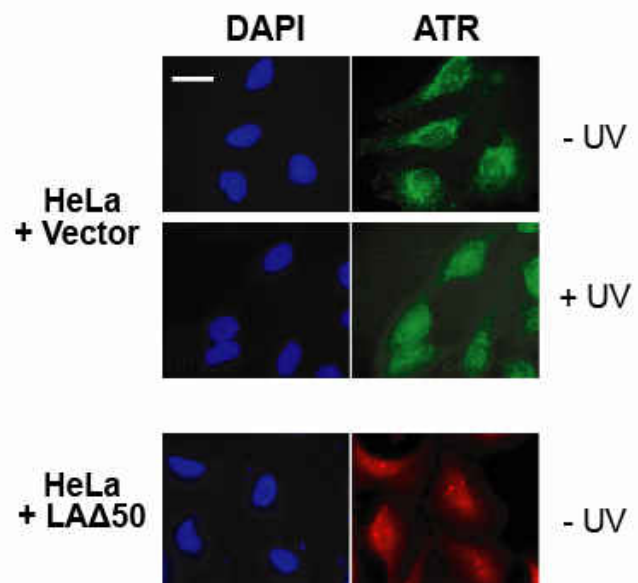
**A****B****C**

Figure 4-2. Activation of ATM and ATR in HGPS and RD cells

(A) CPT treatment was done by incubating the cells with 4  $\mu$ M camptothecin for 1 hour. Cells with or without treatment were fixed with cold methanol ( $-20^{\circ}\text{C}$ ) followed by immunofluorescence microscopy with ATM antibody staining. Blue, DAPI; red, ATM. (B) UV treatment was carried out by irradiating the cells with 20  $\text{J}/\text{m}^2$  UV. Two hours after the treatment, the cells with or without treatment were fixed and stained with ATR antibody for immunofluorescence microscopy. Blue, DAPI; red, ATR. (C) HeLa cells grown on coverslips were transfected with the plasmid for expressing progerin (LA $\Delta$ 50) or empty parent vector. Twenty-four hours after transfection, the cells were irradiated with 20  $\text{J}/\text{m}^2$  UV or mock treated. After additional 2-hour culture, the cells were processed for immunofluorescence microscopy. Blue DAPI; green or red, ATR. Photomicrographs were taken at x63 magnification. Scale bar, 50  $\mu\text{m}$ .

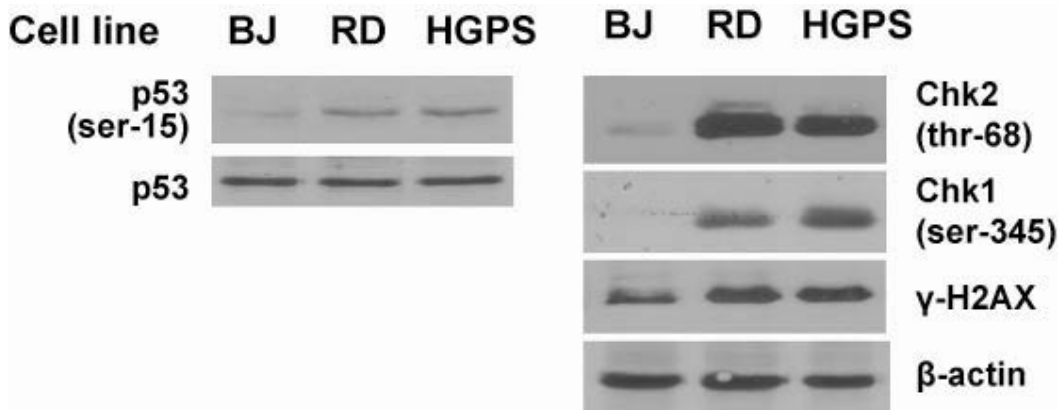


Figure 4-3. Phosphorylation of Chk1, Chk2, and p53 in HGPS and RD cells

Western blotting was performed as described in Materials and Methods. The phosphorylation status of p53 was determined with p53 Ser-15 phosphorylation-specific antibody. The total p53 was probed as the loading control to ensure that the same amounts of p53 were loaded for BJ, RD, and HGPS cells. In the right panel,  $\beta$ -actin was probed to ensure that similar amounts of proteins were loaded for the three cell lines.

## Restoration of Replication Activity by Inactivation of ATM and ATR

DNA damage checkpoint responses are complex signaling pathways orchestrated by the PIKK family including ATM and ATR (Abraham, 2001). Cells with deficient ATM and/or ATR are defective in initiating DNA damage-induced cell-cycle arrest (Shiloh, 2003). To test whether inactivation of ATM and ATR could abolish the premature senescence observed in the patient cells, we treated cells with 5 mM caffeine, an ATM and ATR inhibitor (Sarkaria et al., 1999), and measured their DNA synthesis by [methyl-<sup>3</sup>H] thymidine labeling. As shown in Figure 4-4A (page 107), both ATM and ATR were efficiently knocked down in BJ and HGPS cells transfected with ATR and ATM siRNAs. The observation of lower cellular levels of ATM and ATR in GFP siRNA-transfected HGPS cells than their levels in corresponding BJ cells could be due to the tight chromatin association of ATM and ATR in the checkpoint-activated HGPS cells. These proteins could be partially resistant to extraction for Western blot analysis. However, regardless of the basis for the lowered levels of ATM and ATR in the controls, a relative knockdown by the siRNAs was observed. As shown in Figure 4-4B (page 107), the knockdown significantly increased DNA synthesis in HGPS cells while having no obvious effect on that of the control BJ cells. Similar data were produced by treating the cells with caffeine (Figure 4-4B, page 107). These results confirm that DNA damage checkpoints were activated in the patient cells and demonstrate that the replicative senescence of these patient cells can be reversed by inactivation of checkpoint kinases.

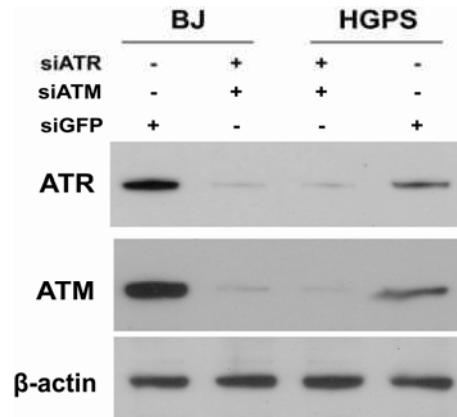
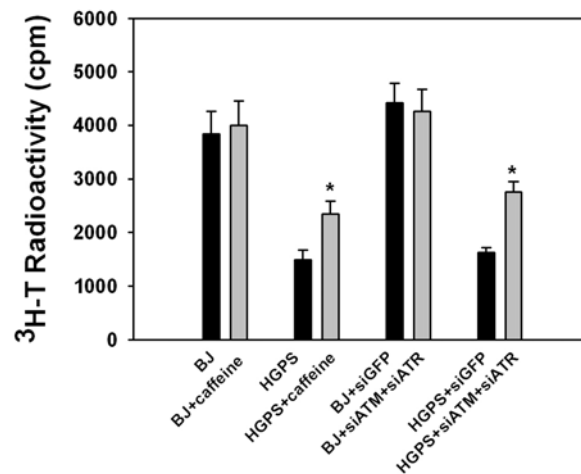
**A****B**

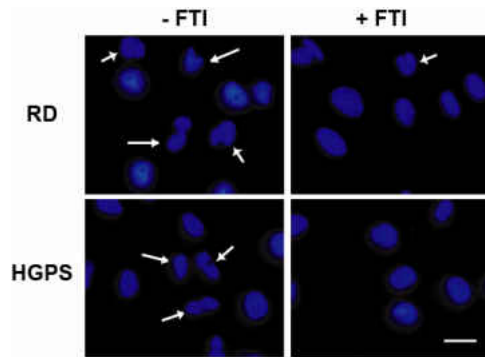
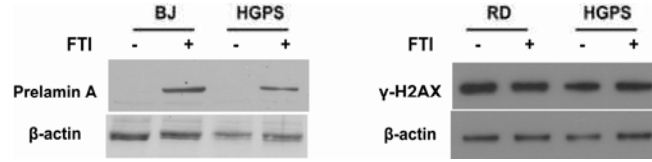
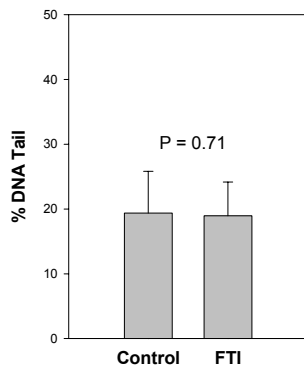
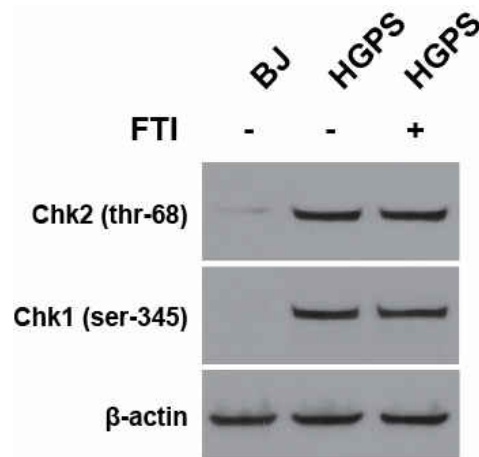
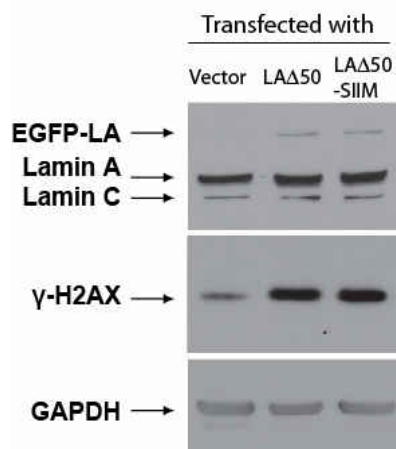
Figure 4-4. Restoration of replication activity in HGPS cells by inactivation of ATM and ATR (A) Western blotting shows the knockdown of ATR and ATM in BJ and HGPS cells by RNAi.  $\beta$ -actin was used as sample loading control. (B) The replication assay was carried out with [methyl- $^3\text{H}$ ] thymidine labeling as described in Materials and Methods. BJ cells and HGPS cells used were at passage 12. The symbol \* indicates a significant difference between HGPS with treatment and HGPS with mock treatment,  $P < 0.05$ .

## FTI Treatment, A Potential Therapy for HGPS and RD?

Recent studies showed that FTI treatment can correct aberrant nuclear morphology in HGPS fibroblasts (Capell et al., 2005; Mallampalli et al., 2005; Toth et al., 2005) and RD fibroblasts (Toth et al., 2005). FTI treatment also ameliorates disease phenotypes in *Zmpste24*-deficient mice (Fong et al., 2006). Because DNA damage accumulation is believed to be one of the major causes of accelerated aging, cellular senescence and normal aging (d'Adda di Fagagna et al., 2003; Gorbunova and Seluanov, 2005; Kirkwood, 2005; Lees-Miller, 2005; Lombard et al., 2005; Misteli and Scaffidi, 2005; von Zglinicki et al., 2005), it is of great interest to test whether FTIs also can reduce the accumulated DNA damage in these cells. As shown in Figure 4-5A (page 110), treatment of HGPS and RD fibroblasts of passage 15 with L-744832, a potent FTI (Capell et al., 2005), significantly reduced the percentage of cells with misshapen nuclei (from 47% to 11% for RD cells,  $P < 0.005$ ; from 33% to 6% for HGPS cells,  $P < 0.001$ ). The misshapen nuclei were defined as nuclei with blebs, folds, or gross irregularities in shape (Toth et al., 2005), and the counting was carried out by two observers who randomly chose 200 cells from each experiment group. This result confirms that FTI treatment can normalize the nuclear morphology of the patient cells. Consistent with these results, FTI treatment of BJ and HGPS fibroblasts caused accumulation of prelamin A in these cells as analyzed by Western blotting (Figure 4-5B, page 110) with prelamin A specific antibody (Sinensky et al., 1994a), demonstrating the efficacy of the FTI in blocking farnesylation in cells. By contrast, however, no substantial reduction of DSBs was detected in HGPS and RD cells after FTI treatment, as evidenced by the amount of  $\gamma$ -H2AX analyzed by Western blotting (Figure 4-5B, page 110). The same HGPS cells were also subjected to single cell gel (SCG) electrophoresis or comet assays that directly measured the DSBs in cells. As shown in Figure 4-5C (page 110), there was no

substantial difference in the amount of DNA damage generated in the cells with and without FTI treatments. In addition, ATM and ATR damage checkpoint signaling was also examined. As shown in Figure 4-5D (page 110), both the checkpoint substrates, Chk1 and Chk2, of ATR and ATM were well phosphorylated in FTI treated and untreated HGPS cells, indicating their activation. Importantly, the phosphorylation was equally efficient in the cells with or without FTI treatment. These observations indicated that FTI treatment was unable to reduce the accumulated DNA damage in these cells despite its capacity to improve the nuclear morphology.

To further confirm the results, pEGFP-LA $\Delta$ 50 and pEGFP-LA $\Delta$ 50-SIIM plasmid constructs, respectively, were transfected into HeLa cells. pEGFP-LA $\Delta$ 50-SIIM is a construct for expression of the LA $\Delta$ 50 with a mutation at its farnesylation site, making the progerin prenylation-incompetent (Capell et al., 2005). Unlike FTI treatment that may not be able to completely abolish the farnesylation of progerin, expression of pEGFP-LA $\Delta$ 50-SIIM produces only the unfarnesylated LA $\Delta$ 50. As shown in Figure 4-5E (page 110), the expression of LA $\Delta$ 50 and prenylation incompetent LA $\Delta$ 50-SSIM in HeLa cells induced similar levels of  $\gamma$ -H2AX accumulation, indicating that farnesylation had no substantial effect on the cellular DNA damage accumulation induced by progerin. This is consistent with the above results obtained with HGPS cells. Our results also suggested that DNA damage accumulation and misshapen nuclei are perhaps two independent phenotypes produced by prelamin A accumulation in HGPS and RD.

**A****B****C****D****E**

### Figure 4-5. FTI treatment of HGPS and RD cells

(A) Improvement of nuclear shapes of HGPS and RD cells by FTI treatment. The patient cells were treated with FTI and prepared for immunofluorescence microscopy as described in Materials and Methods. The nuclei were stained with DAPI. Misshapen nuclei were indicated by arrows. Photomicrographs were taken at x63 magnification. Scale bar, 50  $\mu\text{m}$ . (B) FTI treatment blocked farnesylation of prelamin A but did not change the production of  $\gamma\text{-H2AX}$ , a molecular marker for DSBs. In the left panel, BJ and HGPS cells were lysed in 2 x SDS gel loading buffer and probed with the antibody directed against prelamin A. In the right panel, HGPS and RD cells were lysed and probed with the antibody for  $\gamma\text{-H2AX}$ .  $\beta\text{-actin}$  was loaded to ensure similar amounts of samples were used for each pair of experiment groups. (C) Comet assays were carried out with HGPS cells in the presence and absence of FTI as described in Materials and Methods. DSBs of 50 randomly chosen cells were quantitated as the percentage of DNA in tail. (D) Phosphorylation of Chk1 and Chk2 in HGPS cells with or without FTI treatment. The FTI treatment of BJ and HGPS and Western blotting were performed as described in Materials and Methods. The phosphorylation statuses of Chk1 at Ser-345 and Chk2 at Thr-68 were determined with corresponding antibodies.  $\beta\text{-actin}$  was probed as a loading control. (E) Accumulation of  $\gamma\text{-H2AX}$  in cells expressing prelamin A mutants. HeLa cells were transfected with plasmid pEGFP, pEGFP-LA $\Delta$ 50, or pEGFP-LA $\Delta$ 50-SSIM, followed by Western blot analysis. GAPDH was probed as a loading control.

### Discussion

DNA damage is believed to contribute to both aging and cellular senescence (Lombard et al., 2005) that has been regarded as a permanently maintained DNA damage response state (von Zglinicki et al., 2005). Defects in several DNA repair proteins lead to DNA damage accumulation and damage responses that cause phenotypes reminiscent of premature ageing (Lombard et al., 2005). As there is no evidence for any mutations in DNA repair genes in HGPS and RD cells, we, and others, hypothesize that prelamin A accumulation affects DNA repair in these syndromes. In this study, we present direct evidence that DNA damage checkpoints were



constantly activated in HGPS and RD cells due to accumulated DNA damage. We also demonstrated that the subcellular distribution of checkpoint kinases ATM and ATR may be used as an indicator for their activation *in vivo*. Inactive ATM is homogeneously distributed in the nucleus, while nuclear focus formation of ATM indicates its activation. In unstressed cells, ATR is mainly localized in cytosol but translocates into the nucleus upon DNA damaging stress such as UV irradiation. Our finding is contradictory to that of Manju et al. (Manju et al., 2006) who recently reported that ATR was normally localized in the nucleus. The explanation for this discrepancy may lie in the fact that FLAG-ATR was ectopically expressed in cells in the Manju et al. study, while we used normal cells and stained endogenous ATR directly. The expression of exogenous proteins likely induces stress to the cells, which may cause the translocation of ATR from cytosol to the nucleus. In the present study, activation of ATR and ATM in the patient cells as evidenced by immunofluorescence determination was confirmed by the phosphorylation of their downstream substrates Chk1, Chk2, and p53 as analyzed by Western blotting.

Interestingly, inactivation of ATM and ATR in HGPS cells partially restored cell-cycle progression into S phase. This confirms that a form of prelamin A (progerin) activated DNA damage responses, leading to replicative senescence. Importantly, this senescence can be suppressed by inactivating DNA damage response pathways in HGPS cells. That only partial restoration of S-phase progression is observed is likely due to the incomplete repression of the DNA damage responses as even a residual kinase activity could be sufficient to enforce a DNA damage checkpoint (Cortez et al., 2001). Varela et al. showed that p53 knockout completely recovered the proliferative capacity of *Zmpste24*<sup>-/-</sup> mouse cells (Varela et al., 2005). We expect that a highly efficient checkpoint inhibition would permit a significant recovery of cell division and alleviate many other senescence-associated phenotypes in progeroid cells.

Aberrant nuclear morphology is the most obvious phenotype caused by prelamin A accumulation in HGPS and RD fibroblasts (Goldman et al., 2004; Toth et al., 2005). Recent studies showed that FTI treatment could correct the nuclear morphology defects of progeroid cells (Capell et al., 2005; Glynn and Glover, 2005; Mallampalli et al., 2005; Toth et al., 2005). However, we found that FTI treatment could not reduce the accumulated DSBs in both HGPS and RD cells. This suggests that DNA damage accumulation and misshapen nuclei are probably two unrelated phenotypes caused by prelamin A accumulation in HGPS and RD. Consistent with this notion, p53 knockout can restore proliferative capacity of *Zmpste24*<sup>-/-</sup> mouse cells but only partially reverse other disease phenotypes (Varela et al., 2005), suggesting that independent pathological pathways exist and cooperate with each other in the generation of progeroid phenotypes. Thus, strategies for treatment of HGPS need to combine elimination of DNA damage accumulation as well as normalization of nuclear morphology.

## References

**Abraham, R. T.** (2001). Cell cycle checkpoint signaling through the ATM and ATR kinases. *Genes Dev* **15**, 2177-96.

**Capell, B. C., Erdos, M. R., Madigan, J. P., Fiordalisi, J. J., Varga, R., Conneely, K. N., Gordon, L. B., Der, C. J., Cox, A. D. and Collins, F. S.** (2005). Inhibiting farnesylation of progerin prevents the characteristic nuclear blebbing of Hutchinson-Gilford progeria syndrome. *Proc Natl Acad Sci U S A* **102**, 12879-84.

**Cortez, D., Guntuku, S., Qin, J. and Elledge, S. J.** (2001). ATR and ATRIP: partners in checkpoint signaling. *Science* **294**, 1713-6.

**d'Adda di Fagagna, F., Reaper, P. M., Clay-Farrace, L., Fiegler, H., Carr, P., Von Zglinicki, T., Saretzki, G., Carter, N. P. and Jackson, S. P.** (2003). A DNA damage checkpoint response in telomere-initiated senescence. *Nature* **426**, 194-8.

**De Sandre-Giovannoli, A., Bernard, R., Cau, P., Navarro, C., Amiel, J., Boccaccio, I., Lyonnet, S., Stewart, C. L., Munnich, A., Le Merrer, M. et al.** (2003). Lamin a truncation in Hutchinson-Gilford progeria. *Science* **300**, 2055.

**Eriksson, M., Brown, W. T., Gordon, L. B., Glynn, M. W., Singer, J., Scott, L., Erdos, M. R., Robbins, C. M., Moses, T. Y., Berglund, P. et al.** (2003). Recurrent de novo point mutations in lamin A cause Hutchinson-Gilford progeria syndrome. *Nature* **423**, 293-8.

**Fong, L. G., Frost, D., Meta, M., Qiao, X., Yang, S. H., Coffinier, C. and Young, S. G.** (2006). A protein farnesyltransferase inhibitor ameliorates disease in a mouse model of progeria. *Science* **311**, 1621-3.

**Glynn, M. W. and Glover, T. W.** (2005). Incomplete processing of mutant lamin A in Hutchinson-Gilford progeria leads to nuclear abnormalities, which are reversed by farnesyltransferase inhibition. *Hum Mol Genet* **14**, 2959-69.

**Goldman, R. D., Gruenbaum, Y., Moir, R. D., Shumaker, D. K. and Spann, T. P.** (2002). Nuclear lamins: building blocks of nuclear architecture. *Genes Dev* **16**, 533-47.

**Goldman, R. D., Shumaker, D. K., Erdos, M. R., Eriksson, M., Goldman, A. E., Gordon, L. B., Gruenbaum, Y., Khuon, S., Mendez, M., Varga, R. et al.** (2004). Accumulation of mutant lamin A causes progressive changes in nuclear architecture in Hutchinson-Gilford progeria syndrome. *Proc Natl Acad Sci U S A* **101**, 8963-8.

**Gorbunova, V. and Seluanov, A.** (2005). Making ends meet in old age: DSB repair and aging. *Mech Ageing Dev* **126**, 621-8.

**Helt, C. E., Cliby, W. A., Keng, P. C., and Bambara, R. A.** (2005). Ataxia Telangiectasia Mutated (ATM) and ATM and Rad3-related protein exhibit selective target specificities in response to different forms of DNA damage. *J Biol Chem* **280**, 1186-1192.

**Kirkwood, T. B.** (2005). Understanding the odd science of aging. *Cell* **120**, 437-47.

**Lees-Miller, S. P.** (2005). Dysfunction of lamin A triggers a DNA damage response and cellular senescence. *DNA Repair (Amst)*.

**Li, L. and Zou, L.** (2005). Sensing, signaling, and responding to DNA damage: organization of the checkpoint pathways in mammalian cells. *J Cell Biochem* **94**, 298-306.

**Liu, B., Wang, J., Chan, K. M., Tjia, W. M., Deng, W., Guan, X., Huang, J. D., Li, K. M., Chau, P. Y., Chen, D. J. et al.** (2005a). Genomic instability in laminopathy-based premature aging. *Nat Med* **11**, 780-5.

**Liu, Y., Kvaratskhelia, M., Hess, S., Qu, Y. and Zou, Y.** (2005b). Modulation of replication protein A function by its hyperphosphorylation-induced conformational change involving DNA binding domain B. *J Biol Chem* **280**, 32775-83.

**Lombard, D. B., Chua, K. F., Mostoslavsky, R., Franco, S., Gostissa, M. and Alt, F. W.** (2005). DNA repair, genome stability, and aging. *Cell* **120**, 497-512.

**Mallampalli, M. P., Huyer, G., Bendale, P., Gelb, M. H. and Michaelis, S.** (2005). Inhibiting farnesylation reverses the nuclear morphology defect in a HeLa cell model for Hutchinson-Gilford progeria syndrome. *Proc Natl Acad Sci U S A* **102**, 14416-21.

**Manju, K., Muralikrishna, B. and Parnaik, V. K.** (2006). Expression of disease-causing lamin A mutants impairs the formation of DNA repair foci. *J Cell Sci* **119**, 2704-14.

**McGowan, C. H. and Russell, P.** (2004). The DNA damage response: sensing and signaling. *Curr Opin Cell Biol* **16**, 629-33.

**Misteli, T. and Scaffidi, P.** (2005). Genome instability in progeria: when repair gets old. *Nat Med* **11**, 718-9.

**Navarro, C. L., Cadinanos, J., De Sandre-Giovannoli, A., Bernard, R., Courrier, S., Boccaccio, I., Boyer, A., Kleijer, W. J., Wagner, A., Giuliano, F. et al.** (2005). Loss of ZMPSTE24 (FACE-1) causes autosomal recessive restrictive dermopathy and accumulation of Lamin A precursors. *Hum Mol Genet* **14**, 1503-13.

**Sancar, A., Lindsey-Boltz, L. A., Unsal-Kacmaz, K. and Linn, S.** (2004). Molecular mechanisms of mammalian DNA repair and the DNA damage checkpoints. *Annu Rev Biochem* **73**, 39-85.

**Sarkaria, J. N., Busby, E. C., Tibbetts, R. S., Roos, P., Taya, Y., Karnitz, L. M. and Abraham, R. T.** (1999). Inhibition of ATM and ATR kinase activities by the radiosensitizing agent, caffeine. *Cancer Res* **59**, 4375-82.

**Scaffidi, P. and Misteli, T.** (2006). Lamin A-dependent nuclear defects in human aging. *Science* **312**, 1059-63.

**Sedelnikova, O. A., Rogakou, E. P., Panyutin, I. G. and Bonner, W. M.** (2002). Quantitative detection of (125)IdU-induced DNA double-strand breaks with gamma-H2AX antibody. *Radiat Res* **158**, 486-92.

**Shao, R. G., Cao, C. X., Shimizu, T., O'Connor, P. M., Kohn, K. W. and Pommier, Y.** (1997). Abrogation of an S-phase checkpoint and potentiation of camptothecin cytotoxicity by 7-hydroxystaurosporine (UCN-01) in human cancer cell lines, possibly influenced by p53 function. *Cancer Res* **57**, 4029-35.

**Shiloh, Y.** (2003). ATM and related protein kinases: safeguarding genome integrity. *Nature Rev. Cancer* **3**, 155-168.

**Sinensky, M., Fantle, K. and Dalton, M.** (1994a). An antibody which specifically recognizes prelamin A but not mature lamin A: application to detection of blocks in farnesylation-dependent protein processing. *Cancer Res* **54**, 3229-32.

**Sinensky, M., Fantle, K., Trujillo, M., McLain, T., Kupfer, A. and Dalton, M.** (1994b). The processing pathway of prelamin A. *J Cell Sci* **107 (Pt 1)**, 61-7.

**Steinert, S., Shay, J. W. and Wright, W. E.** (2000). Transient expression of human telomerase extends the life span of normal human fibroblasts. *Biochem Biophys Res Commun* **273**, 1095-8.

**Toth, J. I., Yang, S. H., Qiao, X., Beigneux, A. P., Gelb, M. H., Moulson, C. L., Miner, J. H., Young, S. G. and Fong, L. G.** (2005). Blocking protein farnesyltransferase improves nuclear shape in fibroblasts from humans with progeroid syndromes. *Proc Natl Acad Sci U S A* **102**, 12873-8.

**Varela, I., Cadinanos, J., Pendas, A. M., Gutierrez-Fernandez, A., Folgueras, A. R., Sanchez, L. M., Zhou, Z., Rodriguez, F. J., Stewart, C. L., Vega, J. A. et al.** (2005).

Accelerated ageing in mice deficient in Zmpste24 protease is linked to p53 signalling activation. *Nature* **437**, 564-8.

**von Zglinicki, T., Saretzki, G., Ladhoff, J., d'Adda di Fagagna, F. and Jackson, S. P.** (2005). Human cell senescence as a DNA damage response. *Mech Ageing Dev* **126**, 111-7.

**Wu, X., Shell, S. M., Yang, Z. and Zou, Y.** (2006). Phosphorylation of nucleotide excision repair factor xeroderma pigmentosum group A by ataxia telangiectasia mutated and Rad3-related-dependent checkpoint pathway promotes cell survival in response to UV irradiation. *Cancer Res* **66**, 2997-3005.

## CHAPTER 5

### XERODERMA PIGMENTOSUM GROUP A (XPA) INHIBITS REPAIR OF DNA DOUBLE-STRAND BREAKS IN LAMINOPATHY-BASED PREMATURE AGING CELLS

#### Abstract

Cellular accumulation of DNA damage has been widely implicated in cellular senescence, aging, and premature aging. In Hutchinson-Gilford progeria syndrome (HGPS) and restrictive dermopathy (RD), premature aging is linked to accumulation of DNA double-strand breaks (DSBs) that results in genome instability. However, how DSBs accumulate in cells despite the presence of intact DNA repair proteins remains unknown. Here we report that the recruitment of DSB repair factors Rad50 and Rad51 to the laminopathy-related DSB sites, as marked by  $\gamma$ -H2AX, was impaired in human HGPS cells and *Zmpste24*-deficient cells, making the DSBs unrepairable. By contrast, a significant amount of nuclear foci of XPA, a unique nucleotide excision repair protein, formed in the progeroid cells even without DNA damage agent treatment. Strikingly, these foci massively colocalized with the unrepairable laminopathy-induced DSBs but not to the repairable DSBs induced by camptothecin. RNAi knockdown of XPA in HGPS cells significantly restored DSB repair as evidenced by Western blot analysis, immunofluorescence, and comet assays. Our results suggest that the uncharacteristic localization of XPA to DSBs may inhibit DSB repair in the progeroid cells so that XPA dysfunction may play an important role in accumulating DSBs for development of progeroid laminopathies. Our results also provide a potential strategy for treatment of these devastating premature aging diseases.

## Introduction

Hutchinson-Gilford progeria syndrome (HGPS) is a dominant premature aging disease caused by formation of a carboxyl-terminal truncated form (progerin) of the lamin A precursor, prelamin A (De Sandre-Giovannoli et al., 2003; Eriksson et al., 2003). Lamin A is an intermediate filament protein in the nuclear lamina, a scaffold underlying the inner nuclear membrane that structurally supports the nucleus and organizes chromatin (Goldman et al., 2002). Homozygous deficiency of *Zmpste24*, an endoproteinase essential for the proteolytic maturation of prelamin A, results in restrictive dermopathy (RD), which is a lethal perinatal progeroid disorder (Navarro et al., 2005). Loss of *Zmpste 24* proteinase activity arrests the processing of prelamin A at a stage similar to HGPS, although progerin instead of prelamin A is accumulated in HGPS cells. These two diseases have been suggested to be manifestations of the same cellular problem to different degrees (Misteli and Scaffidi, 2005).

It has been recently shown that HGPS and RD cells exhibit DSB accumulation, impairment of DNA repair, and activation of the p53-dependent stress signaling pathway (Liu et al., 2005; Manju et al., 2006; Varela et al., 2005), suggesting that genome instability caused by HGPS and RD might contribute to premature aging. The DSB accumulation in HGPS and *Zmpste24*-deficient cells as well as in senescing and aging mammalian cells appears to be due to unrepairable DSBs (Sedelnikova et al., 2004). However, the underlying mechanism of the repair defect is still poorly understood. We asked the question of how DNA repair is compromised in HGPS and RD cells even though there is no evidence of mutations in repair genes.

In the present study, using immunofluorescence microscopy and chromatin immunoprecipitation (ChIP) assay, we examined the localization of DNA repair proteins in relation to  $\gamma$ -H2AX, a molecular marker for DSBs, in the progeroid cells. We found that DSB



repair proteins Rad51 and Rad50 were not localized to the DNA damage sites, while XPA, a unique nucleotide excision repair protein, largely colocalized with the DSBs formed due to laminopathies in HGPS and RD cells. This suggests that the mislocalization of XPA to DSBs may be responsible for the unreparability of laminopathy-phenotyped DNA damage in the progeria cells. In support, RNAi knockdown of XPA in HGPS cells significantly restored DSB repair. We speculated that XPA dysfunction may play an important role in the development of progeroid laminopathies.

## Materials and Methods

### Cell Cultures

Fibroblasts from a HGPS patient with the point mutation of 1824C → T were obtained from Coriell Cell Repository (no. AG11513A). Human RD fibroblasts were a gift from Dr. J.H. Miner (Washington University School of Medicine, St Louis, MO). The normal human fibroblasts, BJ cells, were purchased from American Type Culture Collection (ATCC, no. CRL-2522). All cultures were maintained in DMEM (for RD cells) or EMEM (for HGPS and BJ cells) supplemented with 10% FBS and antibiotics.

### Immunofluorescence Microscopy

Cells grown on coverslips were fixed with cold methanol (-20°C) or extracted with 0.5% IGEPAL CA-630 followed by fixation with methanol. The fixed cells were then incubated with primary antibodies against  $\gamma$ -H2AX (rabbit, Bethyl; or mouse, Stressgen), XPA (mouse, Kamiya; or rabbit, Santa Cruz), Rad51 (rabbit, Santa Cruz), Rad50 (rabbit, Bethyl), and XPC (rabbit, GeneTex). Secondary antibodies used include Alexa fluor 488-conjugated donkey anti-rabbit

IgG and Alexa fluor 568-conjugated goat anti-mouse IgG (Molecular Probes). Cells were counterstained with DAPI to visualize nuclear DNA. Focus counting was performed by two blinded observers who randomly chose 50 cells for each experiment.

### Western Blotting

For immunoblotting of XPA and lamin proteins, whole-cell extracts were prepared from  $\sim 10^7$  cells. The samples were separated by SDS-PAGE and immunoblotted with antibodies against XPA (GeneTex), prelamin A (Sinensky et al., 1994) or lamin A/C (Santa Cruz), or  $\beta$ -actin (Santa Cruz).

### $\gamma$ -H2AX Association Assay and Co-Immunoprecipitation

The  $\gamma$ -H2AX association assay used in this study was modified from the histone association assay described by Ricke et al. (Ricke and Bielinsky, 2005). Briefly, cells were treated with formaldehyde to crosslink interacting protein-DNA as well as protein-protein complexes. Nuclei were prepared by fractionation. The chromatin was sheared into 200-1500 bp fragments by sonication. The sheared chromatin was incubated with  $\gamma$ -H2AX antibody, followed by precipitation with protein G Sepharose beads. The immunoprecipitates were boiled for at least 30 minutes to reverse the crosslinks (Ricke and Bielinsky, 2005). Proteins that co-precipitate with chromatin were detected by Western blotting.

The co-immunoprecipitation was performed using a Nuclear Complex Co-IP kit (Active Motif, CA), following the manufacture's instructions.

## Comet Assay

The neutral comet assay was performed to assess DNA strand breaks in cells. The first layer of agarose on microscope slides were prepared by dipping the slides into 1% normal melting point agarose (NMA) followed by drying. Eighty-five microliters of 0.5% low melting point agarose (LMA) containing  $4 \times 10^5$  cells was made by mixing 10  $\mu$ l of cell suspension with 75  $\mu$ l of LMA. The mixture was then poured onto the pre-coated slides. Slides were immersed in freshly prepared ice-cold buffer (2.5 M NaCl, 100 mM Na<sub>2</sub>EDTA, 10 mM Tris-HCl, 1% Triton X-100, pH 10) to lyse the cells for at least 1 hour at 4 °C in the dark. The slides were then placed in the alkaline buffer (0.3 M NaOH, 1 mM EDTA, pH > 13) for 30 minutes for DNA unwinding. The slides were equilibrated in TBE buffer for 5 minutes twice followed by electrophoresis at 1 volt/cm in TBE buffer for 10 minutes. The slides were then dipped in 70% ethanol for 5 minutes and dried at room temperature for 1 hour. Fifty microliters of 600  $\mu$ M DAPI was used for staining. All steps described above were conducted under dimmed light to prevent additional DNA damage. The quantification of the comets was conducted for randomly chosen 50 cells, and DNA damage was expressed as the percentage of DNA in tail.

## Results

### Accumulation of DSBs in HGPS Cells and RD Cells

We first examined accumulation of DSBs in HGPS and RD fibroblasts by probing  $\gamma$ -H2AX focus formation using immunofluorescence (IF) microscopy. The normal human diploid fibroblasts, BJ cells, were used here as a control. The expression of wild-type prelamin A and/or progerin in HGPS and RD cells or normal lamin A in BJ cells was confirmed by Western blotting (Figure 5-1a, page 123). By using IF, we observed  $\gamma$ -H2AX foci in approximately 61%

RD cells and 53% HGPS cells (passage 16), but only in about 8% BJ cells at the same passage. The number of  $\gamma$ -H2AX foci in RD ( $13.8 \pm 3.3$  per cell) and HGPS fibroblasts ( $10.5 \pm 3.0$  per cell) was significantly higher than that in the control BJ fibroblasts ( $0.4 \pm 0.3$  per cell) (Figure 5-1b, page 123). Although  $\gamma$ -H2AX foci were also observed in human M-phase cells in the absence of

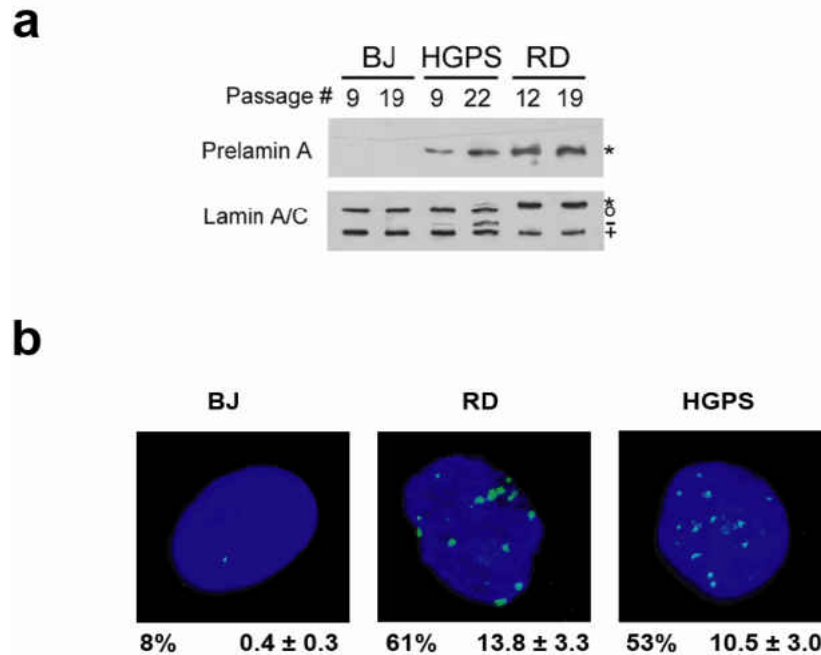


Figure 5-1. Prelamin A and DSB accumulation in BJ, HGPS and RD fibroblasts

(a) Western blot analysis of prelamin A. Cells were grown for the indicated number of passages, and Western blot analyses of cell extracts were performed with antibodies specific for: *Top*, prelamin A, (specific for the extreme C terminus) and *Bottom*, lamin A/C (binds to both lamin A and lamin C). Symbols indicate the following: (\*) = Prelamin A, (o) = mature Lamin A, (-) = LAA50 and (+) = Lamin C. (b) DSB formation as revealed by  $\gamma$ -H2AX foci. Cells were stained with anti- $\gamma$ -H2AX antibody. Blue, DAPI; green,  $\gamma$ -H2AX. The percentage of cells containing  $\gamma$ -H2AX foci is shown on the left bottom of each subpanel; the number of  $\gamma$ -H2AX foci per cell is shown on the right bottom.

DSBs and DNA damage signaling (Ichijima et al., 2005), these foci were locally condensed in nuclei and the pattern/type was very different from that of the DSBs-induced discrete foci formed throughout the whole nuclei (Ichijima et al., 2005). In the present study, only discrete foci have been considered. Importantly, our control BJ cells that had similar percentage (25-30%) of G2/M-phase population as HGPS and RD cells (data not shown and refs. (Liu et al., 2005; Varela et al., 2005)) showed little discrete focus formation as compared to that of progeria cells. In HGPS and RD cells, discrete  $\gamma$ -H2AX foci appeared in more than half of the population. Furthermore, direct evidence from comet assays confirmed that more than half of HGPS cells had DSBs (Figure 5-6c, page 132). The DSBs in HGPS and RD cells were also confirmed by the activated DNA damage responses in these progeria cells involving ATM, ATR, and downstream phosphor-kinases Chk1 and Chk2 (Chapter 4). The significant increase of  $\gamma$ -H2AX foci in lamin A-defective cells indicates that defects in lamin A maturation is correlated with DSB formation in cells.

#### Mislocalization of DSB Repair Proteins and Colocalization of XPA with DSBs

In an effort to determine the mechanism by which DSBs are resistant to being repaired and thus accumulate in HGPS and RD cells, we examined the nuclear localization of several DNA repair proteins. We found that the HGPS and RD cells showing  $\gamma$ -H2AX foci also contained foci of the DSB repair protein Rad51 (Figure 5-2a, page 125). The massive fluorescent staining of Rad51 in HGPS and RD cells indicates that some Rad51 protein may aggregate in the patient cells. However, colocalization of Rad51 and  $\gamma$ -H2AX was random (only about 5% and 2% for RD and HGPS cells, respectively) (Figure 5-2a, page 125). This suggests that Rad51 was unable to localize to the DSB sites for DNA damage repair. In contrast, discrete Rad51 foci were

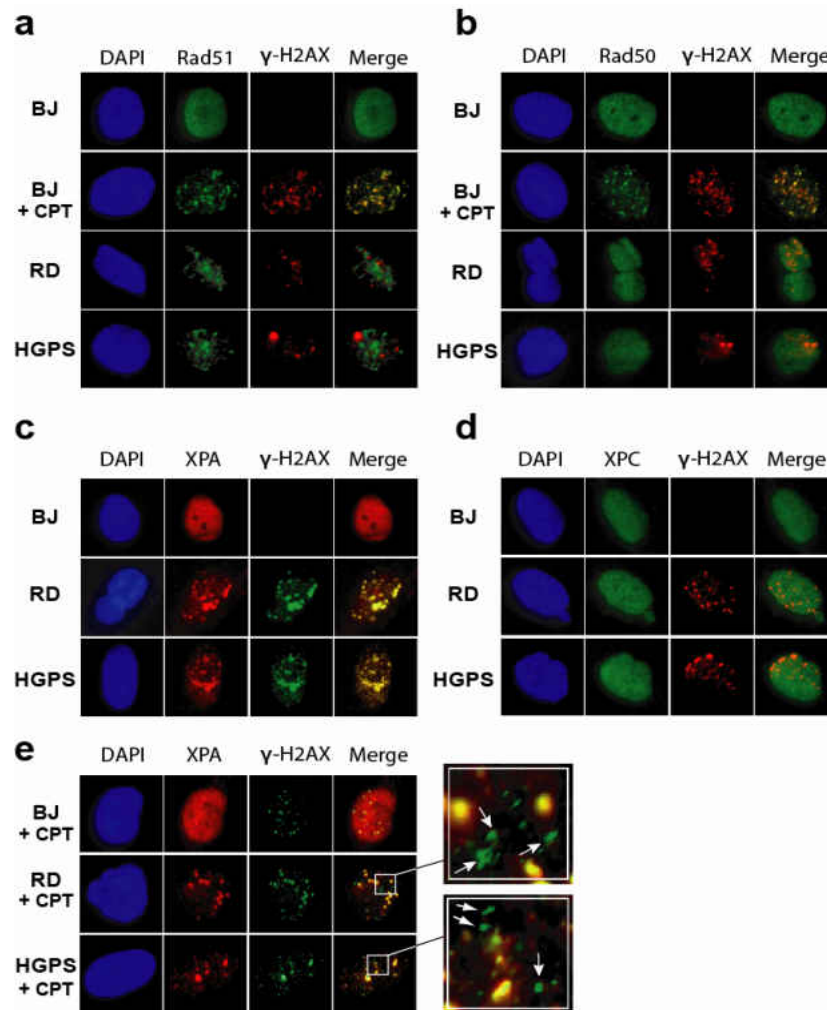


Figure 5-2. Colocalization of  $\gamma$ -H2AX foci and the foci of DNA repair proteins in BJ, HGPS and RD fibroblasts

Nuclear focus localization of Rad51 (a), Rad50 (b), XPA (c and e), and XPC (d) relative to  $\gamma$ -H2AX foci were detected with corresponding antibodies by immunofluorescence microscopy. Uniform staining of the given protein throughout nucleus indicates homogenous distribution of the protein without foci formation. CPT treatment of cells was conducted by incubating the cells with 4  $\mu$ M CPT for 1 hour before fixation. The green foci in the Merge subpanel of (e) represent the CPT-induced DSBs (arrows) that were not colocalized with XPA foci. The nucleus is visualized by DAPI staining.

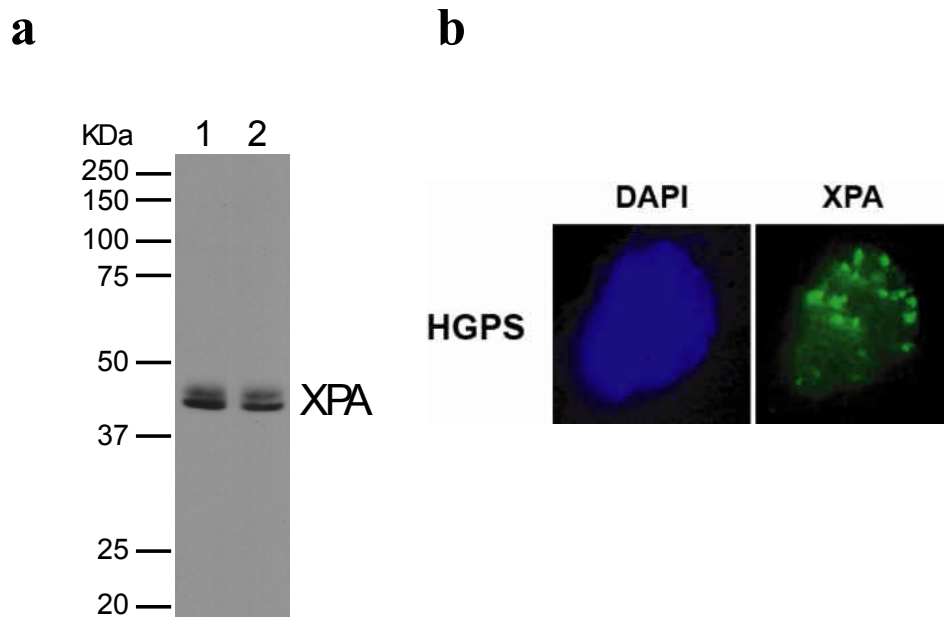


Figure 5-3. Specificity of human XPA antibodies used in this study

(a) Western blot analysis of whole cell extracts by human XPA antibody (mouse, Kamiya). The XPA was visualized as a doublet of bands. (b) Formation of XPA foci in HGPS cells identified by human XPA antibody raised from rabbits (Santa Cruz).

formed and perfectly colocalized with DSBs as marked by  $\gamma$ -H2AX foci in BJ cells treated with camptothecin (CPT), a DSBs inducer (Figure 5-2a, page 125). The same results were also obtained with Rad50 (Figure 5-2b, page 125), a subunit of Mre11/Rad50/Nbs1 (MRN) complex involved in DSB damage signaling and repair (Lee and Paull, 2004; Lee and Paull, 2005; Paull and Lee, 2005; Sancar et al., 2004). These results suggest that the defective repair of DSBs in HGPS and RD fibroblasts is probably due to a disruption of recruitment of DSB repair factors such as MRN and Rad51 to the damage sites.

Our further investigation led to a surprising finding that xeroderma pigmentosum group A (XPA), a unique nucleotide excision repair (NER) factor, formed a large number of nuclear

foci in HGPS and RD cells. Strikingly, these foci colocalized almost completely with  $\gamma$ -H2AX foci (Figure 5-2c, page 125). Specificity of the human XPA antibody (mouse) used in the detection was confirmed by Western blotting of whole cell extracts and by the similar immunofluorescence measurement with different XPA antibody (rabbit) from a different company (Santa Cruz) (Figure 5-3, page 126). The specificity was also verified by the siRNA knockdown experiments (Figure 5-6a, page 132). By contrast, other NER proteins, XPC (xeroderma pigmentosum group C), and RPA (replication protein A), showed no focus formation in HGPS and RD cells (Figure 5-2d, page 125, and data not shown). XPA and XPC are DNA damage-recognition proteins in NER and have no role in DSB repair (Sancar et al., 2004). RPA also is a DNA damage recognition protein and the main single-stranded DNA (ssDNA) binding protein in human cells (Zou et al., 2006). These results suggest that the colocalization of XPA and  $\gamma$ -H2AX was specific and NER-unrelated. This is consistent with the specificity of NER that neither processes DSBs nor generates DSB intermediates (Sancar et al., 2004). As shown in Figure 5-2e (page 125), evidence that further supports the specificity of XPA- $\gamma$ -H2AX colocalization in HGPS and RD cells came from the observation that XPA did not colocalize with CPT-induced  $\gamma$ -H2AX foci (arrowed green foci in the merged images in Figure 5-2e, page 125) in BJ, RD or HGPS cells. This indicates that the DSBs induced by genotoxic agents were different from those formed due to the lamin A defect that disrupts the chromatin-supporting scaffold.

It is possible that the DNA damage arising in HGPS or RD cells may have a particular structural signature or readout that is recognized by XPA. Alternatively, XPA could be recruited to the DSB sites by other cellular factors due to laminopathies. To explore the underlying



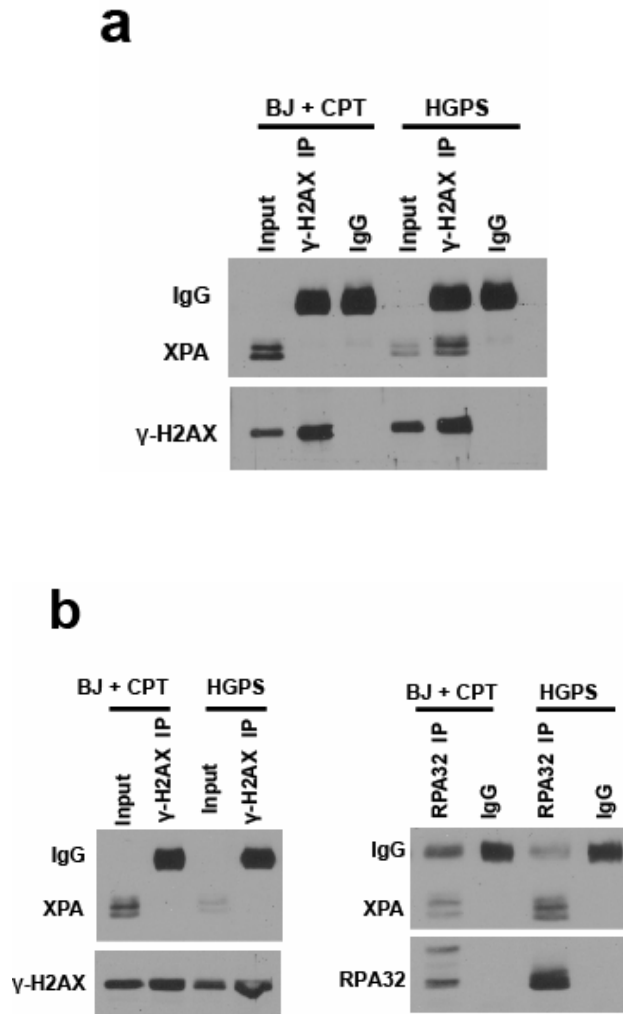


Figure 5-4. Chromatin-mediated XPA- $\gamma$ -H2AX interaction

(a)  $\gamma$ -H2AX association assay was performed as described in Materials and Methods. HGPS and BJ cells were treated with the crosslinking agent formaldehyde. BJ cells were treated with 4  $\mu$ M camptothecin for 1 hour before the formaldehyde fixation. Immunoprecipitated proteins were analyzed by Western blotting with indicated antibodies. IP with IgG was used as a negative control to demonstrate the specificity of  $\gamma$ -H2AX antibody. (b) Co-immunoprecipitation was performed with nuclease treatment. The nuclear extracts (Input) and precipitated proteins were analyzed by immunoblotting with indicated antibodies. IP with RPA32 antibody was carried out in parallel, which served as a positive control demonstrating that the Co-IP conditions used herein preserved protein-protein interactions.

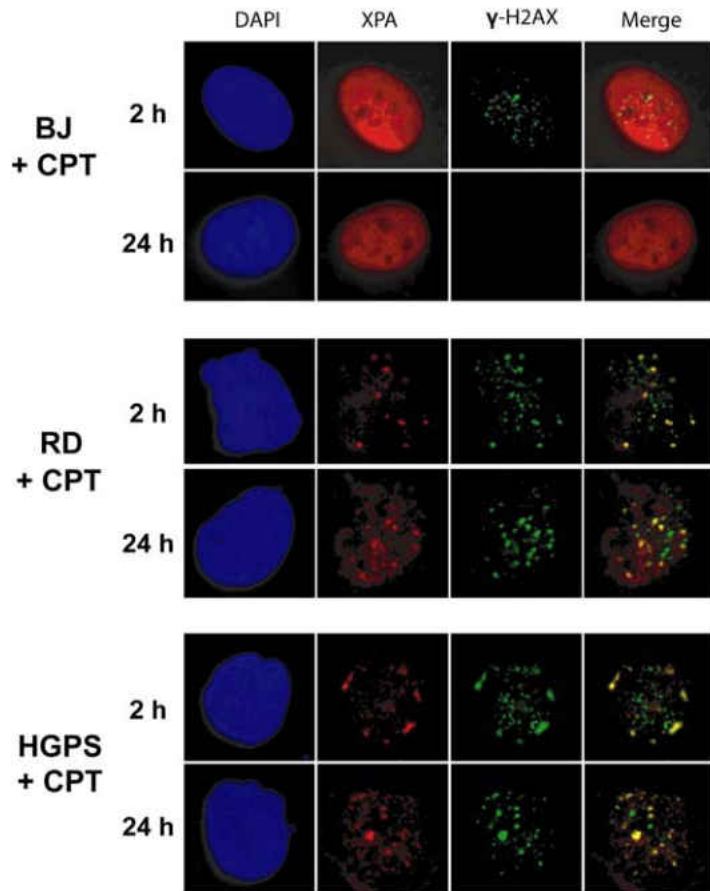
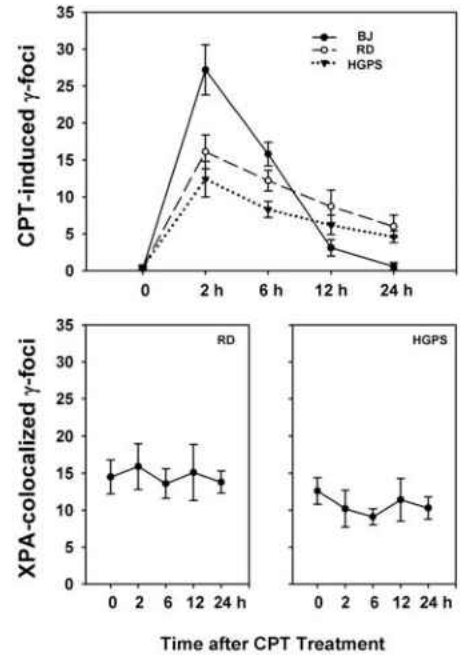
**a****b**

Figure 5-5. Laminopathy-induced DSBs are unreparable

(a) Cells were treated with 4  $\mu$ M CPT and then harvested at the indicated times for immunofluorescence analysis. The  $\gamma$ -H2AX foci that did not colocalize with XPA were CPT-induced  $\gamma$ -foci. (b) Focus counting was performed by two blinded observers who randomly chose 50 cells for each experiment. The number of foci was plotted against time post treatment with CPT.

mechanism by which XPA is localized to the DSB sites, the association of XPA with  $\gamma$ -H2AX in HGPS cells was examined using co-immunoprecipitation assay and a modified ChIP (chromatin immunoprecipitation) assay. In the modified ChIP assay, cells were first treated with formaldehyde to crosslink protein-DNA and protein-protein complexes. After shearing the chromatin into 200-1500-bp fragments, the crosslinked chromatin-associated  $\gamma$ -H2AX in cell extracts was immunoprecipitated with anti- $\gamma$ -H2AX antibody, followed by reversal of the cross-linking. As shown in Figure 5-4a (page 128), Western blot analysis of the immunoprecipitates indicated that XPA was associated with  $\gamma$ -H2AX either through direct interaction or mediated by DNA or other proteins. By contrast, no association between  $\gamma$ -H2AX and XPA was observed for BJ cells treated with CPT. To determine whether there was a direct interaction between  $\gamma$ -H2AX and XPA, co-immunoprecipitation (Co-IP) was performed after nuclease treatment using a Nuclear Complex Co-IP kit (Active Motif, CA). As shown in Figure 5-4b (page 128), the nuclease digestion of DNA resulted in the loss of XPA- $\gamma$ -H2AX association, suggesting that their association in these progeria cells was mediated by chromatin. As a positive control, XPA was efficiently co-immunoprecipitated with RPA (Figure 5-4b, page 128).

#### Persistence of XPA-Localized DSBs

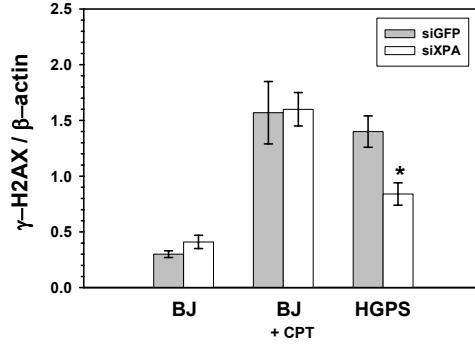
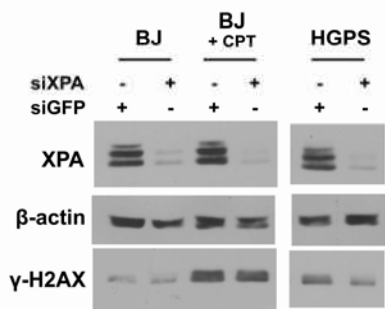
To confirm the accumulated XPA-localized DSBs in the patient cells are resistant to repair, we compared their repair rate to that of CPT-induced DSBs. As shown in Figure 5-5a (page 129), the XPA- $\gamma$ -H2AX colocalized foci remained unrepaired in HGPS and RD cells 24 hrs after CTP treatment. By contrast, the number of CPT-induced  $\gamma$ -H2AX foci (not colocalized with XPA foci) was significantly reduced in the progeroid or BJ cells, although repair in the patient cells occurred at much slower rates. Further quantitative analysis of the DSB repair as the

function of time confirmed the results (Figure 5-5b, page 129), supporting that the XPA-localized DSBs in the patient cells are resistant to repair.

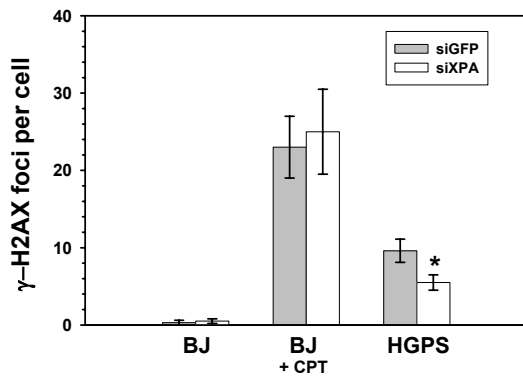
#### Effects of XPA Knockdown on DSB Repair in HGPS Cells

The appearance of XPA at unrepairable DSB sites may suggest a physiological role of XPA in the accumulation and persistence of DSBs in progeroid cells. To test this notion, XPA was knocked down in HGPS cells using XPA-specific siRNA (Figure 5-6a, page 132), followed by examination for the knockdown effects on accumulation of  $\gamma$ -H2AX in these cells using Western blotting. As shown in Figure 5-6a (page 132), XPA knockdown consistently resulted in 37-45% reduction of  $\gamma$ -H2AX formation in HGPS cells as compared to that of GFP siRNA transfected HGPS cells. However, XPA knockdown had no effect on the formation of CPT-induced  $\gamma$ -H2AX in BJ cells (Figure 5-6a, page 132). These results were also confirmed by the method of immunofluorescence. The number of  $\gamma$ -H2AX foci was significantly decreased after XPA knockdown (from  $9.6 \pm 1.6$  to  $5.5 \pm 1.1$  foci per cell in HGPS fibroblasts,  $P = 0.03$ ; from  $14.4 \pm 2.5$  to  $8.0 \pm 2.1$  foci per cell in RD fibroblasts,  $P = 0.03$ ) (Figure 5-6b, page 132), while XPA knockdown had no effect on the formation of CPT-induced  $\gamma$ -H2AX foci in BJ cells (Figure 5-6b, page 132). More direct evidence came from the comet assay of single cell electrophoresis that also showed significant reduction in DNA double-strand breaks in HGPS cells with XPA knockdown as compared with the control HGPS cells transfected with GFP-siRNA (Figure 5-6c, page 132). These results strongly support that XPA may inhibit DSB repair in HGPS and XPA knockdown by siRNA can partially restore the repair.

**a**



**b**



**c**

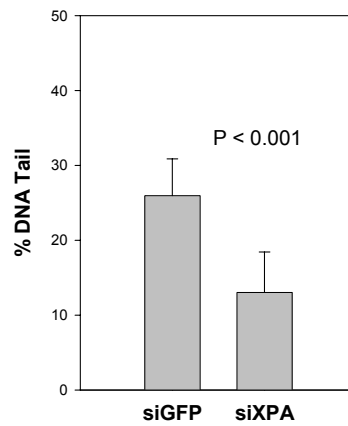
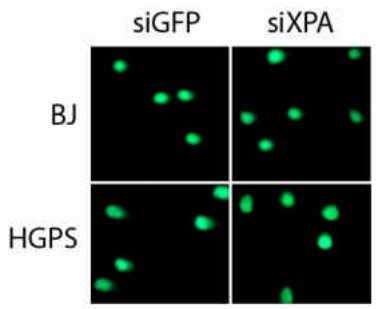


Figure 5-6. DSB repair in HGPS cells with XPA knockdown by RNAi

(a) Knockdown of XPA reduces DSB accumulation. For the knockdown of XPA by RNAi, the cells were transfected with XPA siRNA (Santa Cruz), or GFP siRNA as a control, using TransIT-TKO transfection reagent (Mirus) following manufacture's instruction. Western blotting was performed to analyze the knockdown efficiency 96 hours after transfection. XPA was shown as a known doublet of bands plus a weak third band due to phosphorylation siRNA (Wu et al., 2006). The amount of  $\gamma$ -H2AX was quantified against  $\beta$ -actin, the loading control, by densitometry. Standard deviations was generated from three independent experiments. The symbol \* indicates  $P < 0.05$ . (b) Number of  $\gamma$ -H2AX foci in the XPA-siRNA or GFP-siRNA transfected cells. The symbol \* indicates  $P < 0.05$ . (c) Comet assays were carried out with XPA-siRNA or GFP-siRNA transfected BJ cells and HGPS cells as described in Materials and Methods. DNA damage was quantified and expressed as the percentage of DNA in tail.

### Discussion

Recent studies have shown that DSBs typically accumulated in HGPS cells and RD cells and the resulted genome instability might contribute to premature aging (Liu et al., 2005; Manju et al., 2006; Varela et al., 2005). The accumulation is likely due to the deficiency in DNA repair in these progeria cells. In the effort to address the important question of why and how DNA repair is compromised in HGPS and RD cells that appear to have intact DNA repair proteins, we found that DSB repair proteins Rad51 and Rad50 were absent at the laminopathy-related DNA damage sites, at least partially contributing to the deficiency of DSB repair in the patient cells. The absence of Rad50 and Rad51 at DSBs was surprisingly concurrent with the formation of a significant amount of NER protein XPA foci and the localization of XPA to the unreparable DSBs. These uncharacteristic XPA focus formation and localization occurred exclusively in progeria cells but not in normal fibroblasts. It is possible that the localization of XPA to the laminopathy-induced DSB sites may deny accessibility of the damage sites to DSB-repair

factors, thus inhibiting DNA repair. If this is the case, removal of XPA should reduce the resistance to repair. Indeed, RNAi knockdown of XPA in HGPS cells restored DSB repair by a significant factor. Consistently, a portion of Rad51 foci was re-localized to  $\gamma$ -H2AX foci after XPA knockdown as shown in Figure 5-7. However, a large amount of Rad51 remains in aggregation in HGPS cells, which explains why only partial recovery of DNA repair capacity has been observed by XPA knockdown. These results suggest that XPA is at least partially responsible for the DSB repair deficiency in the patient cells.

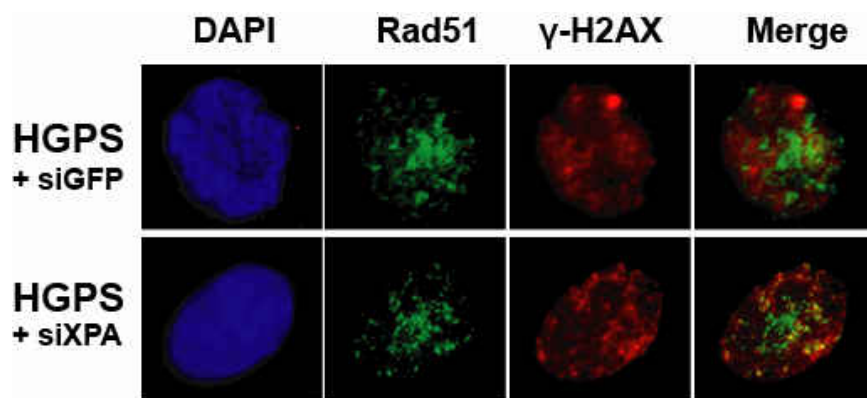


Figure 5-7. The localization of Rad51 foci and  $\gamma$ -H2AX foci in HGPS cells with or without XPA knockdown.

Although it has been well documented that XPA is involved in recognition of DNA bulky lesions in NER, it has no role in DSB repair. Our results from the modified ChIP and co-immunoprecipitation assays (Figure 5-4, page 128) indicated that the association of XPA with  $\gamma$ -H2AX appeared to be mediated by chromatin. It is possible that disruption of the chromatin-supporting scaffolds formed with nuclear lamins in HGPS and RD cells may produce broken chromosomes with unique DNA structures recognized by XPA. In support of this notion, we recently identified a novel activity of XPA for recognition of double-strand/single-strand DNA

(ds-ssDNA) junctions with 3'- and/or 5'-ssDNA overhangs (unpublished data). The binding affinity of XPA for these sites is between one and two orders of magnitude higher than its ability to bind to damaged DNA. This type of DNA structures form as intermediates during some DNA metabolic pathways including replication and DSB repair. In addition, a recent study demonstrated that XPA, but not NER-mediated damage processing, is required for UV-induced S-phase ATR checkpoint activation (Bomgardner et al., 2006) that is replication-dependent. Interestingly, DSBs could result from replication fork stalling and collapse. In the cases of HGPS and RD, more details of the uncharacteristic XPA-DNA binding in the progeria cells need to be defined in the future.

Findings presented in this study serve as the first step towards uncovering the underlying mechanism of DSB accumulation in premature aging HGPS and RD cells. Our results suggest a potential pathological role of XPA in development of human progeria diseases in contrast to its indispensable role in NER to counter NER-deficient diseases. This understanding also provides a potential strategy for alleviating laminopathy-related progeria syndromes by interfering with XPA function. In addition, recent studies showed that inhibiting farnesylation of progerin or prelamin A with farnesyltransferase inhibitors (FTIs) in RD and HGPS fibroblasts could reverse the aberrant nuclear morphology caused by deficiency in lamin A maturation (Capell et al., 2005; Glynn and Glover, 2005; Mallampalli et al., 2005; Toth et al., 2005). The inhibition also showed amelioration of the disease in a mouse model of progeria (Fong et al., 2006). However, we recently found that FTI treatment could not reduce the accumulated DSBs in both HGPS and RD cells (Chapter 4). This suggests that DNA damage accumulation and misshapen nuclei are probably two independent phenotypes caused by lamin A dysfunction in progeria. Thus, elimination of DNA damage accumulation and improvement of nuclear morphology would be



potential goals in development of an effective strategy for treatment of progeroid syndromes. Finally, DNA damage accumulation is believed to be one of the major causes to cellular senescence and normal aging (d'Adda di Fagagna et al., 2003; Gorbunova and Seluanov, 2005; Kirkwood, 2005; Lees-Miller, 2005; Lombard et al., 2005; Misteli and Scaffidi, 2005; von Zglinicki et al., 2005) and the similar unreparability of DSBs has been reported in senescing human cells (Sedelnikova et al., 2004). Importantly, lamin A-dependent nuclear defects were recently found in normal human aging (Scaffidi and Misteli, 2006). Thus, it is of great interest to determine if XPA plays a role in these processes.

## Reference

**Bomgarden, R. D., Lupardus, P. J., Soni, D. V., Yee, M. C., Ford, J. M. and Cimprich, K. A.** (2006). Opposing effects of the UV lesion repair protein XPA and UV bypass polymerase eta on ATR checkpoint signaling. *Embo J* **25**, 2605-14.

**Capell, B. C., Erdos, M. R., Madigan, J. P., Fiordalisi, J. J., Varga, R., Conneely, K. N., Gordon, L. B., Der, C. J., Cox, A. D. and Collins, F. S.** (2005). Inhibiting farnesylation of progerin prevents the characteristic nuclear blebbing of Hutchinson-Gilford progeria syndrome. *Proc Natl Acad Sci U S A* **102**, 12879-84.

**d'Adda di Fagagna, F., Reaper, P. M., Clay-Farrace, L., Fiegler, H., Carr, P., Von Zglinicki, T., Saretzki, G., Carter, N. P. and Jackson, S. P.** (2003). A DNA damage checkpoint response in telomere-initiated senescence. *Nature* **426**, 194-8.

**De Sandre-Giovannoli, A., Bernard, R., Cau, P., Navarro, C., Amiel, J., Boccaccio, I., Lyonnet, S., Stewart, C. L., Munnich, A., Le Merrer, M. et al.** (2003). Lamin a truncation in Hutchinson-Gilford progeria. *Science* **300**, 2055.

**Eriksson, M., Brown, W. T., Gordon, L. B., Glynn, M. W., Singer, J., Scott, L., Erdos, M. R., Robbins, C. M., Moses, T. Y., Berglund, P. et al.** (2003). Recurrent de novo point mutations in lamin A cause Hutchinson-Gilford progeria syndrome. *Nature* **423**, 293-8.

**Fong, L. G., Frost, D., Meta, M., Qiao, X., Yang, S. H., Coffinier, C. and Young, S. G.** (2006). A protein farnesyltransferase inhibitor ameliorates disease in a mouse model of progeria. *Science* **311**, 1621-3.

**Glynn, M. W. and Glover, T. W.** (2005). Incomplete processing of mutant lamin A in Hutchinson-Gilford progeria leads to nuclear abnormalities, which are reversed by farnesyltransferase inhibition. *Hum Mol Genet* **14**, 2959-69.

**Goldman, R. D., Gruenbaum, Y., Moir, R. D., Shumaker, D. K. and Spann, T. P.** (2002). Nuclear lamins: building blocks of nuclear architecture. *Genes Dev* **16**, 533-47.

**Gorbunova, V. and Seluanov, A.** (2005). Making ends meet in old age: DSB repair and aging. *Mech Ageing Dev* **126**, 621-8.

**Ichijima, Y., Sakasai, R., Okita, N., Asahina, K., Mizutani, S. and Teraoka, H.** (2005). Phosphorylation of histone H2AX at M phase in human cells without DNA damage response. *Biochem Biophys Res Commun* **336**, 807-12.

- Kirkwood, T. B.** (2005). Understanding the odd science of aging. *Cell* **120**, 437-47.
- Lee, J. H. and Paull, T. T.** (2004). Direct activation of the ATM protein kinase by the Mre11/Rad50/Nbs1 complex. *Science* **304**, 93-6.
- Lee, J. H. and Paull, T. T.** (2005). ATM activation by DNA double-strand breaks through the Mre11-Rad50-Nbs1 complex. *Science* **308**, 551-4.
- Lees-Miller, S. P.** (2005). Dysfunction of lamin A triggers a DNA damage response and cellular senescence. *DNA Repair (Amst)*.
- Liu, B., Wang, J., Chan, K. M., Tjia, W. M., Deng, W., Guan, X., Huang, J. D., Li, K. M., Chau, P. Y., Chen, D. J. et al.** (2005). Genomic instability in laminopathy-based premature aging. *Nat Med* **11**, 780-5.
- Lombard, D. B., Chua, K. F., Mostoslavsky, R., Franco, S., Gostissa, M. and Alt, F. W.** (2005). DNA repair, genome stability, and aging. *Cell* **120**, 497-512.
- Mallampalli, M. P., Huyer, G., Bendale, P., Gelb, M. H. and Michaelis, S.** (2005). Inhibiting farnesylation reverses the nuclear morphology defect in a HeLa cell model for Hutchinson-Gilford progeria syndrome. *Proc Natl Acad Sci U S A* **102**, 14416-21.
- Manju, K., Muralikrishna, B. and Parnaik, V. K.** (2006). Expression of disease-causing lamin A mutants impairs the formation of DNA repair foci. *J Cell Sci* **119**, 2704-14.
- Misteli, T. and Scaffidi, P.** (2005). Genome instability in progeria: when repair gets old. *Nat Med* **11**, 718-9.
- Navarro, C. L., Cadinanos, J., De Sandre-Giovannoli, A., Bernard, R., Courrier, S., Boccaccio, I., Boyer, A., Kleijer, W. J., Wagner, A., Giuliano, F. et al.** (2005). Loss of ZMPSTE24 (FACE-1) causes autosomal recessive restrictive dermopathy and accumulation of Lamin A precursors. *Hum Mol Genet* **14**, 1503-13.
- Paull, T. T. and Lee, J. H.** (2005). The Mre11/Rad50/Nbs1 complex and its role as a DNA double-strand break sensor for ATM. *Cell Cycle* **4**, 737-40.
- Ricke, R. M. and Bielinsky, A. K.** (2005). Easy detection of chromatin binding proteins by the Histone Association Assay. *Biol Proced Online* **7**, 60-9.
- Sancar, A., Lindsey-Boltz, L. A., Unsal-Kacmaz, K. and Linn, S.** (2004). Molecular mechanisms of mammalian DNA repair and the DNA damage checkpoints. *Annu Rev Biochem* **73**, 39-85.

**Scaffidi, P. and Misteli, T.** (2006). Lamin A-Dependent Nuclear Defects in Human Aging. *Science*.

**Sedelnikova, O. A., Horikawa, I., Zimonjic, D. B., Popescu, N. C., Bonner, W. M. and Barrett, J. C.** (2004). Senescing human cells and ageing mice accumulate DNA lesions with unrepairable double-strand breaks. *Nat Cell Biol* **6**, 168-70.

**Sinensky, M., Fantle, K. and Dalton, M.** (1994). An antibody which specifically recognizes prelamin A but not mature lamin A: application to detection of blocks in farnesylation-dependent protein processing. *Cancer Res* **54**, 3229-32.

**Toth, J. I., Yang, S. H., Qiao, X., Beigneux, A. P., Gelb, M. H., Moulson, C. L., Miner, J. H., Young, S. G. and Fong, L. G.** (2005). Blocking protein farnesyltransferase improves nuclear shape in fibroblasts from humans with progeroid syndromes. *Proc Natl Acad Sci U S A* **102**, 12873-8.

**Varela, I., Cadinanos, J., Pendas, A. M., Gutierrez-Fernandez, A., Folgueras, A. R., Sanchez, L. M., Zhou, Z., Rodriguez, F. J., Stewart, C. L., Vega, J. A. et al.** (2005). Accelerated ageing in mice deficient in Zmpste24 protease is linked to p53 signalling activation. *Nature* **437**, 564-8.

**von Zglinicki, T., Saretzki, G., Ladhoff, J., d'Adda di Fagagna, F. and Jackson, S. P.** (2005). Human cell senescence as a DNA damage response. *Mech Ageing Dev* **126**, 111-7.

**Wu, X., Shell, S. M., Yang, Z. and Zou, Y.** (2006). Phosphorylation of nucleotide excision repair factor xeroderma pigmentosum group A by ataxia telangiectasia mutated and Rad3-related-dependent checkpoint pathway promotes cell survival in response to UV irradiation. *Cancer Res* **66**, 2997-3005.

**Zou, Y., Liu, Y., Wu, X. and Shell, S. M.** (2006). Functions of human replication protein A (RPA): from DNA replication to DNA damage and stress responses. *J Cell Physiol* **208**, 267-73.

## CHAPTER 6

### SUMMARY AND CONCLUSIONS

The maintenance of genomic integrity is a fundamental requirement for cells and organisms to survive from generation to generation. To contend with both internal and external insults to the genome, cells have evolved many pathways. These include DNA repair for removing DNA damage and DNA damage checkpoints for arresting cell cycle progression so as to allow sufficient time for repair, thus preventing the conversion of DNA lesions to inheritable mutations. An important player in this complex pathway network is RPA, whose extensive involvement in DNA metabolism is mediated by its interactions with ssDNA and numerous proteins engaged in cellular processes. RPA has been extensively studied for nearly 20 years. However, the exact role of RPA in DNA damage recognition in NER is still unclear. The present study shows that RPA has a lower binding affinity for damaged ssDNA than for non-damaged ssDNA, and there was a lack of substantial direct contacts between RPA residues and the lesion itself. This result indicates that RPA has no direct recognition power for DNA damage. This is in line with a recent model suggesting that GGR subpathway of NER utilizes XPC-hHR23B as the initial factor for detecting DNA damage, whereas XPA-RPA functions in verifying the presence of the DNA lesion (Evans et al., 1997; Missura et al., 2001; Sugasawa et al., 1998; Thoma and Vasquez, 2003). But how the DNA lesions are verified remains to be elucidated. Our results would also help answer how the recognition complexes spatially arrange on the adducted DNA. Because of higher affinity for undamaged ssDNA, RPA may bind to the undamaged single

strand of the DNA duplex induced by lesions and leave the damaged strand for incision by endonucleases. The exact spatial arrangement of the repair factors needs further investigation.

RPA hyperphosphorylation has recently become an interestedly studied area (Binz et al., 2004; Block et al., 2004; Iftode et al., 1999; Liu and Weaver, 1993; Zernik-Kobak et al., 1997; Zou et al., 2006). We compared the structural characteristics of full-length native and hyperphosphorylated RPAs using mass spectrometric protein footprinting, fluorescence spectroscopy, and limited proteolysis (Liu et al., 2005b). Our data showed that upon hyperphosphorylation of RPA32N, RPA undergoes a conformational change involving the single-stranded DNA binding cleft of DBD-B. We propose that an interdomain interaction occurs between the hyp-RPA32N and DBD-B. Further study showed that a synthesized peptide (aa 11-37 of RPA32) containing phosphorylated Thr-21, Ser-23, and Ser-33, which mimicks hyp-RPA32N, can bind to RPA and quench the tryptophan fluorescence of Trp-361 in DBD-B. Moreover, the equilibrium dissociation constant ( $K_{d,obs}$ ) for the binding was calculated to be  $973 \pm 101$  nM (unpublished data). These data strongly suggest that hyp-RPA32N could affect RPA-DNA and RPA-protein interactions (with dissociation constants on the order of  $10^{-7}$  M) by competitively binding to DBD-B.

The proposed competitive binding model may provide a regulatory mechanism for the modulation of RPA in DNA metabolic pathways. Bochkareva et al. (Bochkareva et al., 2005) suggested that ssDNA may structurally compete with p53 for binding to the OB fold of RPA70N based on a NMR study, which explains why p53-RPA complex formation is affected by the presence of ssDNA. The acidic N-terminal peptide of Rad51 and ssDNA may compete for the binding to the OB fold of RPA70A (Stauffer and Chazin, 2004a). The competition for the multiple binding sites of RPA by DNA and many proteins may contribute to the ordered hand-

off of DNA from protein to protein in DNA metabolism and switch RPA between pathways (Stauffer and Chazin, 2004b). The highly acidic free hyp-RPA32N, if not bound by other factors, may also affect RPA-protein interactions by interfering with the function of acidic RPA32C, which is a protein-protein interacting domain. A clear direction for future study is the identification of protein factors that specifically interact with phosphorylated RPA or hyp-RPA32N. Because of the competitive mechanism for switching between pathways, *in vivo* experiments are needed to reveal the overall role of RPA phosphorylation in DNA metabolism.

Cellular accumulation of DNA damage has been widely implicated in cellular senescence, aging, and premature aging. In Hutchinson-Gilford progeria syndrome (HGPS) and restrictive dermopathy (RD), premature aging is caused by defective maturation of nuclear structural protein lamin A and linked to accumulation of DNA DSBs. The perplexity for these laminopathies is that the identified disease-causing genes seem to have no direct relation to the disease phenotype. In Chapter 4, we showed evidence that in HGPS and RD fibroblasts, DNA damage checkpoints are persistently activated and the recruitment of DSB repair factors Rad50 and Rad51 to the laminopathy-related DSB sites was impaired. Strikingly, XPA, a unique NER protein, formed foci and colocalized with the unrepairable DSBs in the patient cells. The data clearly demonstrated that lamin A dysfunction resulted in genomic instability. This observation is in agreement with the fact that one of the functions of the lamins is to tether the nuclear envelope to chromatin. Previous studies also showed that the nuclear lamins play major roles in chromatin organization, DNA replication and RNA polymerase II-dependent gene expression (Burke and Ellenberg, 2002; Burke and Stewart, 2002; Gruenbaum et al., 2005; Taddei et al., 2004). It is possible that disruption of the chromatin-supporting scaffolds formed with nuclear lamins in HGPS and RD cells may produce broken chromosomes with unique DNA structures

recognized by XPA. The most significant findings of the present study are that inactivation of checkpoint kinases ATM and ATR in these patient cells can partially overcome their early replication arrest, and RNAi knockdown of XPA in HGPS cells significantly restored DSB repair. This provides a potential strategy for treatment of these devastating premature aging diseases. More experiments are needed to examine the effects of kinase inactivation and/or XPA knockdown on the senescence of the patient cells. The generation and analysis of XPA<sup>-/-</sup> Zmpste24<sup>-/-</sup> mice could provide more information for the development of treatment strategy.



## COMPREHENSIVE REFERENCES

- Abraham, R.T. (2001) Cell cycle checkpoint signaling through the ATM and ATR kinases. *Genes Dev*, **15**, 2177-2196.
- Abramova, N.A., Russell, J., Botchan, M. and Li, R. (1997) Interaction between replication protein A and p53 is disrupted after UV damage in a DNA repair-dependent manner. *Proc Natl Acad Sci U S A*, **94**, 7186-7191.
- Arunkumar, A.I., Stauffer, M.E., Bochkareva, E., Bochkarev, A. and Chazin, W.J. (2003) Independent and coordinated functions of replication protein A tandem high affinity single-stranded DNA binding domains. *J Biol Chem*, **278**, 41077-41082.
- Barr, S.M., Leung, C.G., Chang, E.E. and Cimprich, K.A. (2003) ATR kinase activity regulates the intranuclear translocation of ATR and RPA following ionizing radiation. *Curr Biol*, **13**, 1047-1051.
- Bastin-Shanower, S.A. and Brill, S.J. (2001) Functional analysis of the four DNA binding domains of replication protein A. The role of RPA2 in ssDNA binding. *J Biol Chem*, **276**, 36446-36453.
- Bennett, K.L., Matthiesen, T. and Roepstorff, P. (2000) Probing protein surface topology by chemical surface labeling, crosslinking, and mass spectrometry. *Methods Mol Biol*, **146**, 113-131.
- Binz, S.K., Lao, Y., Lowry, D.F. and Wold, M.S. (2003) The phosphorylation domain of the 32-kDa subunit of replication protein A (RPA) modulates RPA-DNA interactions. Evidence for an intersubunit interaction. *J Biol Chem*, **278**, 35584-35591.
- Binz, S.K., Sheehan, A.M. and Wold, M.S. (2004) Replication protein A phosphorylation and the cellular response to DNA damage. *DNA Repair (Amst)*, **3**, 1015-1024.
- Blackwell, L.J. and Borowiec, J.A. (1994) Human replication protein A binds single-stranded DNA in two distinct complexes. *Mol Cell Biol*, **14**, 3993-4001.
- Block, W.D., Yu, Y. and Lees-Miller, S.P. (2004) Phosphatidyl inositol 3-kinase-like serine/threonine protein kinases (PIKKs) are required for DNA damage-induced phosphorylation of the 32 kDa subunit of replication protein A at threonine 21. *Nucleic Acids Res*, **32**, 997-1005.

- Bochkarev, A. and Bochkareva, E. (2004) From RPA to BRCA2: lessons from single-stranded DNA binding by the OB-fold. *Curr Opin Struct Biol*, **14**, 36-42.
- Bochkarev, A., Bochkareva, E., Frappier, L. and Edwards, A.M. (1999) The crystal structure of the complex of replication protein A subunits RPA32 and RPA14 reveals a mechanism for single-stranded DNA binding. *Embo J*, **18**, 4498-4504.
- Bochkarev, A., Pfuetzner, R.A., Edwards, A.M. and Frappier, L. (1997) Structure of the single-stranded-DNA-binding domain of replication protein A bound to DNA. *Nature*, **385**, 176-181.
- Bochkareva, E., Belegu, V., Korolev, S. and Bochkarev, A. (2001) Structure of the major single-stranded DNA-binding domain of replication protein A suggests a dynamic mechanism for DNA binding. *Embo J*, **20**, 612-618.
- Bochkareva, E., Frappier, L., Edwards, A.M. and Bochkarev, A. (1998) The RPA32 subunit of human replication protein A contains a single-stranded DNA-binding domain. *J Biol Chem*, **273**, 3932-3936.
- Bochkareva, E., Kaustov, L., Ayed, A., Yi, G.S., Lu, Y., Pineda-Lucena, A., Liao, J.C., Okorokov, A.L., Milner, J., Arrowsmith, C.H. and Bochkarev, A. (2005) Single-stranded DNA mimicry in the p53 transactivation domain interaction with replication protein A. *Proc Natl Acad Sci U S A*, **102**, 15412-15417.
- Bochkareva, E., Korolev, S. and Bochkarev, A. (2000) The role for zinc in replication protein A. *J Biol Chem*, **275**, 27332-27338.
- Bochkareva, E., Korolev, S., Lees-Miller, S.P. and Bochkarev, A. (2002) Structure of the RPA trimerization core and its role in the multistep DNA-binding mechanism of RPA. *Embo J*, **21**, 1855-1863.
- Bomgardner, R.D., Lupardus, P.J., Soni, D.V., Yee, M.C., Ford, J.M. and Cimprich, K.A. (2006) Opposing effects of the UV lesion repair protein XPA and UV bypass polymerase eta on ATR checkpoint signaling. *Embo J*, **25**, 2605-2614.
- Bootsma, D., Kraemer, K. H., Cleaver, J. E., and Hoeijmakers, J. H. (2002) *Nucleotide excision repair syndromes: Xeroderma pigmentosum, Cockayne syndrome, and trichothiodystrophy. The genetic basis of human cancer*. McGraw-Hill, Medical Pub. Division, New York.

- Boubnov, N.V. and Weaver, D.T. (1995) scid cells are deficient in Ku and replication protein A phosphorylation by the DNA-dependent protein kinase. *Mol Cell Biol*, **15**, 5700-5706.
- Brill, S.J. and Bastin-Shanower, S. (1998) Identification and characterization of the fourth single-stranded-DNA binding domain of replication protein A. *Mol Cell Biol*, **18**, 7225-7234.
- Brush, G.S., Anderson, C.W. and Kelly, T.J. (1994) The DNA-activated protein kinase is required for the phosphorylation of replication protein A during simian virus 40 DNA replication. *Proc Natl Acad Sci U S A*, **91**, 12520-12524.
- Brush, G.S., Morrow, D.M., Hieter, P. and Kelly, T.J. (1996) The ATM homologue MEC1 is required for phosphorylation of replication protein A in yeast. *Proc Natl Acad Sci U S A*, **93**, 15075-15080.
- Burke, B. and Ellenberg, J. (2002) Remodelling the walls of the nucleus. *Nat Rev Mol Cell Biol*, **3**, 487-497.
- Burke, B. and Stewart, C.L. (2002) Life at the edge: the nuclear envelope and human disease. *Nat Rev Mol Cell Biol*, **3**, 575-585.
- Burns, J.L., Guzder, S.N., Sung, P., Prakash, S. and Prakash, L. (1996) An affinity of human replication protein A for ultraviolet-damaged DNA. *J Biol Chem*, **271**, 11607-11610.
- Capell, B.C., Erdos, M.R., Madigan, J.P., Fiordalisi, J.J., Varga, R., Conneely, K.N., Gordon, L.B., Der, C.J., Cox, A.D. and Collins, F.S. (2005) Inhibiting farnesylation of progerin prevents the characteristic nuclear blebbing of Hutchinson-Gilford progeria syndrome. *Proc Natl Acad Sci U S A*, **102**, 12879-12884.
- Carty, M.P., Zernik-Kobak, M., McGrath, S. and Dixon, K. (1994) UV light-induced DNA synthesis arrest in HeLa cells is associated with changes in phosphorylation of human single-stranded DNA-binding protein. *Embo J*, **13**, 2114-2123.
- Clifford, D.M., Marinco, S.M. and Brush, G.S. (2004) The meiosis-specific protein kinase Ime2 directs phosphorylation of replication protein A. *J Biol Chem*, **279**, 6163-6170.
- Clugston, C.K., McLaughlin, K., Kenny, M.K. and Brown, R. (1992) Binding of human single-stranded DNA binding protein to DNA damaged by the anticancer drug cis-diamminedichloroplatinum (II). *Cancer Res*, **52**, 6375-6379.
- Cortez, D., Guntuku, S., Qin, J. and Elledge, S.J. (2001) ATR and ATRIP: partners in checkpoint signaling. *Science*, **294**, 1713-1716.

- Cosman, M., Ibanez, V., Geacintov, N.E. and Harvey, R.G. (1990) Preparation and isolation of adducts in high yield derived from the binding of two benzo[a]pyrene-7,8-dihydroxy-9,10-oxide stereoisomers to the oligonucleotide d(ATATGTATA). *Carcinogenesis*, **11**, 1667-1672.
- Cruet-Hennequart, S., Coyne, S., Glynn, M.T., Oakley, G.G. and Carty, M.P. (2006) UV-induced RPA phosphorylation is increased in the absence of DNA polymerase eta and requires DNA-PK. *DNA Repair (Amst)*, **5**, 491-504.
- d'Adda di Fagagna, F., Reaper, P.M., Clay-Farrace, L., Fiegler, H., Carr, P., Von Zglinicki, T., Saretzki, G., Carter, N.P. and Jackson, S.P. (2003) A DNA damage checkpoint response in telomere-initiated senescence. *Nature*, **426**, 194-198.
- Dart, D.A., Adams, K.E., Akerman, I. and Lakin, N.D. (2004) Recruitment of the cell cycle checkpoint kinase ATR to chromatin during S-phase. *J Biol Chem*, **279**, 16433-16440.
- de Laat, W.L., Appeldoorn, E., Sugawara, K., Weterings, E., Jaspers, N.G. and Hoeijmakers, J.H. (1998) DNA-binding polarity of human replication protein A positions nucleases in nucleotide excision repair. *Genes Dev*, **12**, 2598-2609.
- De Sandre-Giovannoli, A., Bernard, R., Cau, P., Navarro, C., Amiel, J., Boccaccio, I., Lyonnet, S., Stewart, C.L., Munnich, A., Le Merrer, M. and Levy, N. (2003) Lamin a truncation in Hutchinson-Gilford progeria. *Science*, **300**, 2055.
- Din, S., Brill, S.J., Fairman, M.P. and Stillman, B. (1990) Cell-cycle-regulated phosphorylation of DNA replication factor A from human and yeast cells. *Genes Dev*, **4**, 968-977.
- Doll, R. and Peto, R. (1981) The causes of cancer: quantitative estimates of avoidable risks of cancer in the United States today. *J Natl Cancer Inst*, **66**, 1191-1308.
- Dutta, A. and Stillman, B. (1992) cdc2 family kinases phosphorylate a human cell DNA replication factor, RPA, and activate DNA replication. *Embo J*, **11**, 2189-2199.
- Eriksson, M., Brown, W.T., Gordon, L.B., Glynn, M.W., Singer, J., Scott, L., Erdos, M.R., Robbins, C.M., Moses, T.Y., Berglund, P., Dutra, A., Pak, E., Durkin, S., Csoka, A.B., Boehnke, M., Glover, T.W. and Collins, F.S. (2003) Recurrent de novo point mutations in lamin A cause Hutchinson-Gilford progeria syndrome. *Nature*, **423**, 293-298.
- Evans, E., Moggs, J.G., Hwang, J.R., Egly, J.M. and Wood, R.D. (1997) Mechanism of open complex and dual incision formation by human nucleotide excision repair factors. *Embo J*, **16**, 6559-6573.

- Fong, L.G., Frost, D., Meta, M., Qiao, X., Yang, S.H., Coffinier, C. and Young, S.G. (2006) A protein farnesyltransferase inhibitor ameliorates disease in a mouse model of progeria. *Science*, **311**, 1621-1623.
- Fried, L.M., Koumenis, C., Peterson, S.R., Green, S.L., van Zijl, P., Allalunis-Turner, J., Chen, D.J., Fishel, R., Giaccia, A.J., Brown, J.M. and Kirchgessner, C.U. (1996) The DNA damage response in DNA-dependent protein kinase-deficient SCID mouse cells: replication protein A hyperphosphorylation and p53 induction. *Proc Natl Acad Sci U S A*, **93**, 13825-13830.
- Gately, D.P., Hittle, J.C., Chan, G.K. and Yen, T.J. (1998) Characterization of ATM expression, localization, and associated DNA-dependent protein kinase activity. *Mol Biol Cell*, **9**, 2361-2374.
- Geacintov, N.E., Gagliano, A.G., Ibanez, V. and Harvey, R.G. (1982) Spectroscopic characterizations and comparisons of the structures of the covalent adducts derived from the reactions of 7, 8-dihydroxy-7,8,9,10-tetrahydrobenzo [a] pyrene-9,10-oxide, and the 9, 10-epoxides of 7,8,9,10-tetrahydrobenzo [a] pyrene and 9,10,11,12-tetrahydrobenzo [e] pyrene with DNA. *Carcinogenesis*, **3**, 247-253.
- Geacintov, N.E., Solntsev, k., Johnson, L.W., Chen, J.X., Kolbanovskiy, A.D., Liu, T.M. and Shafirovich, V.Y. (1998) Photoinduced electron transfer and strand cleavage in pyrenyl-DNA complexes and adducts. *J. Phys. Org. Chem.*, **11**, 561-565.
- Geacintov, N.E., Zinger, D., Ibanez, V., Santella, R., Grunberger, D. and Harvey, R.G. (1987) Properties of covalent benzo[a]pyrene diol epoxide-DNA adducts investigated by fluorescence techniques. *Carcinogenesis*, **8**, 925-935.
- Glynn, M.W. and Glover, T.W. (2005) Incomplete processing of mutant lamin A in Hutchinson-Gilford progeria leads to nuclear abnormalities, which are reversed by farnesyltransferase inhibition. *Hum Mol Genet*, **14**, 2959-2969.
- Goldman, R.D., Gruenbaum, Y., Moir, R.D., Shumaker, D.K. and Spann, T.P. (2002) Nuclear lamins: building blocks of nuclear architecture. *Genes Dev*, **16**, 533-547.
- Goldman, R.D., Shumaker, D.K., Erdos, M.R., Eriksson, M., Goldman, A.E., Gordon, L.B., Gruenbaum, Y., Khuon, S., Mendez, M., Varga, R. and Collins, F.S. (2004) Accumulation of mutant lamin A causes progressive changes in nuclear architecture in Hutchinson-Gilford progeria syndrome. *Proc Natl Acad Sci U S A*, **101**, 8963-8968.

- Gomes, X.V., Henricksen, L.A. and Wold, M.S. (1996) Proteolytic mapping of human replication protein A: evidence for multiple structural domains and a conformational change upon interaction with single-stranded DNA. *Biochemistry*, **35**, 5586-5595.
- Gorbunova, V. and Seluanov, A. (2005) Making ends meet in old age: DSB repair and aging. *Mech Ageing Dev*, **126**, 621-628.
- Gruenbaum, Y., Margalit, A., Goldman, R.D., Shumaker, D.K. and Wilson, K.L. (2005) The nuclear lamina comes of age. *Nat Rev Mol Cell Biol*, **6**, 21-31.
- He, Z., Henricksen, L.A., Wold, M.S. and Ingles, C.J. (1995) RPA involvement in the damage-recognition and incision steps of nucleotide excision repair. *Nature*, **374**, 566-569.
- Helt, C.E., Cliby, W. A., Keng, P. C., and Bambara, R. A. (2005) Ataxia Telangiectasia Mutated (ATM) and ATM and Rad3-related protein exhibit selective target specificities in response to different forms of DNA damage. *J Biol Chem*, **280**, 1186-1192.
- Henricksen, L.A., Carter, T., Dutta, A. and Wold, M.S. (1996) Phosphorylation of human replication protein A by the DNA-dependent protein kinase is involved in the modulation of DNA replication. *Nucleic Acids Res*, **24**, 3107-3112.
- Hey, T., Lipps, G. and Krauss, G. (2001) Binding of XPA and RPA to damaged DNA investigated by fluorescence anisotropy. *Biochemistry*, **40**, 2901-2910.
- Heyduk, E. and Heyduk, T. (1994) Mapping protein domains involved in macromolecular interactions: a novel protein footprinting approach. *Biochemistry*, **33**, 9643-9650.
- Huang, W., Amin, S. and Geacintov, N.E. (2002) Fluorescence characteristics of site-specific and stereochemically distinct benzo[a]pyrene diol epoxide-DNA adducts as probes of adduct conformation. *Chem Res Toxicol*, **15**, 118-126.
- Ichijima, Y., Sakasai, R., Okita, N., Asahina, K., Mizutani, S. and Teraoka, H. (2005) Phosphorylation of histone H2AX at M phase in human cells without DNA damage response. *Biochem Biophys Res Commun*, **336**, 807-812.
- Iftode, C., Daniely, Y. and Borowiec, J.A. (1999) Replication protein A (RPA): the eukaryotic SSB. *Crit Rev Biochem Mol Biol*, **34**, 141-180.
- Jackson, D., Dhar, K., Wahl, J.K., Wold, M.S. and Borgstahl, G.E. (2002) Analysis of the human replication protein A:Rad52 complex: evidence for crosstalk between RPA32, RPA70, Rad52 and DNA. *J Mol Biol*, **321**, 133-148.

- Jackson, S.P. (2002) Sensing and repairing DNA double-strand breaks. *Carcinogenesis*, **23**, 687-696.
- Jacobs, D.M., Lipton, A.S., Isern, N.G., Daughdrill, G.W., Lowry, D.F., Gomes, X. and Wold, M.S. (1999) Human replication protein A: global fold of the N-terminal RPA-70 domain reveals a basic cleft and flexible C-terminal linker. *J Biomol NMR*, **14**, 321-331.
- Karanjawala, Z.E. and Lieber, M.R. (2004) DNA damage and aging. *Mech Ageing Dev*, **125**, 405-416.
- Kerr, I.D., Wadsworth, R.I., Cubeddu, L., Blankenfeldt, W., Naismith, J.H. and White, M.F. (2003) Insights into ssDNA recognition by the OB fold from a structural and thermodynamic study of Sulfolobus SSB protein. *Embo J*, **22**, 2561-2570.
- Kim, C., Paulus, B.F. and Wold, M.S. (1994) Interactions of human replication protein A with oligonucleotides. *Biochemistry*, **33**, 14197-14206.
- Kim, C., Snyder, R.O. and Wold, M.S. (1992) Binding properties of replication protein A from human and yeast cells. *Mol Cell Biol*, **12**, 3050-3059.
- Kim, C. and Wold, M.S. (1995) Recombinant human replication protein A binds to polynucleotides with low cooperativity. *Biochemistry*, **34**, 2058-2064.
- Kim, H.S. and Brill, S.J. (2003) MEC1-dependent phosphorylation of yeast RPA1 in vitro. *DNA Repair (Amst)*, **2**, 1321-1335.
- Kirkwood, T.B. (2005) Understanding the odd science of aging. *Cell*, **120**, 437-447.
- Kolodner, R.D., Putnam, C.D. and Myung, K. (2002) Maintenance of genome stability in *Saccharomyces cerevisiae*. *Science*, **297**, 552-557.
- Kolpashchikov, D.M., Weissart, K., Nasheuer, H.P., Khodyreva, S.N., Fanning, E., Favre, A. and Lavrik, O.I. (1999) Interaction of the p70 subunit of RPA with a DNA template directs p32 to the 3'-end of nascent DNA. *FEBS Lett*, **450**, 131-134.
- Kvaratskhelia, M., Miller, J.T., Budihas, S.R., Pannell, L.K. and Le Grice, S.F. (2002) Identification of specific HIV-1 reverse transcriptase contacts to the viral RNA:tRNA complex by mass spectrometry and a primary amine selective reagent. *Proc Natl Acad Sci U S A*, **99**, 15988-15993.
- Lao, Y., Gomes, X.V., Ren, Y., Taylor, J.S. and Wold, M.S. (2000) Replication protein A interactions with DNA. III. Molecular basis of recognition of damaged DNA. *Biochemistry*, **39**, 850-859.

- Lao, Y., Lee, C.G. and Wold, M.S. (1999) Replication protein A interactions with DNA. 2. Characterization of double-stranded DNA-binding/helix-destabilization activities and the role of the zinc-finger domain in DNA interactions. *Biochemistry*, **38**, 3974-3984.
- Lavrik, O.I., Kolpashchikov, D.M., Weisshart, K., Nasheuer, H.P., Khodyreva, S.N. and Favre, A. (1999) RPA subunit arrangement near the 3'-end of the primer is modulated by the length of the template strand and cooperative protein interactions. *Nucleic Acids Res*, **27**, 4235-4240.
- Lee, J.H. and Paull, T.T. (2004) Direct activation of the ATM protein kinase by the Mre11/Rad50/Nbs1 complex. *Science*, **304**, 93-96.
- Lee, J.H. and Paull, T.T. (2005) ATM activation by DNA double-strand breaks through the Mre11-Rad50-Nbs1 complex. *Science*, **308**, 551-554.
- Lee, S.H. and Kim, D.K. (1995) The role of the 34-kDa subunit of human replication protein A in simian virus 40 DNA replication in vitro. *J Biol Chem*, **270**, 12801-12807.
- Lees-Miller, S.P. (2005) Dysfunction of lamin A triggers a DNA damage response and cellular senescence. *DNA Repair (Amst)*.
- Leite, J.F. and Cascio, M. (2002) Probing the topology of the glycine receptor by chemical modification coupled to mass spectrometry. *Biochemistry*, **41**, 6140-6148.
- Li, L. and Zou, L. (2005) Sensing, signaling, and responding to DNA damage: organization of the checkpoint pathways in mammalian cells. *J Cell Biochem*, **94**, 298-306.
- Liu, B., Wang, J., Chan, K.M., Tjia, W.M., Deng, W., Guan, X., Huang, J.D., Li, K.M., Chau, P.Y., Chen, D.J., Pei, D., Pendas, A.M., Cadinanos, J., Lopez-Otin, C., Tse, H.F., Hutchison, C., Chen, J., Cao, Y., Cheah, K.S., Tryggvason, K. and Zhou, Z. (2005a) Genomic instability in laminopathy-based premature aging. *Nat Med*, **11**, 780-785.
- Liu, J.S., Kuo, S.R. and Melendy, T. (2006a) Phosphorylation of replication protein A by S-phase checkpoint kinases. *DNA Repair (Amst)*, **5**, 369-380.
- Liu, V.F. and Weaver, D.T. (1993) The ionizing radiation-induced replication protein A phosphorylation response differs between ataxia telangiectasia and normal human cells. *Mol Cell Biol*, **13**, 7222-7231.
- Liu, Y., Kvaratskhelia, M., Hess, S., Qu, Y. and Zou, Y. (2005b) Modulation of replication protein A function by its hyperphosphorylation-induced conformational change involving DNA binding domain B. *J Biol Chem*, **280**, 32775-32783.



- Liu, Y., Rusinol, A., Sinensky, M., Wang, Y. and Zou, Y. (2006b) DNA damage responses in progeroid syndromes arising from defective maturation of prelamin A. *J Cell Sci*, (**in press**).
- Liu, Y., Yang, Z., Utzat, C.D., Liu, Y., Geacintov, N.E., Basu, A.K. and Zou, Y. (2005c) Interactions of human replication protein A with single-stranded DNA adducts. *Biochem J*, **385**, 519-526.
- Lombard, D.B., Chua, K.F., Mostoslavsky, R., Franco, S., Gostissa, M. and Alt, F.W. (2005) DNA repair, genome stability, and aging. *Cell*, **120**, 497-512.
- Mallampalli, M.P., Huyer, G., Bendale, P., Gelb, M.H. and Michaelis, S. (2005) Inhibiting farnesylation reverses the nuclear morphology defect in a HeLa cell model for Hutchinson-Gilford progeria syndrome. *Proc Natl Acad Sci U S A*, **102**, 14416-14421.
- Manju, K., Muralikrishna, B. and Parnaik, V.K. (2006) Expression of disease-causing lamin A mutants impairs the formation of DNA repair foci. *J Cell Sci*, **119**, 2704-2714.
- Mass, G., Nethanel, T., Lavrik, O.I., Wold, M.S. and Kaufmann, G. (2001) Replication protein A modulates its interface with the primed DNA template during RNA-DNA primer elongation in replicating SV40 chromosomes. *Nucleic Acids Res*, **29**, 3892-3899.
- McGowan, C.H. and Russell, P. (2004) The DNA damage response: sensing and signaling. *Curr Opin Cell Biol*, **16**, 629-633.
- Mer, G., Bochkarev, A., Gupta, R., Bochkareva, E., Frappier, L., Ingles, C.J., Edwards, A.M. and Chazin, W.J. (2000) Structural basis for the recognition of DNA repair proteins UNG2, XPA, and RAD52 by replication factor RPA. *Cell*, **103**, 449-456.
- Missura, M., Buterin, T., Hindges, R., Hubscher, U., Kasparikova, J., Brabec, V. and Naegeli, H. (2001) Double-check probing of DNA bending and unwinding by XPA-RPA: an architectural function in DNA repair. *Embo J*, **20**, 3554-3564.
- Misteli, T. and Scaffidi, P. (2005) Genome instability in progeria: when repair gets old. *Nat Med*, **11**, 718-719.
- Mu, D., Hsu, D.S. and Sancar, A. (1996) Reaction mechanism of human DNA repair excision nuclease. *J Biol Chem*, **271**, 8285-8294.
- Murzin, A.G. (1993) OB(oligonucleotide/oligosaccharide binding)-fold: common structural and functional solution for non-homologous sequences. *Embo J*, **12**, 861-867.

- Navarro, C.L., Cadinanos, J., De Sandre-Giovannoli, A., Bernard, R., Courrier, S., Boccaccio, I., Boyer, A., Kleijer, W.J., Wagner, A., Giuliano, F., Beemer, F.A., Freije, J.M., Cau, P., Hennekam, R.C., Lopez-Otin, C., Badens, C. and Levy, N. (2005) Loss of ZMPSTE24 (FACE-1) causes autosomal recessive restrictive dermopathy and accumulation of Lamin A precursors. *Hum Mol Genet*, **14**, 1503-1513.
- Niu, H., Erdjument-Bromage, H., Pan, Z.Q., Lee, S.H., Tempst, P. and Hurwitz, J. (1997) Mapping of amino acid residues in the p34 subunit of human single-stranded DNA-binding protein phosphorylated by DNA-dependent protein kinase and Cdc2 kinase in vitro. *J Biol Chem*, **272**, 12634-12641.
- Nuss, J.E., Patrick, S.M., Oakley, G.G., Alter, G.M., Robison, J.G., Dixon, K. and Turchi, J.J. (2005) DNA damage induced hyperphosphorylation of replication protein A. 1. Identification of novel sites of phosphorylation in response to DNA damage. *Biochemistry*, **44**, 8428-8437.
- Oakley, G.G., Loberg, L.I., Yao, J., Risinger, M.A., Yunker, R.L., Zernik-Kobak, M., Khanna, K.K., Lavin, M.F., Carty, M.P. and Dixon, K. (2001) UV-induced hyperphosphorylation of replication protein a depends on DNA replication and expression of ATM protein. *Mol Biol Cell*, **12**, 1199-1213.
- Oakley, G.G., Patrick, S.M., Yao, J., Carty, M.P., Turchi, J.J. and Dixon, K. (2003) RPA phosphorylation in mitosis alters DNA binding and protein-protein interactions. *Biochemistry*, **42**, 3255-3264.
- Pan, Z.Q., Amin, A.A., Gibbs, E., Niu, H. and Hurwitz, J. (1994) Phosphorylation of the p34 subunit of human single-stranded-DNA-binding protein in cyclin A-activated G1 extracts is catalyzed by cdk-cyclin A complex and DNA-dependent protein kinase. *Proc Natl Acad Sci U S A*, **91**, 8343-8347.
- Park, C.J. and Choi, B.S. (2006) The protein shuffle. Sequential interactions among components of the human nucleotide excision repair pathway. *Febs J*, **273**, 1600-1608.
- Park, J.S., Park, S.J., Peng, X., Wang, M., Yu, M.A. and Lee, S.H. (1999) Involvement of DNA-dependent protein kinase in UV-induced replication arrest. *J Biol Chem*, **274**, 32520-32527.
- Patrick, S.M., Oakley, G.G., Dixon, K. and Turchi, J.J. (2005) DNA Damage Induced Hyperphosphorylation of Replication Protein A. 2. Characterization of DNA Binding

- Activity, Protein Interactions, and Activity in DNA Replication and Repair. *Biochemistry*, **44**, 8438-8448.
- Patrick, S.M. and Turchi, J.J. (1999) Replication protein A (RPA) binding to duplex cisplatin-damaged DNA is mediated through the generation of single-stranded DNA. *J Biol Chem*, **274**, 14972-14978.
- Patrick, S.M. and Turchi, J.J. (2001) Stopped-flow kinetic analysis of replication protein A-binding DNA: damage recognition and affinity for single-stranded DNA reveal differential contributions of k(on) and k(off) rate constants. *J Biol Chem*, **276**, 22630-22637.
- Paull, T.T. and Lee, J.H. (2005) The Mre11/Rad50/Nbs1 complex and its role as a DNA double-strand break sensor for ATM. *Cell Cycle*, **4**, 737-740.
- Pestryakov, P.E., Khlimankov, D.Y., Bochkareva, E., Bochkarev, A. and Lavrik, O.I. (2004) Human replication protein A (RPA) binds a primer-template junction in the absence of its major ssDNA-binding domains. *Nucleic Acids Res*, **32**, 1894-1903.
- Pestryakov, P.E., Weisshart, K., Schlott, B., Khodyreva, S.N., Kremmer, E., Grosse, F., Lavrik, O.I. and Nasheuer, H.P. (2003) Human replication protein A. The C-terminal RPA70 and the central RPA32 domains are involved in the interactions with the 3'-end of a primer-template DNA. *J Biol Chem*, **278**, 17515-17524.
- Reardon, J.T. and Sancar, A. (2002) Molecular anatomy of the human excision nuclease assembled at sites of DNA damage. *Mol Cell Biol*, **22**, 5938-5945.
- Reardon, J.T. and Sancar, A. (2003) Recognition and repair of the cyclobutane thymine dimer, a major cause of skin cancers, by the human excision nuclease. *Genes Dev*, **17**, 2539-2551.
- Ricke, R.M. and Bielinsky, A.K. (2005) Easy detection of chromatin binding proteins by the Histone Association Assay. *Biol Proced Online*, **7**, 60-69.
- Riedl, T., Hanaoka, F. and Egly, J.M. (2003) The comings and goings of nucleotide excision repair factors on damaged DNA. *Embo J*, **22**, 5293-5303.
- Sakasai, R., Shinohe, K., Ichijima, Y., Okita, N., Shibata, A., Asahina, K. and Teraoka, H. (2006) Differential involvement of phosphatidylinositol 3-kinase-related protein kinases in hyperphosphorylation of replication protein A2 in response to replication-mediated DNA double-strand breaks. *Genes Cells*, **11**, 237-246.
- Sancar, A. (1996) DNA excision repair. *Annu Rev Biochem*, **65**, 43-81.

- Sancar, A., Lindsey-Boltz, L.A., Unsal-Kacmaz, K. and Linn, S. (2004) Molecular mechanisms of mammalian DNA repair and the DNA damage checkpoints. *Annu Rev Biochem*, **73**, 39-85.
- Sarkaria, J.N., Busby, E.C., Tibbetts, R.S., Roos, P., Taya, Y., Karnitz, L.M. and Abraham, R.T. (1999) Inhibition of ATM and ATR kinase activities by the radiosensitizing agent, caffeine. *Cancer Res*, **59**, 4375-4382.
- Scaffidi, P. and Misteli, T. (2006a) Lamin A-dependent nuclear defects in human aging. *Science*, **312**, 1059-1063.
- Scaffidi, P. and Misteli, T. (2006b) Lamin A-Dependent Nuclear Defects in Human Aging. *Science*.
- Schweizer, U., Hey, T., Lipps, G. and Krauss, G. (1999) Photocrosslinking locates a binding site for the large subunit of human replication protein A to the damaged strand of cisplatin-modified DNA. *Nucleic Acids Res*, **27**, 3183-3189.
- Sedelnikova, O.A., Horikawa, I., Zimonjic, D.B., Popescu, N.C., Bonner, W.M. and Barrett, J.C. (2004) Senescing human cells and ageing mice accumulate DNA lesions with unreparable double-strand breaks. *Nat Cell Biol*, **6**, 168-170.
- Sedelnikova, O.A., Rogakou, E.P., Panyutin, I.G. and Bonner, W.M. (2002) Quantitative detection of (125)IdU-induced DNA double-strand breaks with gamma-H2AX antibody. *Radiat Res*, **158**, 486-492.
- Shao, R.G., Cao, C.X., Shimizu, T., O'Connor, P.M., Kohn, K.W. and Pommier, Y. (1997) Abrogation of an S-phase checkpoint and potentiation of camptothecin cytotoxicity by 7-hydroxystaurosporine (UCN-01) in human cancer cell lines, possibly influenced by p53 function. *Cancer Res*, **57**, 4029-4035.
- Shao, R.G., Cao, C.X., Zhang, H., Kohn, K.W., Wold, M.S. and Pommier, Y. (1999) Replication-mediated DNA damage by camptothecin induces phosphorylation of RPA by DNA-dependent protein kinase and dissociates RPA:DNA-PK complexes. *Embo J*, **18**, 1397-1406.
- Shell, S.M., Hess, S., Kvaratskhelia, M. and Zou, Y. (2005) Mass spectrometric identification of lysines involved in the interaction of human replication protein a with single-stranded DNA. *Biochemistry*, **44**, 971-978.

- Shiloh, Y. (2003) ATM and related protein kinases: safeguarding genome integrity. *Nature Rev. Cancer*, **3**, 155-168.
- Shivji, M.K., Podust, V.N., Hubscher, U. and Wood, R.D. (1995) Nucleotide excision repair DNA synthesis by DNA polymerase epsilon in the presence of PCNA, RFC, and RPA. *Biochemistry*, **34**, 5011-5017.
- Sinensky, M., Fantle, K. and Dalton, M. (1994a) An antibody which specifically recognizes prelamin A but not mature lamin A: application to detection of blocks in farnesylation-dependent protein processing. *Cancer Res*, **54**, 3229-3232.
- Sinensky, M., Fantle, K., Trujillo, M., McLain, T., Kupfer, A. and Dalton, M. (1994b) The processing pathway of prelamin A. *J Cell Sci*, **107 (Pt 1)**, 61-67.
- Smith, G.C. and Jackson, S.P. (1999) The DNA-dependent protein kinase. *Genes Dev*, **13**, 916-934.
- Stauffer, M.E. and Chazin, W.J. (2004a) Physical interaction between replication protein A and Rad51 promotes exchange on single-stranded DNA. *J Biol Chem*, **279**, 25638-25645.
- Stauffer, M.E. and Chazin, W.J. (2004b) Structural mechanisms of DNA replication, repair, and recombination. *J Biol Chem*, **279**, 30915-30918.
- Steinert, S., Shay, J.W. and Wright, W.E. (2000) Transient expression of human telomerase extends the life span of normal human fibroblasts. *Biochem Biophys Res Commun*, **273**, 1095-1098.
- Suckau, D., Mak, M. and Przybylski, M. (1992) Protein surface topology-probing by selective chemical modification and mass spectrometric peptide mapping. *Proc Natl Acad Sci U S A*, **89**, 5630-5634.
- Sugasawa, K., Ng, J.M., Masutani, C., Iwai, S., van der Spek, P.J., Eker, A.P., Hanaoka, F., Bootsma, D. and Hoeijmakers, J.H. (1998) Xeroderma pigmentosum group C protein complex is the initiator of global genome nucleotide excision repair. *Mol Cell*, **2**, 223-232.
- Taddei, A., Hediger, F., Neumann, F.R. and Gasser, S.M. (2004) The function of nuclear architecture: a genetic approach. *Annu Rev Genet*, **38**, 305-345.
- Thoma, B.S. and Vasquez, K.M. (2003) Critical DNA damage recognition functions of XPC-hHR23B and XPA-RPA in nucleotide excision repair. *Mol Carcinog*, **38**, 1-13.

- Toth, J.I., Yang, S.H., Qiao, X., Beigneux, A.P., Gelb, M.H., Moulson, C.L., Miner, J.H., Young, S.G. and Fong, L.G. (2005) Blocking protein farnesyltransferase improves nuclear shape in fibroblasts from humans with progeroid syndromes. *Proc Natl Acad Sci U S A*, **102**, 12873-12878.
- Treuner, K., Okuyama, A., Knippers, R. and Fackelmayer, F.O. (1999) Hyperphosphorylation of replication protein A middle subunit (RPA32) in apoptosis. *Nucleic Acids Res*, **27**, 1499-1504.
- Varela, I., Cadinanos, J., Pendas, A.M., Gutierrez-Fernandez, A., Folgueras, A.R., Sanchez, L.M., Zhou, Z., Rodriguez, F.J., Stewart, C.L., Vega, J.A., Tryggvason, K., Freije, J.M. and Lopez-Otin, C. (2005) Accelerated ageing in mice deficient in Zmpste24 protease is linked to p53 signalling activation. *Nature*, **437**, 564-568.
- Vassin, V.M., Wold, M.S. and Borowiec, J.A. (2004) Replication protein A (RPA) phosphorylation prevents RPA association with replication centers. *Mol Cell Biol*, **24**, 1930-1943.
- Volker, M., Mone, M.J., Karmakar, P., van Hoffen, A., Schul, W., Vermeulen, W., Hoeijmakers, J.H., van Driel, R., van Zeeland, A.A. and Mullenders, L.H. (2001) Sequential assembly of the nucleotide excision repair factors in vivo. *Mol Cell*, **8**, 213-224.
- von Zglinicki, T., Saretzki, G., Ladhoff, J., d'Adda di Fagagna, F. and Jackson, S.P. (2005) Human cell senescence as a DNA damage response. *Mech Ageing Dev*, **126**, 111-117.
- Wakasugi, M. and Sancar, A. (1999) Order of assembly of human DNA repair excision nuclease. *J Biol Chem*, **274**, 18759-18768.
- Wold, M.S. (1997) Replication protein A: a heterotrimeric, single-stranded DNA-binding protein required for eukaryotic DNA metabolism. *Annu Rev Biochem*, **66**, 61-92.
- Wu, X., Shell, S.M., Yang, Z. and Zou, Y. (2006) Phosphorylation of nucleotide excision repair factor xeroderma pigmentosum group A by ataxia telangiectasia mutated and Rad3-related-dependent checkpoint pathway promotes cell survival in response to UV irradiation. *Cancer Res*, **66**, 2997-3005.
- Wu, X., Shell, S.M., and Zou, Y. (2005) Interaction and co-localization of Rad9/Rad1/HUS1 checkpoint complex with replication protein A in human cells. *Oncogene*, **24**, 4728-4735.
- Yamasaki, R.B., Vega, A. and Feeney, R.E. (1980) Modification of available arginine residues in proteins by p-hydroxyphenylglyoxal. *Anal Biochem*, **109**, 32-40.

- Yang, Z.G., Liu, Y., Mao, L.Y., Zhang, J.T. and Zou, Y. (2002) Dimerization of human XPA and formation of XPA2-RPA protein complex. *Biochemistry*, **41**, 13012-13020.
- Zappacosta, F., Pessi, A., Bianchi, E., Venturini, S., Sollazzo, M., Tramontano, A., Marino, G. and Pucci, P. (1996) Probing the tertiary structure of proteins by limited proteolysis and mass spectrometry: the case of Minibody. *Protein Sci*, **5**, 802-813.
- Zernik-Kobak, M., Vasunia, K., Connelly, M., Anderson, C.W. and Dixon, K. (1997) Sites of UV-induced phosphorylation of the p34 subunit of replication protein A from HeLa cells. *J Biol Chem*, **272**, 23896-23904.
- Zhou, B.B. and Elledge, S.J. (2000) The DNA damage response: putting checkpoints in perspective. *Nature*, **408**, 433-439.
- Zou, Y., Bassett, H., Walker, R., Bishop, A., Amin, S., Geacintov, N.E. and Van Houten, B. (1998) Hydrophobic forces dominate the thermodynamic characteristics of UvrA-DNA damage interactions. *J Mol Biol*, **281**, 107-119.
- Zou, Y., Liu, Y., Wu, X. and Shell, S.M. (2006b) Functions of human replication protein A (RPA): from DNA replication to DNA damage and stress responses. *J Cell Physiol*, **208**, 267-273.

## APPENDIX

### ABBREVIATIONS

6-4PP, pyrimidine (6-4) pyrimidone photoproduct  
aa, amino acid  
AAF, *N*-acetyl-2-acetylaminofluorene  
AF, aminofluorene  
AP, 1-aminopyrene  
ATM, ataxia telangiectasia mutated  
ATR, ATM- and Rad3-related  
BER, base excision repair  
BPDE, benzo[*a*]pyrene diol epoxide  
Cdk, cyclin-dependent kinase  
ChIP, chromatin immunoprecipitation  
Chk1, check point kinase 1  
Chk2, check point kinase 2  
CIP, calf intestinal phosphatase  
CPD, cyclobutane pyrimidine dimer CS, Cockayne Syndrome  
CPT, camptothecin  
DAPI, 4',6-diamidino-2-phenylindole  
DBD, DNA binding domain  
DMEM, Dulbecco's modified Eagle medium  
DNA-PK, DNA-dependent protein kinase  
DSB, DNA double-strand break  
dsDNA, double-stranded DNA  
DTT, Dithiothreitol  
EDTA, Ethylenediamine Tetraacetic acid  
EMEM, Eagles minimum essential medium  
ERCC1, excision-repair cross-complementing group 1  
FPLC, Fast protein, peptide and polynucleotide liquid chromatography



FTI, farnesyltransferase inhibitor  
GFP, Green fluorescent protein  
GGR, global genomic repair  
HEPES, N-2-hydroxyethylpiperazine-N'-2-ethanesulfonic acid  
HGPS, Hutchinson-Gilford progeria syndrome  
HPG, *p*-hydroxyphenylglyoxal  
HR, homologous recombination  
hyp-RPA, hyperphosphorylated RPA  
hyp-RPA32N, hyperphosphorylated RPA32 N-terminus  
IF, immunofluorescence  
 $K_{d,obs}$ , equilibrium dissociation constant  
LMA, low melting point agarose  
MALDI-TOF, matrix-assisted laser desorption time of flight  
MEF, mouse embryonic fibroblasts  
MMR, mismatch repair  
MRN complex, Mre11/Rad50/Nbs1 complex  
MS, mass spectrometry  
NER, nucleotide excision repair  
NHEJ, nonhomologous end-joining  
NHS-biotin, *N*-hydroxysuccinimidobiotin  
NMA, normal melting point agarose  
NMR, Nuclear Magnetic Resonance  
OB-fold, oligosaccharide/oligonucleotides binding fold  
PCNA, proliferating cell nuclear antigen  
PI, Isoelectric point  
PIKK, phosphoinositide 3-kinase-like kinase  
PVDF, polyvinylidene difluoride  
Q-TOF, quadrupole-time of flight  
RD, restrictive dermopathy  
RFC, replication factor C  
RNAi, RNA interference

RPA, replication protein A  
RPA32C, RPA32 C-terminus  
RPA32N, RPA32 N-terminus  
SDS-PAGE, Sodium Dodecyl Sulfate- Polyacrylamide Gel Electrophoresis  
siRNA, small interfering RNA  
SSB, single-stranded DNA binding  
ssDNA, single-stranded DNA  
SV40, simian virus 40  
TCA, trichloroacetic acid  
TCR, transcription coupled repair  
TFIIH, transcription factor II H  
TTD, trichothiodystrophy  
UV, ultraviolet  
XP, xeroderma pigmentosum  
XPA, XPB etc., xeroderma pigmentosum group A, B etc.  
XPC-hHR23B, xeroderma pigmentosum protein C-human homolog of RAD23B  
XRCC4, x-ray repair cross-complementing protein 4

## VITA

YIYONG LIU

### Personal Data:

Place of Birth: Nangcheng, Jiangxi Province, China

Nationality: China

Marital Status: Married

### Education:

East Tennessee State University, Johnson City, Tennessee, Ph.D. in Biomedical Science, 2006

Sichuan University, Sichuan, China, M.S. in Biochemistry and Molecular Biology, 2002

Sichuan University, Sichuan, China, B.E. in Biochemical Engineering, 1996

### Professional Experience:

Graduate Assistant, East Tennessee State University, Johnson City, Tennessee, 2002-2006

Graduate Assistant, Sichuan University, Sichuan, China, 1999-2002

Research Assistant, North China Pharmaceutical Corporation, Shijiazhuang, China, 1996-1999

### Publications:

1. Liu, Y., Rusinol, A., Shell, S.M., Sinensky, M., Wang Y. and Zou, Y. (2006) Xeroderma Pigmentosum Group A (XPA) Inhibits Repair of DNA Double-Strand Breaks in Laminopathy-Based Premature Aging Cells. Submitted.
2. Liu, Y., Rusinol, A., Sinensky, M. Wang, Y., and Zou, Y. (2006) DNA Damage Responses in Progeroid Syndromes Arising from Defective Maturation of Prelamin A. *J Cell Sci* (in press).
3. Liu, Y. and Zou, Y. (2006) New insights into the roles of XPA and RPA in DNA repair and DNA damage responses. *Current Chemical Biology* (in press).

4. Wu X, Shell SM, Liu Y and Zou Y (2006) ATR-Dependent Checkpoint Modulates XPA Nuclear Import in Response to UV Irradiation. *Oncogene* Jul 24; [Epub ahead of print].
5. Zou, Y., Liu, Y., Wu, X. and Shell, S.M. (2006) Functions of human replication protein A (RPA): From DNA replication to DNA damage and stress responses. *J Cell Physiol*, 208, 267-273.
6. Liu, Y., Kvaratskhelia, M., Hess, S., Qu, Y. and Zou, Y. (2005) Modulation of replication protein A function by its hyperphosphorylation-induced conformational change involving DNA binding domain B. *J Biol Chem*, 280, 32775-32783.
7. Liu, Y., Yang, Z., Utzat, C.D., Liu, Y., Geacintov, N.E., Basu, A.K. and Zou, Y. (2005) Interactions of human replication protein A with single-stranded DNA adducts. *Biochem J*, 385, 519-526.
8. Liu, Y., Liu, Y., Yang, Z., Utzat, C., Wang, G., Basu, A.K. and Zou, Y. (2005) Cooperative interaction of human XPA stabilizes and enhances specific binding of XPA to DNA damage. *Biochemistry*, 44, 7361-7368.
9. Wu, X., Yang, Z., Liu, Y. and Zou, Y. (2005) Preferential localization of hyperphosphorylated replication protein A to double-strand break repair and checkpoint complexes upon DNA damage. *Biochem J*, 391, 473-480.
10. Liu, Y., Zhou, H., Wang, X., Sun, J. and Bao, J. (2001) Study on Tryptophan modification and fluorescence spectrum of Sophora Flavescens Lectin. *Journal of Sichuan University*, 38, 738-743.

#### Honors and Awards:

ASBMB Graduate/Postdoctoral Travel Award in April, 2006

ETSU Graduate Student Travel Award in April, 2006

ETSU Graduate Student Travel Award in May, 2005

Second Place in Division II, 2004 Appalachian Student Research Forum, East Tennessee State University, Johnson City, Tennessee, 2004